

GEOSPATIAL MODELLING AND MAPPING OF AVALANCHE HAZARD

A thesis submitted to the
University of Petroleum and Energy Studies

For the Award of
Doctor of Philosophy
In
Computer Science & Engineering

By
SATISH KUMAR
(SAP ID - 500042710)

July 2020

Supervisor
Dr. Pankaj Kumar Srivastava
Professor
Department of Petroleum Engineering and Earth Sciences,
University of Petroleum and Energy Studies,
Dehradun, India

External Supervisor
Dr. Snehmani
Sc. 'F', and Joint Director
Snow and Avalanche Study Establishment,
Defence Research & Development Organization,
Chandigarh, India



UNIVERSITY WITH A PURPOSE

Department of Information Technology
School of Computer Science
University of Petroleum and Energy Studies
Dehradun-248007: Uttarakhand

APRIL 2021

DECLARATION

I declare that the thesis entitled **“Geospatial Modelling and Mapping of Avalanche Hazard”** has been prepared by me under the guidance of Dr. Pankaj Kumar Srivastava, Professor of the Department of Petroleum Engineering & Earth Sciences, University of Petroleum and Energy Studies, Dehradun and Dr. Snehmani, Scientist ‘F’, Joint Director, Snow & Avalanche Study Establishment, Research & Development Centre, DRDO, Chandigarh. No part of this thesis has formed the basis for the award of any degree or fellowship previously.



(SATISH KUMAR)

SAP ID: 500042710

Ph.D. Research Scholar

Department of Information Technology,

School of Computer Science,

University of Petroleum & Energy Studies (UPES),

Village & Post Office-Bidholi, Via-Premnagar,

Dehradun-248007

Date: 02.04.2021

CERTIFICATE

I certify that **Mr. Satish Kumar (SAP ID: 500042710)** has prepared his thesis entitled **“Geospatial Modelling and Mapping of Avalanche Hazard”** for the award of the degree of Doctor of Philosophy (Engineering-Computer Science) from the University of Petroleum & Energy Studies, under my guidance. He has carried out the work at the Department of Information Technology, University of Petroleum & Energy Studies.

Internal Supervisor


(Dr. Pankaj Kumar Srivastava)

Professor

Department of Petroleum Engineering & Earth Sciences,
School of Engineering, University of Petroleum & Energy Studies (UPES),
Village & Post Office-Bidholi, Via-Premnagar,
Dehradun-248007

Email id: pksrivastava@ddn.upes.ac.in

Date: 16/7/2020

Tel : +91-172-2699804-06
Fax: +91-172-2699802/2699970
Mail: snehmani@sase.drdo.in
M: 9417839240



Govt of India
Ministry of Defence, DRDO
Snow & Avalanche Study Est (SASE)
Research & Development Center (RDC)
Him Parisar, Plot No 1, Sector 37-A
Chandigarh-160 036 (UT)

No.: SASE/Tech/9505/RSG

22-Jun-2020

CERTIFICATE

This is to certify that the thesis entitled **“Geospatial Modelling and Mapping of Avalanche Hazard”** by **Satish Kumar (SAP ID: 500042710)** in completion of the requirements for the award of the degree of Doctor of Philosophy (Engineering-Computer Science) is an original work carried out by him under our joint supervision and guidance.

It is certified that the work has not been submitted anywhere else for the award of any other diploma or degree of this or any other university. This thesis is fully adequate, in scope and quality for the award of the degree of Doctor of Philosophy (Engineering-Computer Science).

External Supervisor

A handwritten signature in blue ink, appearing to be 'Snehmani'.

(Dr. Snehmani)
Scientist 'F', Joint Director,
Head-Remote Sensing Group

ABSTRACT

Snow avalanche is known as a most dangerous natural hazard in snow-bound regions of the Indian Himalaya. Detection of potential avalanche areas and generation of avalanche susceptibility maps assist decision-makers and planners in executing suitable measures to reduce the avalanche risk. The base of the research is development and implementation of geospatial models for avalanche hazard mapping using avalanche occurrence parameters. The geospatial models implemented in the present study are Probabilistic Frequency Ratio, Multicriteria Decision Analysis-Analytical Hierarchy Process (MCDA-AHP), and Fuzzy-Frequency Ratio (Fuzzy-FR) Models. The most prominent avalanche occurrence parameters were used in proposed models. The avalanche occurrence parameters are divided into two categories as: (i) Terrain-based and (ii) meteorological-based parameters. The terrain-based avalanche occurrence parameters are slope, aspect, curvature, elevation, terrain roughness and ground cover. The meteorological-based avalanche occurrence parameters are: Air temperature, snow depth, wind speed/direction and relative humidity. ASTER GDEM V2 and Landsat 8 satellite imagery were used to generate considered terrain parameters and vegetation cover. Meteorology datasets were used to generate meteorological parameters. The proposed models were developed and implemented in geospatial domain by using both types of avalanche occurrence parameters to generate susceptibility maps of potential avalanche release areas. For validation of the results, avalanche inventory map of documented avalanche locations was used. The prediction accuracy has been calculated by using the area under the ROC curve (ROC-AUC) method.

ACKNOWLEDGMENTS

I would like to express my gratitude to Dr. Snehmani, Sc. 'F' & Joint Director, Snow and Avalanche Study Establishment, DRDO, Chandigarh for his supervision, advice, and guidance from the very early stage of this research as well as giving me extraordinary experiences throughout the work. Above all and the most needed, he provided me with unflinching encouragement and support in various ways.

I express my sincere gratitude to Dr. Pankaj Kumar Srivastava, Professor, Department of Petroleum Engineering & Earth Sciences, School of Engineering, University of Petroleum & Energy Studies (UPES), for his supervision and encouragement throughout the Ph.D. work.

I am thankful to the administration and staff of Snow and Avalanche Study Establishment, DRDO, Chandigarh for extending all the help required to carry out field work in inhospitable and remote areas.

Finally, I wish to thank all those whose names have not figured above but have helped me directly or indirectly during the course of my research work. Really this thesis would not have been written without any of you.

(SATISH KUMAR)

TABLE OF CONTENTS

• LIST OF FIGURES	x
• LIST OF TABLES.....	xi
1. INTRODUCTION	1
1.1 Overview of avalanche.....	1
1.2 The magnitude of the problem	2
1.3 History and research motivation.....	3
1.4 Research questions and objectives.....	10
1.4.1 Research questions.....	10
1.4.2 Research objectives.....	10
1.5 Outline of the thesis	11
2. LITERATURE REVIEW.....	13
2.1 Background	13
2.2 Identification and monitoring of snow avalanche using remote sensing	14
2.3 Spatial modelling and mapping of avalanche hazard	27
2.4 Research Gap.....	30
2.5 Research objectives.....	31
2.6 The process for the development and implementation of the proposed models	31
2.6.1 Construction of avalanche related database	31
2.6.2 Geospatial modelling and mapping	32
2.6.3 Evaluating the models' performance in the most appropriate fashion using GIS in combination with a statistical tool.....	33
3. STUDY AREA.....	35
3.1 Study Area.....	35
3.2 Data Used	37

3.2.1 Terrain data.....	37
3.2.2 Meteorological data	39
4. INFLUENCE OF TERRAIN AND METEOROLOGICAL PARAMETERS IN AVALANCHE OCCURRENCE	40
4.1 Analysis of avalanche occurrence terrain parameters.....	40
4.1.1 Slope	40
4.1.2 Aspect.....	41
4.1.3 Elevation	42
4.1.4 Curvature.....	42
4.1.5 Vegetation cover.....	43
4.1.6 Terrain roughness	43
4.2 Analysis of avalanche occurrence meteorological parameters.....	44
4.2.1 Air Temperature Map	44
4.2.2 Relative Humidity Map.....	46
4.2.3 Snow Depth Map.....	48
4.2.4 Wind Speed and Direction Map	51
5. GEOSPATIAL MODELLING AND MAPPING OF AVALANCHE HAZARD.....	55
5.1 Rationale	55
5.2 Preparation of Avalanche inventory map.....	55
5.3 Analysis of avalanche occurrence factors and generation of thematic GIS layers.....	56
5.4 Probabilistic frequency ratio model for avalanche susceptibility mapping...61	
5.5 Multi-Criteria Decision Analysis-Analytical Hierarchy Process (MCDA- AHP) Model.....	70
5.5.1 MCDA-AHP Model.....	70

5.5.2	Avalanche susceptibility mapping using MCDA-AHP model.....	73
5.6	Fuzzy Frequency Ratio (Fuzzy-FR) Model for Avalanche Susceptibility Mapping	79
5.6.1	Theoretical background of fuzzy set theory and frequency ratio method... ..	79
5.6.2	Methodology for fuzzy-frequency ratio modelling	81
5.6.3	Fuzzy-Frequency Ratio Modelling for avalanche susceptibility mapping... ..	81
5.6.3.1	Frequency ratio values for each class of avalanche occurrence factors	83
5.6.3.2	Fuzzification of FR based avalanche occurrence factors.....	83
5.6.3.3	Fuzzy overlay analysis to obtain fuzzified avalanche susceptibility index.....	84
6.	RESULTS AND DISCUSSION.....	89
6.1	Probabilistic Frequency Ratio Model	89
6.2	Multi-Criteria Decision Analysis-Analytical Hierarchy Process (MCDA-AHP) Model.....	92
6.3	Fuzzy Frequency Ratio (Fuzzy-FR) Model	96
6.4	Comparison of results between FR, MCDA-AHP and Fuzzy-FR models... ..	100
7.	CONCLUSION AND FUTURE RESEARCH	103
7.1	Conclusion.....	103
7.2	Future research	106
8.	REFERENCES	107
	APPENDICES.....	125
	APPENDIX 1: FIRST PAGE OF PLAGIARISM REPORT	125
	APPENDIX -2: CURRICULUM VITAE.....	126
	APPENDIX -3: LIST OF PUBLICATIONS	130

LIST OF FIGURES

Figure 1.1: Maximum speed and thrust exerted by an avalanche (McClung and Schaerer, 2006).....	3
Figure 1.2: Destruction caused by March 1979 avalanche in Lahaul and Spiti Valley Himachal Pradesh, India. Half of the Guiskar village was wiped away by the avalanche.	4
Figure 1.3: Avalanches in Kashmir's Gurez sector (Source: NDTV).....	5
Figure 1.4: An Indian Kashmiri villager in Gund, located 70 km from Srinagar. Several people, including soldiers killed by avalanches. (Source: CBC).....	5
Figure 1.5: Year-wise fatalities due to avalanche accidents in the Indian Himalaya. On average, about 35–40 deaths due to avalanches every year in the (SASE internal report, 2010, 2016 and 2018).	6
Figure 1.6: Villages affected by avalanches in Himachal (SASE internal report, 2010, 2014, 2016 and 2018).....	6
Figure 1.7: Villages affected by avalanches in Jammu and Kashmir (SASE internal report, 2010, 2014, 2016 and 2018).	7
Figure 1.8: Villages affected by avalanches in Uttarakhand (SASE internal report, 2010, 2014, 2016 and 2018).....	7
Figure 1.9: Avalanche vulnerability map of Himachal Pradesh (SASE internal report, 2010).....	8
Figure 3.1: Location map of the study area.....	35
Figure 3.2: Avalanche affects 40 percent of various road axes in the western Himalayan region.	36
Figure 4.1: Profile of air-temperature of 25-January-2018.....	44
Figure 4.2: Distance weights of the different stations	45
Figure 4.3: Flow chart of the temperature map generation.....	46
Figure 4.4: Flow chart to generate RH map.....	48

Figure 4.5: Snow depth map preparation workflow	49
Figure 4.6: (a) Air-Temperature (b) Relative-Humidity (c) Snow-Depth and (d) Wind-Speed maps.....	50
Figure 4.7: Process to generate terrain modified wind speed and direction	52
Figure 4.8: Wind rose of three automatic weather stations (AWS).....	53
Figure 4.9: Terrain-modified wind speed/direction.....	53
Figure 4.10: Assessment of observed and terrain modified wind speed at stations 1 and 3 with respect to RMSE, r^2 , and correlation coefficient	54
Figure 4.11: Frequency-distribution of avalanche occurrence with respect to meteorological parameters	54
Figure 5.1: Flow chart of frequency ratio modelling for avalanche susceptibility mapping	64
Figure 5.2: Avalanche occurrence terrain parameters: (A) Slope, (B) Aspect, (C) Curvature, (D) Elevation, (E) Vegetation, and (F) Terrain Roughness.....	65
Figure 5.3: Diagram showing the example process for calculating the FR value of each class of the avalanche occurrence factor.....	68
Figure 5.4: Avalanche susceptibility map of the study area generated using the FR model	68
Figure 5.5: Avalanche susceptibility map of the study area obtained using FR model with observed avalanche polygons overlaid.....	69
Figure 5.6: Partly comparison of avalanche susceptibility maps of terrain and meteorological-based parameters (A: Terrain-based avalanche hazard map; B: Hybrid (Terrain + Meteorological)-based avalanche hazard map)	69
Figure 5.7: Flow chart of MCDA-AHP modelling for avalanche susceptibility mapping	78
Figure 5.8: Partly comparison of avalanche susceptibility maps of terrain and meteorological-based parameters (A: Terrain-based avalanche hazard map; B: Hybrid (Terrain + Meteorological)-based avalanche hazard map)	78

Figure 5.9: Linear membership function.....	80
Figure 5.10: Flow chart of fuzzy-FR modelling for avalanche susceptibility mapping	82
Figure 5.11: Partly comparison of avalanche susceptibility maps of terrain and meteorological-based parameters (A: Terrain-based avalanche hazard map; B: Hybrid (Terrain + Meteorological)-based avalanche hazard map)	83
Figure 6.1: ROC curve for success rate and prediction rate of terrain-based avalanche susceptibility index.....	91
Figure 6.2: ROC curve for success rate and prediction rate of terrain and meteorological parameters based avalanche susceptibility index	92
Figure 6.3: ROC curve analysis of prediction rate for avalanche hazard index based on terrain and meteorological parameters.....	95
Figure 6.4: ROC curve for success rate and prediction rate of terrain-based avalanche susceptibility index.....	99
Figure 6.5: ROC curve for success rate and prediction rate of terrain and meteorological parameters based avalanche susceptibility index	100

LIST OF TABLES

Table 1.1: Avalanche Hazard and the damage occurred (SASE internal report, 2014).....	8
Table 1.2: Avalanche accidents in Himachal Pradesh (SASE internal report, 2014)	9
Table 2.1: The list of most popular space-borne optical satellites/sensors useful for avalanche detection and monitoring.	18
Table 2.2: Most popular space-borne radar satellites/sensors useful for avalanche mapping	27
Table 3.1: Geographical attributes of the study area.	36
Table 3.2: Occurrence parameters used in geospatial modelling of avalanche susceptibility, spatial resolution, and data sources.....	38
Table 3.3: Specifications of Landsat 8 OLI data.....	38
Table 5.1: FR values in the each class of avalanche occurrence terrain factors. ..	66
Table 5.2: FR values in the each class of avalanche occurrence meteorological factors	67
Table 5.3: The importance value scale (Saaty, 1980).....	71
Table 5.4: Random consistency index (Saaty, 2000); n = order of the matrix.	72
Table 5.5: Assignment of ratings for each terrain-based thematic layer/criteria. .	73
Table 5.6: Assignment of ratings for each meteorological-based thematic layer/criteria.	75
Table 5.7: Pairwise comparison matrix and weight values of each terrain-based layer using MCDA-AHP	76
Table 5.8: Pairwise comparison matrix and weight values of each meteorological-based layer using MCDA-AHP.....	76
Table 5.9: Spatial relationship between each terrain-based avalanche conditioning factor, avalanche occurrence and fuzzy membership values	85

Table 5.10: Spatial relationship between each meteorological-based avalanche conditioning factor, avalanche occurrence and fuzzy membership values.....	87
Table 6.1: Fuzzy set of avalanche occurrence factors	97

1. INTRODUCTION

1.1 Overview of avalanche

Avalanche is a rapid downhill flow of snow mass on a slope. This may bring ice, soil, forest and rocks along with it. Snow avalanche is known as most dangerous natural hazard in snow-bound regions of the Indian Himalaya. A snow avalanche is a ubiquitous phenomenon in snow-belt mountainous regions and a threat to human, property, communication, etc., because of the uncertainty associated and poor predictability involved (Brundl et al. 2004; McCammon and Hägeli, 2007).

Generally, snow avalanches are of mainly two types, such as loose snow avalanche and slab avalanche. The avalanche releases at a point which extends over the large area is known as loose snow avalanche. A large amount of snow usually flows down a sloping surface in a triangular pattern (McClung and Schaerer, 2006). A failure in the snow depth initiates slab avalanche, which is commonly in a rectangular shape and completely break down cracks in snow cover. The slab-avalanche is more destructive in nature than loose-snow avalanche. The destructive nature of the slab-avalanche causes more fatalities and property damage property than other type of avalanches (McClung and Schaerer, 2006). The relative magnitude of the shear displacement in slab-avalanche is influenced by the slope angle and type of snow. More than two-thirds of the total deformation is in shear by slope angles of 25° and nearly 90% of the total deformation is in shear when the slope angle reaches 45° (McClung and Schaerer, 2006). When the snow density increases, as would be expected for most slab avalanches, shear deformation becomes even more dominant. The slope dependence of the deformation components is one explanation of the slope angle dependence of slab avalanche formation. Slab avalanches become rare for slope angles near 25° and they increase in frequency as slope angle increases due to higher shear stresses and a more significant percentage of shear deformation (McClung and Schaerer, 2006).

The Indian Himalayan experiences number of avalanches of all types. The various type of avalanche activities reported in the Indian Himalaya ranging from loose-snow to wet slab-avalanche. The loose-snow avalanche activities are

reported during the early winter (Bahadur, 2004). Whereas, wet slab avalanches are noticed in March-April (Bahadur, 2004). The western Indian Himalaya is divided into 03 zones by Sharma and Ganju (2000). The lower, middle and upper-Himalaya are three zones of the western India Himalaya. The frequency of avalanches is fairly high in lower-Himalaya. In this zone, almost all the direct-action avalanches occur in heavy snowfall.

Most of the slab avalanches occurred in peak winter (Sharma and Ganju, 2000). In the lower Himalaya zone, the loose snow avalanches may occur due to radiation in (Sharma and Ganju, 2000). The area covering in this zone is Pir-Panjal range of Jammu & Kashmir and same range in Himachal Pradesh on the windward side. In the middle Himalaya zone, a maximum number of avalanches observed throughout the winter, including slab, loose snow and thaw avalanches. Thaw avalanches are observed in April and May. The snowfall in the upper Himalaya zone is almost dry. In the upper Himalaya zone, the frequency of avalanche activity is low because ground conditions are not favourable to anchor the amount of snowpack. However, delayed action avalanches have been observed in some areas where undulating and rugged slopes provide sufficient anchorage (Sharma and Ganju, 2000).

In worldwide, snow avalanche mostly occurs in spring and winter seasons on slopes without vegetation where snow slide along the inclined slope due to the effect of internal and external forces (Schweizer et al., 2003). Prediction of avalanche is inferior to understand because it mostly affects by dynamic parameters. The dynamic parameters are referred to snowfall, snowpack, wind, temperature, raining, and precipitation intensity. Subsequently, weather conditions also contributing avalanche occurrence (Schweizer et al., 2003).

1.2 The magnitude of the problem

Avalanche can reach speed of upto 200 km/h and exerts pressures upto 50 T/m² (McClung and Schaerer, 2006) (Figure 1.1). Such speed and the pressure are bound to cause soil erosion in soil terrain and forest destruction in a forested area in the first instance. Besides that, several problems are associated with an avalanche that affects mountain people, directly or indirectly. Life in the mountains becomes paralyzed, thus affecting the overall wellbeing of mountain people. Due

to the disruption of traffic, essential supplies to the interior in snowbound areas are affected. Loss of forest cover and soil cover, in addition to road damage, impedes the hill development schemes. While on the one hand, the avalanche debris dams, rivers causing flooding, same avalanche debris on the ground locks up the water required during the spring period. Avalanches affect military operations as well as border area security and safety.

1.3 History and research motivation

Avalanche activities occur in snow-belt mountainous regions worldwide. Avalanche is one of the main natural disasters and threats to humans, property, communication, etc. The oldest recorded avalanche accident in 218 BC, which killed 12,000 soldiers and 2,000 horses (Schweizer et al., 2015). Most of the significant avalanche accidents associated with military operations. The associated military operations are Napoleon in 1800 and Dolomites in 1916 during World-War 1. A recent example was the conflict between India and Pakistan in April 2012. Due to this conflict, an avalanche triggered and killed 130 soldiers (Schweizer et al., 2015).

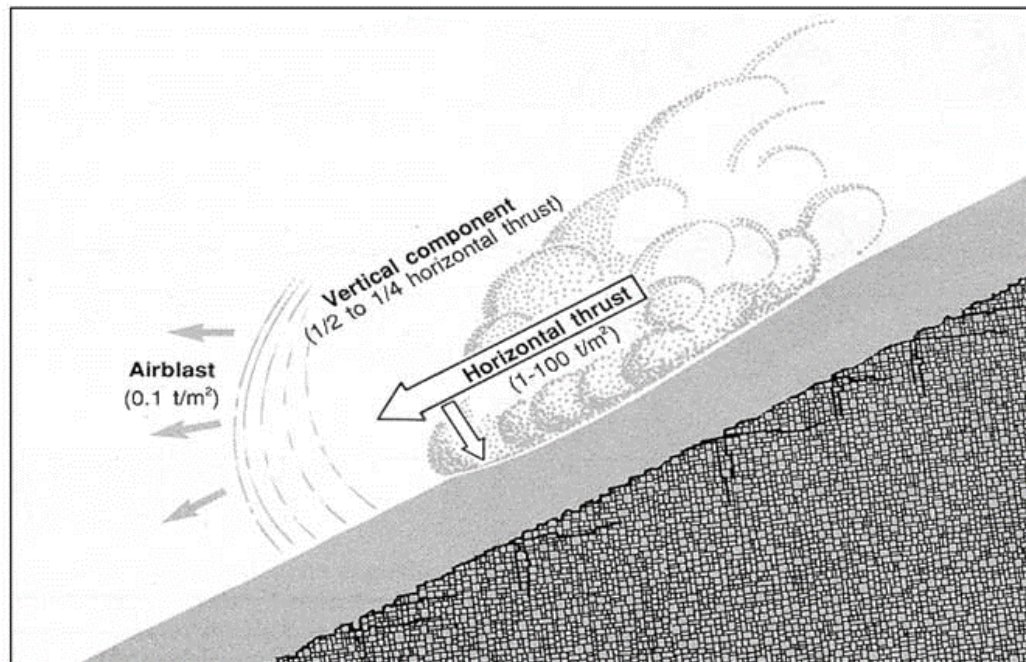


Figure 1.1: Maximum speed and thrust exerted by an avalanche (McClung and Schaerer, 2006).

Avalanche activities in the Western Himalaya are in extreme proportions and vicious in their frequency from January to March (Ganju and Dimri, 2004). In

1838, an avalanche accident was recorded in a village nearby Triloknath temple in Lahaul Himalaya. Due to this massive avalanche, a village near to Triloknath temple was utterly swept away and killed a total of about 60 people and 3,000 cattle (Rao et al., 1988). In northern India, on March 7, 1979, an avalanche moved through the village of Gusikar, destroying several stone buildings and killing 35 residents (Figure 1.2). Widespread avalanche activity existed in the same week across the Indian Himalaya, resulting in the deaths of about 200 people (McClung and Schaerer, 2006).

A total number of deaths due to avalanche accidents reached 869, including 87 army officers upto 11-December-2015. A total of Rs 7505 crore utilized in military operations in 04 years as of 2016. Whereas, the Pakistan army lost 213 soldiers in Siachen region from 2003-2010 (Indian Express 2016).



Figure 1.2: Destruction caused by March 1979 avalanche in Lahaul and Spiti Valley Himachal Pradesh, India. Half of the Guiskar village was wiped away by the avalanche.

A series of 04 avalanches on 25-January-2017 in the Gurez valley killed 24 people (Figure 1.3 and Figure 1.4), known as the Gurez avalanche accident. Twenty India army soldiers and four civilians were claimed in total death of 24 people. In the series of four avalanches, the first avalanche triggered in the morning and killed four people. The second avalanche was also triggered at almost the same time in a tourist place and army camp of Sonmarg. A distance of 150 km from

Sonmarg, two more avalanches triggered in the evening and killed 15 soldiers (Retrieved 26 January 2017, NDTV).



Figure 1.3: Avalanches in Kashmir's Gurez sector (Source: NDTV)



Figure 1.4: An Indian Kashmiri villager in Gund, located 70 km from Srinagar. Several people, including soldiers killed by avalanches. (Source: CBC)

In Western Indian-Himalayan, 30-40 deaths on average and property lost each year because of avalanche accidents (De Scally and Gardner, 1994; Gardner and Saczuk 2004; Ganju et al., 2002; Ganjui and Dimri, 2004; Sharma et al.,

2004). While, total fatalities in worldwide due to avalanche accidents are estimated at about 250 per year (Schweizer et al., 2015).

Analysis of avalanche occurrences data since the last four decades (Figure 1.5) indicates that 35–40 deaths per year. A property worth a million lost every year due to avalanche accidents. The actual loss is likely to be higher since many accidents unreported. Village of Himachal Pradesh, Jammu & Kashmir and Uttarakhand states such as: 109, 91, and 16 number of villages are affected continuously by snow avalanches throughout the winter season (Ganju and Dimri, 2004) (Figure 1.6, Figure 1.7 and Figure 1.8). A certain extent of northeast Sikkim is also affected by snow avalanches.

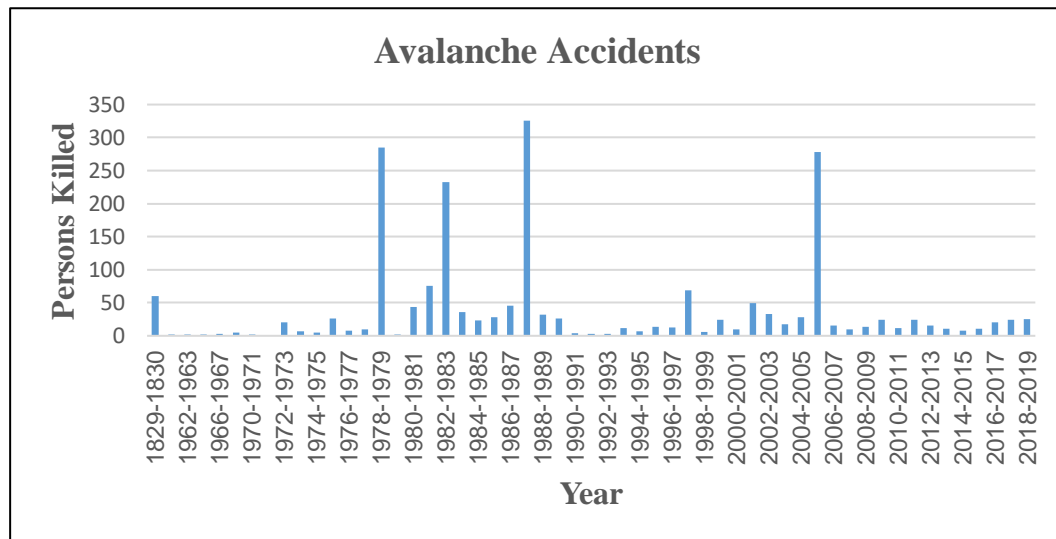


Figure 1.5: Year-wise fatalities due to avalanche accidents in the Indian Himalaya. On average, about 35–40 deaths due to avalanches every year in the (SASE internal report, 2010, 2016 and 2018).

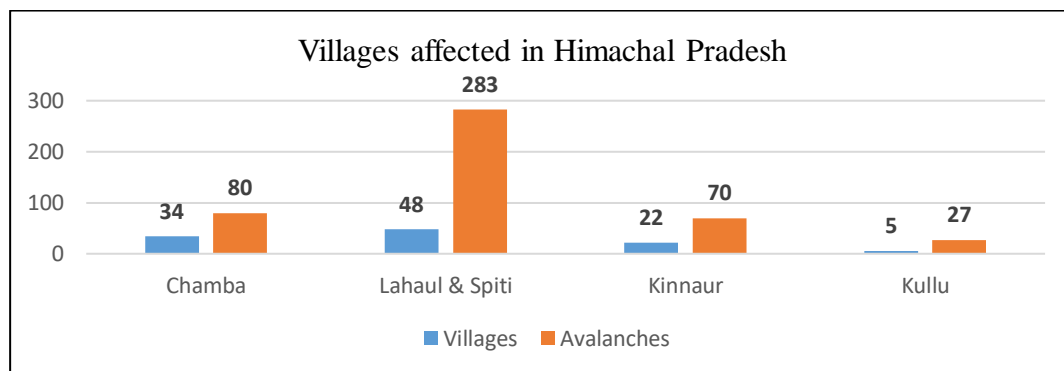


Figure 1.6: Villages affected by avalanches in Himachal (SASE internal report, 2010, 2014, 2016 and 2018).

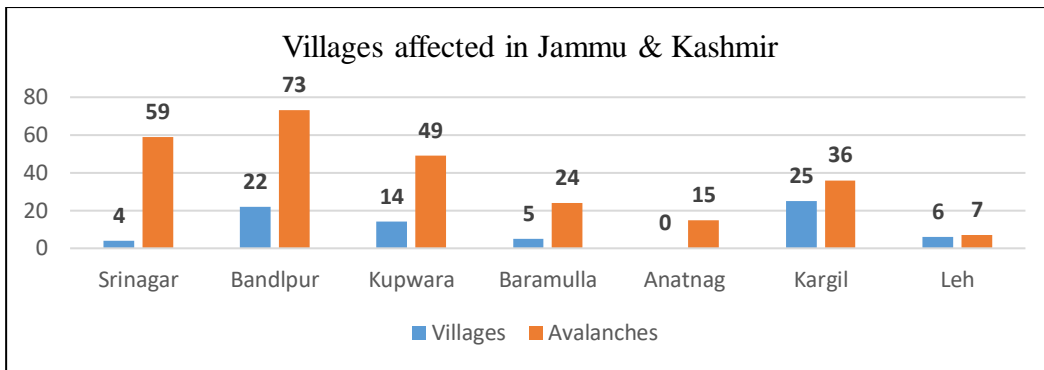


Figure 1.7: Villages affected by avalanches in Jammu and Kashmir (SASE internal report, 2010, 2014, 2016 and 2018).

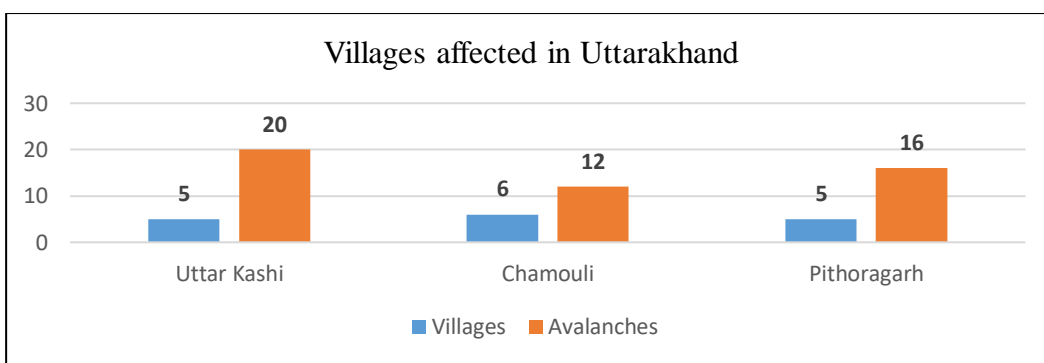


Figure 1.8: Villages affected by avalanches in Uttarakhand (SASE internal report, 2010, 2014, 2016 and 2018).

The primary study area is the Lahaul & Spiti district of Himachal Pradesh (H.P), i.e., Lahaul-Himalaya. The mountainous region falling in Kullu, Chamba, Lahaul & Spiti and Kinnaur districts of H.P. These districts are highly vulnerable to avalanche accidents (Figure 1.9). Various recorded avalanche events and damage caused are given in Table 1.1. Avalanche accidents are break-up in district-wise and given in Table 1.2.

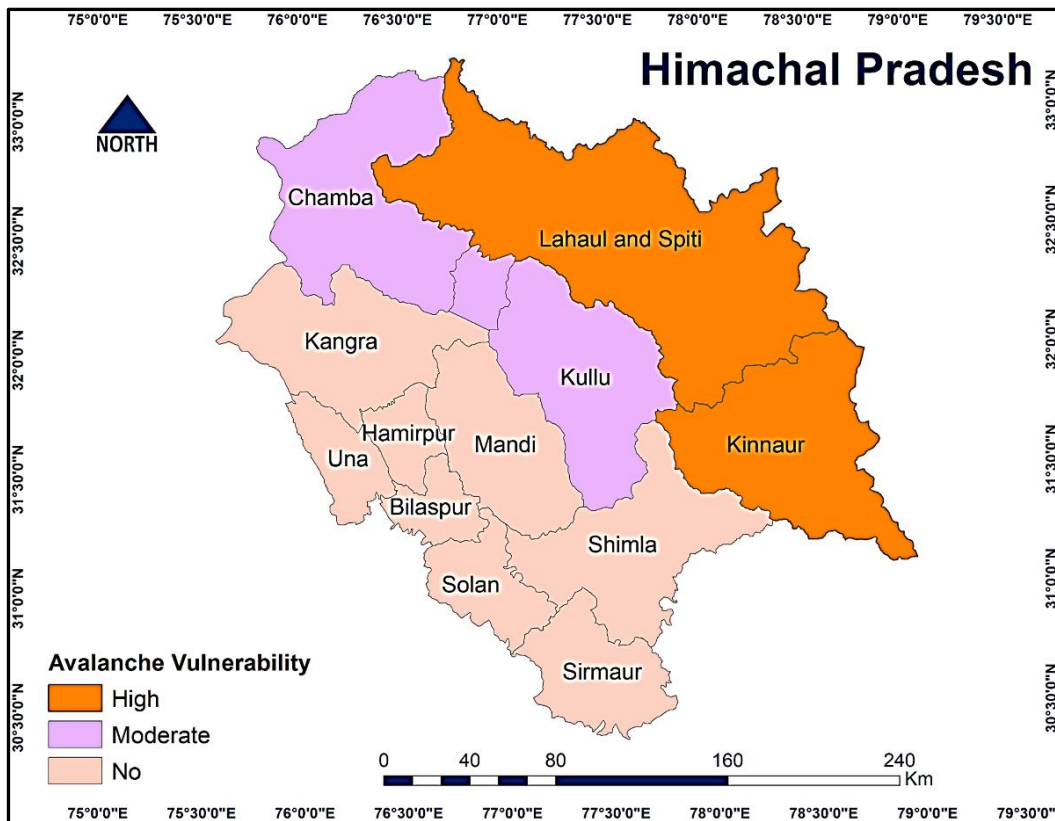


Figure 1.9: Avalanche vulnerability map of Himachal Pradesh (SASE internal report, 2010)

Table 1.1: Avalanche Hazard and the damage occurred (SASE internal report, 2014)

Place	Date	Avalanche Occurrence
Lahaul and Spiti	Jan 1975	The earthquake triggered the avalanche and damaged road network.
	Mar 1978	Damage property, road network and 30 people killed.
	Mar 1979	Damage communication system and 237 people died.
	Mar 1991	Tinku avalanche blocked the road for 40 days.
	Sept.1995	Snow avalanche debris changed to flood.
	Nov 1997	Avalanche occurred alongside the Rani Nala.
	March 2011	Avalanche occurred alongside Pindri Nala and 02 labor men died.

The avalanche hazard vulnerability map of Himachal Pradesh, India, shows that the Kinnaur and of Lahaul-Spiti districts are highly vulnerable districts. Kullu and Chamba are moderate vulnerable districts. Some parts of Shimla and Kangra also fall in moderate vulnerable areas.

Table 1.2: Avalanche accidents in Himachal Pradesh ([SASE internal report, 2014](#))

Sr. No.	District	Accidents	People involved	People killed	People injured
1	Lahaul & Spiti	21	397	298	53
2	Kinnaur	32	144	129	9
3	Chamba	12	59	53	0
4	Kullu	6	13	9	4
5	Shimla	2	6	1	5

Increasing population density, transport, construction and recreational activities in snow-bound mountainous regions leading avalanche risk to greater proportions in the near future ([Ancey, 2001](#); [Ganju and Dimri, 2004](#); [Fuchs and Brundel, 2005](#)). The predictive nature of snow avalanche is very poor because it affects by wind, snowfall, snowpack, temperature, raining, water content and precipitation intensity. Subsequently, weather conditions also contribute to avalanche occurrence ([Schweizer et al., 2003](#)). Although the predictive nature of the avalanche is poor, the susceptibility map of the avalanches provides useful information for avalanche risk assessment, management and planning the protection infrastructure development ([Mears, 1992](#); [Hervas, 2003](#); [Barbolini et al., 2011](#)). Due to a lack of general awareness and an information map of the avalanche hazard area, the threat is likely to constitute serious problems. Therefore, avalanche susceptibility mapping over the large and undocumented mountainous regions is highly in demand nowadays. Through scientific analysis of avalanche activities, avalanche workers can predict avalanche release areas. Hence, minimize the avalanche risk through appropriate preparation. Geospatial modelling is recognized as a significant approach for natural hazards assessment, including avalanche susceptibility ([Selçuk, 2013](#)). In this regard, geospatial technology has tremendous capability to utilize various types of topographical information &

management of the large volume of data and hence, useful for avalanche susceptibility mapping (Selçuk, 2013).

1.4 Research questions and objectives

1.4.1 Research questions

A number of identified research questions related to geospatial modelling of avalanche hazard are given below as:

- (i) What kind of spatial data and geospatial components required to generate an avalanche hazard map?
- (ii) In the geospatial model development for avalanche hazard mapping, what relationships bind the occurrence parameters and spatial components?
- (iii) What is the experience worldwide in the best practice in geospatial modelling of avalanche hazard?
- (iv) How can geospatial models be developed for the assessment of avalanche hazard?
- (v) What are the statistical techniques for evaluating the efficiency of the models in the geospatial domain?
- (vi) How to assess the performance of the models in the most appropriate fashion using GIS in combination with statistical tools?

1.4.2 Research objectives

Research objectives identified in the context of geospatial modelling of avalanche hazard are:

- (i) To analyze the terrain and meteorological data of the study area for identification of the various parameters (constant and dynamic parameters) contributing towards avalanche occurrence.
- (ii) Development and implementation of geospatial models/algorithms for avalanche hazard mapping using avalanche occurrence parameters.
- (iii) Proposed models for avalanche susceptibility mapping are: Probabilistic Frequency Ratio Model, Multi-Criteria Decision Analysis-Analytical

Hierarchy Process (MCDA-AHP) Model, and Fuzzy-Frequency Ratio (Fuzzy-FR) Model.

- (iv) Evaluating the model's performance in the most appropriate fashion using GIS in combination with statistical tools.

1.5 Outline of the thesis

The thesis is outlined in eight chapters, with section, subsection and subsections provided in each chapter.

Chapter 1

Introduction: This chapter presents the overview of a snow avalanche, the nature of the phenomenon of avalanche, the history and research needs. This explains history and motivation for snow avalanche research. Encourage the applications of geospatial technology in avalanche hazard modelling and mapping. The chapter describes the key research objectives followed by research questions.

Chapter 2

Literature review and state-of-the-art: Chapter 2 consists of a study of the literature and state-of-the-art GIS techniques used in modeling avalanches. The advantages and disadvantages of geospatial technology are discussed in this chapter.

Chapter 3

Study area and dataset: Chapter 3 provides a brief overview of the study area and the dataset used.

Chapter 4

Influence of terrain and meteorological factors in avalanche occurrence: Chapter 4 describe the contribution of terrain and meteorological factors in avalanche occurrence. Statistical assessment and development of the relationship between classes of terrain parameters and meteorological factors with avalanche occurrence data.

Chapter 5

Geospatial modelling and mapping of avalanche Hazard: Development and implementation of proposed geospatial models for avalanche susceptibility mapping such as: Probabilistic FR-Model, MCDA-AHP Model, and Fuzzy-FR Model. Evaluation of the model's performance in the most appropriate fashion using GIS in combination with statistical tools.

Chapter 6

Results and discussion: Chapter 6 discusses the outcome of the geospatial models developed for avalanche hazard mapping.

Chapter 7

Conclusion and future research: Chapter 7 talks about the insights and achievements from present research with the proposed future scope.

2. LITERATURE REVIEW

2.1 Background

Avalanche hazard assessment using geospatial technology has a long history of more than thirty years. A snow avalanche is the most dangerous natural hazard in snowbound mountainous regions. Therefore, an avalanche susceptibility map needs to be prepared to know the potential areas and minimize the vulnerability. Geospatial technology, including remote sensing and GIS has tremendous capability to achieve the goal with better results. For two decades, many studies have been performed and algorithms developed in the context of avalanche hazard management. Identification and mapping of snow avalanche sites is a challenging process for a large undocumented mountainous terrain. Due to complex mountainous terrain, there is a lack of avalanche occurrence evidence, occurrence parameters and estimation of avalanche runout distance. Various kinds of parameters which influence the occurrence of avalanche activity are terrain, meteorological, vegetative parameters and snowpack structure. The terrain parameters which influence the avalanche occurrence are slope, aspect, curvature, elevation and terrain roughness. Meteorological parameters are snowfall, snowpack, wind, temperature, and precipitation intensity. The digital elevation model (DEM) in the GIS model helps to generate and apply terrain parameters for the identification and mapping of snow avalanches. Most commonly used ASTER, SRTM and NRSC Cartosat-1 digital elevation models of spatial resolution 30 m are freely available on respective web portals. The processes to generate the digital elevation model from ortho stereo-pair satellite data and generation of terrain parameters are discussed. The influence of various avalanche occurrence parameters and application of geospatial modelling & mapping by utilizing parameters for avalanche hazard are discussed in this chapter.

Geospatial technology and methods applied for mapping and modelling of the snow avalanche are discussed in this chapter. This chapter highlights the modelling and mapping techniques with the advance remote sensing technology and spatial analysis. Present and future challenges, advantages and disadvantages of the technology are also concluded in this chapter.

2.2 Identification and monitoring of snow avalanche using remote sensing

Remote sensing technology is widely used for the collection of data from different kinds of objects on the Earth. The process of acquisition of data without any physical contact with the object through sensors mounted on satellites or airborne platforms. The space-based remote sensing technology is mostly used from early for the acquisition of data of snowbound mountainous regions. (Rango and Itten, 1976; Chang et al., 1982; Dozier, 1989b; Hall et al., 2002; Nolin, 2010; Dong, 2018; Tsai et al., 2019). Space-based remote sensing is considered as most suitable for avalanche related study because the satellite can cover a large area at a time with regular repeatability. The satellite has a capacity to mount a number of remote sensing sensors to provide comprehensive capability data acquisition. Relevant theories and applications of satellite-based remote sensing for snow-related studies by Dozier (1989a), Rees (2006), Scherer et al. (2013), Tedesco (2015) and Xiao et al. (2018) are published.

This section addressed the use of remote sensing for the identification, monitoring, characterization and analysis of avalanche hazard. Remote sensing technology of optical, light detection & ranging (LiDAR) and radio detection & ranging (RADAR) based sensors of different kinds were used worldwide for avalanche related studies. Remote sensing of avalanches depends upon the spectral properties of the snow in the electromagnetic spectrum. Remote sensing is categorized into two types as per the range of electromagnetic spectrum: optical and microwave remote sensing. Further three categories of the optical remote sensing are: panchromatic, multispectral and hyper-spectral as per the spectral information.

2.2.1 Optical remote sensing of snow avalanche hazard

Optical sensor has been used in optical remote sensing which exploits the visible, NIR and SWIR parts of the electromagnetic spectrum. Due to an increase in the snow density, snow depth and surface roughness, the detection of avalanche extent is mostly depending upon the difference in contrast between snowpack structure and avalanche debris. Calculation of snow properties usually affected by the angle of observation and illumination of the optical sensor. Thus, optical remote sensing sensors limits the detection accuracy of a snow avalanche. Three types of

platforms such as: ground-based, airborne and spaceborne, are generally used in optical remote sensing.

At the initial stage, the ground-based optical remote sensing of the avalanche was based on the automatic time-lapse photography (Christiansen, 2001). Continued automated digital photographs were used for the extraction of snow distribution and snow cover maps. In recent time, the time-lapse photography for monitoring the glide cracks, cornice failure and cornice dynamics is popular (van Herwijnen and Simenhois, 2012; Peitzsch et al., 2010; Hendrikx et al., 2012; Feick et al., 2012; Vogel et al., 2012; van Herwijnen and Fierz, 2014). Whereas, glide cracks and cornice dynamics are not easy to understand. To improve the detailed understanding process, a high spatial and temporal photography camera facilitates direct integration with meteorological data. This time-lapse photography facilitates the simple approach to easily monitor the cornice dynamics and cornice failure activity on slope inflections, edges and ridges. Direct integration of continuous time-lapse photographs of high frequency with meteorological data has been successfully applied for easily monitoring of wet-snow avalanche (van Herwijnen et al., 2013).

Digital photogrammetry is very helpful for understanding the interaction of terrain parameters with snow distribution (Wirz et al., 2011). Digital photogrammetry is commonly utilized for three-dimensional (3D) modelling. This technique uses the overlapping photographs of different angles of the same region to extract 3D measurement or geometry. The structure-from-motion (SfM) is one of the advanced techniques to generate 3D information or structure from 2D photographs (Koenderink and van Doorn, 1991). This technique has been successfully demonstrated to study the slab avalanche (Gauthier et al., 2014). This research consists of generating the surface model for extracting the volume and deposition area of a slab avalanche. The SfM technique was also helpful for mapping the fracture lines of the slab avalanche.

Aerial optical remote sensing sensors are beneficial for avalanche detection, monitoring and topographic mapping. Application of data from aerial optical remote sensing sensors is extensively utilized in natural disasters and other environmental studies. Whereas, the application of data from aerial-based optical

remote sensing of avalanche is not thoroughly explored. A few researchers have used aerial optical sensor data for avalanche monitoring. One of the main reasons behind the limited applicability of aerial optical remote sensing technology is that the survey is typically only carried out in summers. This technology is generally used for avalanche applications such as mapping of starting and run-out zones of the avalanche. Aerial optical remote sensing images are also used for avalanche inventory map generation. [Bühler et al. \(2009\)](#) recommended that the avalanche hazard mapping requires airborne optical images of a large scale. For the mapping of avalanche debris, a high radiometric and spatial resolution digital push-broom scanner was used by [Bühler et al. \(2009\)](#). In this study, an avalanche detection accuracy of 94% was achieved for large and medium debris of avalanches. The airborne digital push-broom scanner exploits the spectral, textural and directional information facilitating the medium avalanches differentiation in the shaded area.

The slope angle is most prominent avalanche occurrence parameter. The high-resolution DEM was used for the extraction of the slope angle. Subsequently, avalanche runout was simulated by using a Rapid Mass Movement System (RAMMS) ([Christen et al., 2010](#); [Gilany and Iqbal, 2019](#); [Jarsve et al., 2019](#)). The RAMMS is also known as a numerical simulation model. [Lato et al. \(2012\)](#) also used the airborne remote sensing using a push-broom scanner. The orthoimages were used for the mapping of avalanche debris by applying the object-based technique. In this study, the neighborhood pixels were calculated to identify avalanche. This technique is followed by the classification and segmentation of the airborne remote sensing imagery, which then facilitates the detection of avalanche debris. The object-based technique was applied in two case studies avalanche detection, which demonstrated 95% and 97% accuracy ([Lato et al., 2012](#)).

An aerial platform equipped with optical remote sensing sensors was deployed by [Eckerstorfer et al. \(2015\)](#) to detect the recent avalanche deposits. This system was employed to capture overlapping photographs with a high frequency of time-series. SfM technique was used to generate the full mosaic of ortho-image from captured overlapping photographs of avalanche deposits for further interpretation and calculation, such as volume and outline of deposits.

Space-borne optical remote sensing is commonly applied in various fields such as ground subsidence hazard (Lee et al., 2010; Bianchini et al., 2019; Rehman et al., 2020), landslide susceptibility (Pradhan and Lee, 2010; Umar et al., 2014; Shahabi et al., 2015; Gholami et al., 2019; Ozdemir et al., 2020), groundwater mapping (Oh et al., 2011; Ozdemir, 2011; Naghibi et al., 2015; Falah et al., 2019), debris hazard mapping (Yang et al., 2011) and susceptibility assessment of debris flow (Chen et al., 2015; ; Xiong et al., 2020). Whereas, applications of optical remote sensing data in avalanche studies are not fully exploited. Only a few research scientists have worked on optical remote sensing for study on avalanche mapping. Table 2.1 shows the list of most popular optical space-based satellites/sensors useful for avalanche detection and monitoring. Remote sensing sensors mentioned in Table 2.1, range from low resolution to very high resolution with remote sensing techniques are beneficial for detection and monitoring the avalanche. Lato et al. (2012) and Larsen et al. (2013) have mentioned the techniques for the avalanche detection using space-based optical remote sensing data. Lato et al. (2012) adopted a technique followed by segmentation and classification of QuickBird satellite data for avalanche detection. Space-based optical remote sensing of avalanches is very helpful in those regions where the manual method is not possible due to rugged and high mountainous terrain. In recent years, a combination of manually and space-based optical remote sensing-based techniques were applied for the detection of avalanche deposits in a large area (Eckerstorfer and Malnes, 2015; Eckerstorfer et al., 2014). Landsat-8 OLI satellite data of spatial resolution 15 m was used in this study.

Table 2.1: The list of most popular space-borne optical satellites/sensors useful for avalanche detection and monitoring.

Satellite/Sensor	Spectral resolution	Spatial resolution (m)		Swath (km)	Temporal resolution
		Panchromatic	Multi-spectral		
Quick Bird	NIR, R, G, B, P	0.6	2.4	16.5	1–3.5
Landsat-8	NIR, TIR, R, G, B, P	15	30	185	16
Ikonos	NIR, R, G, B	0.8	3.6	11	3
GeoEye-1	NIR, R, G, B	0.5	2	15.2	3
WorldView-1	P	0.5		17.6	1–5
WorldView-2	P, 8 MS	0.46	2	16.4	1–4
Orbview-3	P, 4 MS	1	4	8	3
Spot-5	NIR, SWIR, R, G, B, P	2.5, 5	10	60	2–3
Formosat-2	NIR, R, G, B, P	2	8	24	1
Kompsat-2	NIR, R, G, B, P	1	4	15	2-3
Kompsat-3	NIR, R, G, B, P	0.7	0.8	15	2-3
Cartosat-2B	P	0.8		9.6	4
Pléiades-1/2	NIR, R, G, B, P	0.7	2	20	1
Sentinel-2A & 2B	NIR, R, G, B, P	10	10	290	5

2.2.2 Light detection and ranging (LiDAR) remote sensing of avalanche hazard

The application of LiDAR technology is divided into two categories (i) ground-based and (ii) airborne LiDAR. Terrestrial laser scanner (TLS) is a ground-

based LiDAR. In snow study, the application of TLS is to measure snow depth (Prokop, 2008). (Prokop, 2008) applied the TLS for the detection of avalanche and known as one of the first researchers for this type of study. This study demonstrated the possibility of detection of avalanches.

At first, the TLS was used for measurement of snow depth within a 500 m distance. An error below 10 cm was reported under normal visibility conditions. The accuracy of TLS was further compared with tachymetry survey data (Prokop et al., 2008), which demonstrated the acceptable results. The case study attempted by Prokop et al. (2013) permits the representation of mass gain and loss on deposits, starting and run-out zones of the snow avalanche. Application of TLS based approach was also applied by Deems et al. (2014) for analysis of relating parameters of avalanches. The relating parameters analyzed in this including various zones of avalanche (starting, tack and run-out zone), slope in snow cover & snow-free conditions. The process in this study was followed by calculating the mass loss at the starting zone, mass gain at the run-out zone and tracking of release area of avalanche (Deems et al. 2014). Change of mass balance of snow cover used for extraction of the volume of avalanche debris. Sovilla et al. (2010) used TLS for the extraction of the snow depth of avalanche debris before and after the avalanche occurrence. This study achieved the vertical resolution of 100 m and 500 m for horizontal, which demonstrated acceptable results instead of a manual photogrammetric approach for estimation of the depth of avalanche debris (Deems et al., 2013).

The second category of LiDAR technology for remote sensing of avalanche is airborne LiDAR. The airborne LiDAR was initially applied by Vallet et al. (2000) in avalanche related study. A laser scanner Optech-ALTM 1020 was used to calculate the avalanche debris volume. The scanner mounted helicopter was used for the collection of recent avalanches data. This study achieves the accuracy from 25 to 30 cm (Vallet et al., 2000). A very high-resolution DEM extracted from airborne LiDAR data was successfully applied for extraction of release area of avalanche (Chrustek and Wezyk (2009). A potential release area (PRA) technique was used in this study. The application of high-resolution DEM demonstrated better results in rugged and steep terrain.

2.2.3 Radar remote sensing of avalanche hazard

Radar remote sensing of avalanche is divided into three categories: (i) ground-based, (ii) airborne and (iii) spaceborne radar. As per knowledge, the remote sensing of avalanche using ground-based radar systems has been initially performed by [Martinez-Vazquez and Fortuny-Guasch \(2008\)](#). This study demonstrated the application of Linear SAR (LISA) operated in C-band with a frequency of 5.8 GHz. In the backscattered arrangement, a high physical change of avalanche represented, which results in the temporal decorrelation. Qualitative measurement of temporal decorrelation is defined as coherence. In coherence, the avalanche release area seemed as low coherence. Decorrelation is also lead by the physical change of the snowpack structure. This decorrelation makes avalanche detection very difficult. Intermediate processes like morphological filtering and spatial averaging were applied to solve the problem by [Martinez-Vazquez and Fortuny-Guasch \(2008\)](#). Finally, an accuracy of 73.5% was achieved for avalanche detection. The false-negative rating was found as 7.4%. The differential interferometry SAR (DInSAR) was also used to extract the avalanche volume by the ground-based SAR ([Martinez-Vazquez and Fortuny-Guasch, 2008](#)). The avalanche identification in dry snow was also performed using C-band of SAR, followed by interferometry processing of paired images ([Martinez-Vazquez and Fortuny-Guasch, 2008](#)). Whereas, the C-band of SAR has the capability of good penetration depth in dry snow. GAMMA Portable Radar Interferometer (GPRI) was used to detect small avalanche ([Wiesmann et al., 2014 and Caduff et al., 2015](#)). The GPRI acquired images with a repeat interval of 3 minutes. This study also revealed that liquid water content in snow affects the coherence.

The second category of radar remote sensing is airborne radar remote sensing. As per knowledge, the avalanche detection study based on airborne radar remote sensing does not exist. Nevertheless, as per the references of existing studies performed based on ground and airborne remote sensing for avalanche detection, it is concluded that the airborne radar remote sensing of avalanche is possible. The SAR system introduced by the German Aerospace Centre, known as E-SAR has the potential for the present application. The E-SAR covers a wavelength ranges of 3-85cm and operates in four bands of frequency. The bands operated in the E-SAR system are X, C, L and P. A repeat pass and single-pass

channel included in measurement modes (DLR, 2014). Another airborne SAR developed by MetaSensing also has the capability for avalanche detection. This SAR system operated in Ku and X-bands. The UAVSAR developed by NASA operated in L-band may also be capable of avalanche related studies. This system used for repeat and single-pass InSAR. The operational elevation of UAVSAR ranges from 2000–18000 m.

Unmanned aerial vehicles (UAV) is a type of aerial platform. UAVs may be operated in lower height to collect data in very high spatial resolution and accuracy. Therefore, UAV can be used as a promising platform for avalanche detection. The capability of UAV to reach in inaccessible remote areas where difficult for the manned aerial platform is an added advantage. The SAR-based UAV has the potential for avalanche detection and related studies. This type of platform may be very beneficial for continuously monitor the avalanche-prone regions of highly complex, rugged and steepness. This technology may also be helpful when satellite coverage is not sufficient. Moreover, the GPR mounted on UAV assists the locations of avalanche victims buried underneath the snow cover (Instanes et al., 2004).

The third category of radar remote sensing is space-borne radar. As per knowledge, space-borne SAR remote sensing of the avalanche was initially performed by Wiesmann et al. (2001). This was performed to detect avalanche debris. The backscattered image from ERS 1/2 was used to detect avalanche. The C-band SAR data of ERS 1/2 was utilized in this study. Backscattered based change detection was applied for detection of avalanches by Bühler et al. (2014b). 02 Terra SAR-X images of different acquisition dates were used to detect avalanche. For the requirement of visual identification of avalanche, the RGB composition was applied. C-band images of Radarsat-2(RS-2 U) were used to detect avalanche release areas (Malnes et al., 2013). The spatial resolution of RS-2 U is 3 m and ground swath is 20 Km. Due to the high backscattering contrast of RS-2 U image, the avalanche can also be visually detected. The backscattering contrast of avalanche snow ranges from 1.5–2.3 dB. RS-2 U images were also used by Eckerstorfer and Malnes (2015) for detection of avalanches in Northern Norway. In these studies, high backscattered contrast between avalanche debris and contiguous snow cover, the small-size avalanches are visually detectable. Optical

remote sensing images and field datasets were also used for the validation of results.

2.2.4 Advantages and disadvantages of remote sensing technology in avalanche study

(i) Advantage and disadvantages of optical remote sensing

Advantage and disadvantage of optical remote sensing is divided into three categories of technology as (i) ground-based, (ii) airborne and (iii) space-borne remote sensing. The ground-based optical remote sensing delivers acceptable data in real-time through automated time-lapse photography to detect and monitor avalanche occurrence. The time-lapse (TL) photography system requires an integrated based high-resolution DSLR camera, weatherproof case, solar panel, charge circuitry and TL controller. At present, many suitable and cost-effectiveness time-lapse photography systems are available in the global market. The scale of the study ranges from low to high as per the resolution of the DSLR camera. In general, the time required to capture a single picture is two minutes to a day, which usually depends upon the application and input power. In wintertime, the power drain quickly, which requires frequent maintenance (Vogel et al., 2012). The probability of system failure also high due to draining the power in the wintertime. The weather conditions also affect the process of optical remote sensing. Unpleasant weather conditions obstruct continuous monitoring of avalanche sites. Spatial coverage of ground-based limited as compare to space-borne and airborne remote sensing.

The 3D model can be generated from SfM photogrammetry by utilizing a pair of overlapping images (Westoby et al., 2012). This technique is highly reliable due to high resolution and accuracy. The main limitation of this technique is that while creating a 3D model, the scale and spatial orientation lost. Therefore, post georeferencing is usually required. Due to the high-resolution camera and high configuration system, an accurate with acceptable resolution (in cm) 3D models may be extracted.

An airborne optical remote sensing system utilizes aerial scanner to capture high spatial and temporal and radiometric resolution images. One of the most popular scanners ADS used to capture high-resolution data at three observational

angles to extract DSM. The difference between summer and winter DSMs are useful for the extraction of snow-depth. A similar study was performed by [Bühler et al. \(2015\)](#) for a large area. Accuracy of around 0.3 m RMSE of snow depth was reported. The spatial resolution of data ranges from 0.5 m to 5 m, which depends upon the flight level and spectral resolution is 5 bands.

The main advantage of this scanner is the NIR band. The NIR band is less prone to image saturation. Due to the sensitivity of these bands with respect to the grain size of snow, the acquired image more contrasted than a simple color photograph ([Bühler et al., 2015](#)). Visually analysis of high-resolution image acquired through an airborne survey is easy for the detection of avalanche-debris manually. Non-experts can also easily identify the avalanche-debris because acquired images are exposed uniformly. However, this process becomes tedious work due to a lack of uniformity over large regions. To overcome this difficulty, the automated classification and segmentation technique provide appropriate results for the detection of avalanches. This technique is beneficial for the detection of a medium and large avalanche. The technique becomes a challenge for the detection of small avalanche because ski lifts and the wind blowing snow are hard to differentiate from avalanche debris. Documented potential release area and terrain parameters of snow-free terrain of avalanche site are essential to enhance the accuracy, reliability and efficiency of the algorithm for automated detection of avalanche debris. However, automated detection of avalanche debris using optical remote sensing is limited because the optical data is more sensitive to unpleasant weather conditions. This technique is based upon the texture differentiation in snow, which requires instant response time. An airborne optical remote sensing system with an ADS scanner is high resource-intensive and costly. The alternate airborne optical remote sensing system is RPAS. The payload carrier in RPAS is least cost and resource-intensive. The aerial survey through RPAS is pre-programmable and fully autonomous for flights. The time taken in the RPAS survey is quick, which can survey a valley in a few hours. The main disadvantage of the RPAS survey is highly dependent upon the weather conditions.

The third category of optical remote sensing technology is space-borne optical remote sensing. At present, many space-borne remote sensing sensors ranges from low to high resolution exist. A high resolution optical remote sensor

namely QuickBird was available for long time which provided the images of spatial resolution 0.6 m and 2.5 m in panchromatic multispectral bands with a swath of 16.5–19 km. Due to these characteristics of the QuickBird satellite sensor, the release area mapping of avalanche is feasible. The QuickBird satellite comes with the high cost because of high temporal, radiometric and spatial resolution. Many optical satellite sensors are available to acquire high-resolution data. The list of high resolution satellite imagery available commercially including WorldView 1, WorldView 2, WorldView 3, WorldView 4, OrbView-3, Ikonos, GeoEye 1, and Pleiades 1A/1B.

WorldView-1 and WorldView-2 satellite sensors have a spatial resolution of 0.46 m in PAN band, 8 and 4 multispectral bands. The spatial resolution of WorldView-3 is 0.31 m in PAN band with 8 multispectral and 8 SWIR bands. The spatial resolution of WorldView-4 is 0.31 m in PAN band with 4 multispectral bands. The spatial resolution of OrbView-3 is 1 m in PAN band with 4 multispectral bands. The spatial resolution of Ikonos is 0.8 m in PAN band with 4 multispectral bands. The spatial resolution of GeoEye-1 is 0.46 m in PAN band with 4 multispectral bands. The spatial resolution of Pleiades 1A/1B is 0.5 m in PAN band with 4 multispectral bands. These satellite images can be used for natural hazards applications like landslide, snow avalanche, debris flow, etc. for detection, monitoring and mapping. The list detailing the available high-resolution optical satellite images are described by [Lato et al. \(2012\)](#). Landsat 8 OLI having a spatial resolution of 15 m in PAN band and 30 m in multispectral bands with a swath 100 Km are freely available for academic exercises. Though, the acquisition time of Landsat 8 OLI is variable and may not cover the area of the interest. Recently, two optical remote sensing satellites Sentinel 2A and Sentinel 2B also launched on 23-June-2015 and 07-March-2017 to acquire medium resolution satellite images. These satellites have visible, NIR, SWIR sensors with 13 multispectral bands of spatial resolution 10, 20 and 60 m with a swath of 290 Km, respectively. Due to the availability of high and medium resolution satellite data, the avalanche detection, monitoring and mapping are feasible nowadays. The only problem is that the optical remote sensing is very highly sensitive to unpleasant weather conditions through which become the tedious task for extraction of adequate information.

(ii) Advantage and disadvantages of LiDAR remote sensing

Riegl initially used the TLS for the detection of avalanche debris. The TLS systems LMS Z420i, LPM-2 K or LPM-i800HA, were used by Reigl (Prokop, 2008) for the avalanche-related study. The acquisition speed of these systems is very slow and outdated as compared to recent years. A few years back, the TLS-based survey was limited to a small range due to scanner wavelength. This scanner takes long scanning time due to slow operating speed and also limited by the availability of power supply. New TLS systems Optech Iiris LR and RieglVZ-6000 have fast acquisition speed and unprecedented range. These TLS systems are portable and work in all weather conditions due to wavelength. The GPS, SLR camera and software used in new TLS are expensive. Therefore, the main disadvantage of new TLS systems is the high price. The airborne LiDAR for avalanche detection does not use significantly and only a little information available. Riegl is considered as the main provider of airborne LiDAR systems. Riegl VQ-580 system is suitable for avalanche related studies. Leica Optec also provides the LiDAR system. Leica LiDAR systems may be suitable for avalanche monitoring. The main advantage of the airborne LiDAR system is the application in large areas. The main disadvantage of airborne LiDAR is high price and logistic challenges.

(iii) Advantage and disadvantages of RADAR remote sensing

Mostly used portable ground-based imaging SAR devices are Ibis-FL, LISALab and GPRI. The data acquisition speed of these systems is fast and less time interval of 30 seconds. Therefore, less time interval makes it regular repeatability of data acquisition. Through ground-based imaging SAR devices, coherence coefficients & temporal backscattered change detection used for the detection of the avalanche. The SAR data should be acquired after and before avalanche occurrence for extraction of occurrence parameters. Preprocessing of SAR data is necessary before application. The preprocessing of SAR data including filtering, calibration, coregistration and classification techniques. Interferometric coherence changes with a change of snowpack structure (Caduff et al., 2015). The main advantage of the ground-based SAR is high spatial and temporal-resolution. Its temporal resolution is around 30 seconds and spatial resolution ranges from 1

m to 8 m in 1 Km distance. Ground-based SAR can detect any minor change in the snow surface. This is very sensitive upto 1 mm of change in the snow surface. The ground-based SAR method is not dependent on light, weather conditions and can be used at any time. However, this system is dependent on enough power supply. The main disadvantage of the ground-based SAR system is limited area monitoring. This system is still expensive to procure, complex to operate and processing.

The space-based i.e., satellite-borne SAR systems provide high-resolution data for avalanche detection but restricted to poor in repeatability. The list of most popular space-based RADAR satellites/sensors is given in [Table 2.2](#). These systems work in all weather and light conditions, but acquisition cost is high. A small avalanche can also detectable in high-resolution SAR data after contrast enhancement and topographical correction.

Sometimes, the detection capability in SAR images is limited to the low incidence angle of radar, which causes layover and foreshortening effects. The SAR data of Sentinel-1A satellite is freely available since 2015 for any region on the globe. Sentinel-1A solved the issue of acquisition cost and poor repeatability. The spatial resolution of the C-band SAR of Sentinel-1A is 10 m and the swath is 250×150 Km. The temporal resolution of Sentinel-1A is 12 days. Medium size avalanche debris can be detected in the Sentinel-1A image ([Malnes et al., 2015](#)). As per [Malnes et al. \(2015\)](#), a Sentinel-1A image can cover the complete county of Troms.

A total 505 number of avalanche release areas were detected manually by [Malnes et al. \(2015\)](#) in a single image. Backscattered-base change detection can also apply with two SAR images of with and without avalanche occurrence ([Eckerstorfer et al., 2016](#)). An avalanche is detectable in high backscattered contrast of the SAR image. High backscattered SAR images of Sentinel-1A with and without avalanche activity were used in automated detection of the avalanche release area algorithm ([NGI, 2015](#)). After comparison with manually detected avalanches, 57.1 % detected avalanches were correct. The satellite-based SAR system has the advantage of acquiring data in high resolution and with large swath. Also, this system is not dependent on weather and light conditions, which can be

used to detect avalanche activity regularly. These factors show the high potential of SAR data for avalanche detection.

Table 2.2: Most popular space-borne radar satellites/sensors useful for avalanche mapping

Sensor	Spatial resolution (m)	Band	Frequency (GHz)	Swath (km)	Polarization
ERS 1/2	30	C	5.3	100	VV
Envisat ASAR IM	30	C	5.3	100	HH/VV
Envisat ASAR WSN	100	C	5.3	500	HH/VV
TerraSAR-X Staring Spotlight	0.25–40	X	9.65	4–270	HH/VV/HV/VH
RS-2 U	3 × 3	C	5.4	20	HH/VV/HV/VH
RS-2 SCWA	100 × 100	C	5.4	300	HH, HV/VV, VH
RS-2 SCNA	50 × 50	C	5.4	500	HH, HV/VV, VH
S-1 IW	20 × 20	C	5.4	250	HH, HV/VV, VH
S-1 EW	40 × 40	C	5.4	500	HH, HV/VV, VH
Cosmo-Skymed Spotlight 2	1 × 1	X	9.65	10	HH, HV/VV, VH
Cosmo-Skymed Strip map	3–15	X	9.65	40–30	HH, HV/VV, VH

2.3 Spatial modelling and mapping of avalanche hazard

In past years, a number of avalanche runout modelling studies are performed with statistical models Alpha-Beta (α - β) and Runout-Ratio Models (Sinickas and Jamieson, 2014), dynamic models such as PCM Model (Perla et al., 1980), PLK Model (Perla et al., 1984), Leading Edge Model (McClung and Mears, 1995), AVAL-1D (Oller et al., 2010), Erosion and Deposition Model (Naaim et al., 2003, 2004), Snow Avalanche Modelling and Simulation Model (SAMOS) (Sailer et al., 2002), the modified version of SAMOS i.e. SamosAT (Sailer et al., 2008) and Voellmy–Salm model (Christen et al., 2010).

There have been various kinds of GIS-based studies performed and models developed for mapping various aspects of avalanche hazard (Gleason 1994; Furdada et al., 1995; Stoffel et al., 1998; Tracy 2001; Hebertson and Jenkins, 2003; Hendriks et al., 2004; Gruber and Bartelt, 2007; Delparte et al., 2008; Biskupic and Barka, 2010; Barbolini et al., 2011; Campbell et al., 2012; Selçuk, 2013, Snehmani et al., 2013; Snehmani et al., 2014; Meer et al., 2020; Yariyan et al., 2020). These models are vital to assess the extent of a particular hazard factor as per the terrain and occurrence zones of the hazard. Maggioni et al. (2002) identified potential avalanche release areas using GIS with respect to topographical parameters and historical avalanche events data. Bühler et al., (2013) also developed an automated snow avalanche release area detection tool over two study sites such as (i) Manali, Himachal, India, and (ii) Davos, Grisons, Switzerland. The tool presented by Bühler et al., (2013) was based on the high-resolution forest cover information and digital elevation models derived from aerial photogrammetric data. Pistocchi and Notarnicola (2013) tested two probabilistic data-driven models to delineate potential avalanche release zones, such as: (i) weights of evidence model, and (ii) logistic regression model in South Tyrol, Italy.

Probabilistic assessment and identification of avalanche occurrence conditions including snow cover and weather are extensively performed by Hendriks et al., (2005); McClung et al., (2006); Jomelli et al., (2007); Schweizer et al., (2009). A few studies based on release area mapping of the avalanche has been done (Pistocchi and Notarnicola, 2013; Bühler et al., 2013) and susceptibility mapping of snow avalanches (Selçuk, 2013, Snehmani et al., 2014).

A heuristic (expert-judgment) method, the analytical hierarchy process (AHP) model (Saaty, 1980) basis of weighting and rating is successfully attempted for avalanche susceptibility mapping (Selçuk, 2013, Snehmani et al., 2014). The modified-AHP (M-AHP) model has been introduced by Nefeslioglu et al. (2013) for natural hazard assessment, especially for avalanches. The primary benefit of this method is the values incorporated in the model depending on the expert judgments. Sometimes, this process could lead to the main drawbacks, specifically for pair-wise comparisons and results in model imperfection. Weight of evidence

(WoE) and logistic regression (LS) models based on data-driven techniques were also attempted for avalanche mapping (Pistocchi and Notarnicola, 2013).

Researchers like McClung and Schaerer (2006), Jomelli et al. (2007), and Schweizer et al. (2009) proposed various methods for probabilistic assessment and identification of snow cover and weather parameters influencing the contribution in avalanche activity.

It is generally assumed that the avalanche events in the future will predominantly repeat themselves at the documented avalanche regions (Hebertson and Jenkins, 2003). Barbolini et al., (2001) suggested frequency analysis of registered or documented avalanche sites as the first step in avalanche susceptibility mapping. Sometimes mapping of large-area avalanche hazard in the mountainous region needed, where an adequate dataset of recorded avalanches are unavailable (Eckert et al., 2007). In this condition, it is significant to use topographical factors for the identification of avalanche-prone areas. Maggioni and Gruber (2003) devised a concept to calculate a relationship between avalanche occurrences and topographical parameters to observe the statistical distribution of documented avalanche sites onto less known areas based on geomorphological characteristics. This concept has found extensive useful in mountainous areas where documentation of past avalanche occurrences does not exist (Maggioni, 2004). Various probabilistic models (Chung and Fabbri, 1993, 1999) initially utilized for mineral exploration and landslide hazard mapping have been successfully adopted for mapping potential avalanche release areas (Ghinoi and Chung, 2005). The approach for applying these probabilistic models is independent of expert judgment and entirely based on data-driven values, which makes the applicability of these models for large regions consistent. However, these probabilistic models have not been further used in avalanche mapping.

On the other hand, modelling of avalanches using a fuzzy and machine learning approach is limited (Jaccard, 1989; Barpi 2004; Ghinoi and Chung, 2005; Zischg et al., 2005; Rahmati et al., 2019; Choubin et al., 2020).

Integration of Fuzzy logic (Zadeh, 1965) with AHP (F-AHP) and frequency ratio approach (Bonham-Carter, 1994) (Fuzzy-FR) are widely applied for natural hazard and geo-environmental problems (Aksoy and Ercanoglu, 2012; Huang et al.,

2012; Kavzoglu et al., 2014; Shahabi et al., 2015; Gholami et al., 2019; Ozdemir, 2020). As per knowledge, these models are not ever developed for avalanche susceptibility mapping. Hence, Probabilistic Frequency ratio and Fuzzy-FR models provide novelty to present investigation.

Fuzzy logic (Zadeh, 1965) is commonly utilized to solve complicated and decision-making problems. The fuzzy-set concept is effectively and widely utilized in diverse disciplines of complex degree of uncertainties (Barpi, 2004; Bui et al., 2012). In the fuzzy set concept, an entity is a member of an entity set if it has a membership degree of 1. On the other hand, if the entity has a membership degree of 0, then it is not a member of the entity set (Hines, 1997). This theory is idealized to map the spatial entities as the members of an entity set (Pourghasemi et al., 2013).

In natural hazard assessment, the FR value is the ratio of the probabilities of hazard occurrence to the non occurrence factors' attributes of the total area (Bonham-Carter, 1994; Pradhan and Lee, 2010). The FR-based methodology provides the capability to calculate the level of the relationship between the dependent and independent parameters (Oh et al., 2011). The FR model has been successfully applied in applications such as ground subsidence hazard (Kim et al., 2006; Lee et al., 2010; Bianchini et al., 2019; Rehman et al., 2020), landslide susceptibility (Pradhan and Lee, 2010; Umar et al., 2014; Shahabi et al., 2014; Shahabi et al., 2015; ; Gholami et al., 2019; Ozdemir et al., 2020) and groundwater mapping (Oh et al., 2011; Ozdemir, 2011; Naghibi et al., 2015; Falah et al., 2019). The theoretical background of the fuzzy logic and frequency ratio method is described in the next sections.

The research initiative presented in the present research is snow avalanche susceptibility mapping using GIS-based probabilistic Frequency Ratio (FR) Model, Multi-Criteria Decision Analysis-Analytical Hierarchy Process (MCDA-AHP) Model and Fuzzy Frequency Ratio (Fuzzy-FR) Model.

2.4 Research Gap

Models/algorithms such as: Probabilistic Frequency Ratio Model, Fuzzy Frequency Ratio (Fuzzy-FR) Model, Fuzzy-Analytical Hierarchy Process (Fuzzy-AHP) Model, Modified Analytical Hierarchy Process (M-AHP) Model

are not developed and utilized for avalanche susceptibility mapping. Application of the most popular & prominent statistical assessment technique the area under the receiver operating characteristics (ROC-AUC) analysis is missing for the performance validation of the model in avalanche susceptibility mapping.

2.5 Research objectives

The main purpose of this research is modelling and mapping of avalanche hazard using geospatial technology. A number of specific research objectives were identified in the context of geospatial modelling of avalanche hazard are:

- (i) To analyze the terrain and meteorological data of the study area for identification of the various parameters (constant and dynamic parameters) contributing towards avalanche occurrence.
- (ii) Development and implementation of geospatial models/algorithms for avalanche hazard mapping using avalanche occurrence parameters.
- (iii) Proposed geospatial models for avalanche susceptibility mapping are: Probabilistic Frequency Ratio Model, Multi-Criteria Decision Analysis-Analytical Hierarchy Process (MCDA-AHP) Model and Fuzzy-Frequency Ratio (Fuzzy-FR) Model,
- (iv) Evaluating the model's performance in the most appropriate fashion using GIS in combination with statistical tools.

2.6 The process for the development and implementation of the proposed models

2.6.1 Construction of avalanche related database

A. Preparation of avalanche inventory map of documented snow avalanches

- a. In order to obtain a comprehensive and detailed avalanche inventory map, exhaustive field surveys and interpretations are carried out in the avalanche-prone regions with well supported high-resolution satellite imagery and Survey of India (SoI) mapsheets.

B. Generation of vegetation cover map:

- a. Preparation of Landsat 8 OLI satellite image including layers stack, mosaick, sub-set, geo-reference and ortho-rectification.
- b. Preparation of vegetation thematic map followed by normalized difference vegetation index.

C. Generation of avalanche occurrence terrain and meteorological parameters

- a. Preparation of digital elevation model including download and mosaic of the ASTER GDEM tiles.
- b. Generation of avalanche occurrence terrain parameters such as slope, aspect, curvature, elevation and terrain roughness by using the spatial analyst tool.
- c. Generation of avalanche meteorological parameters such as snow depth, air temperature, wind speed/direction and relative humidity

D. Generation of thematic layers

- a. Reclassification and generation of thematic layers from slope, aspect, curvature, elevation and terrain roughness parameters generated from ASTER GDEM data.
- b. Derivation of threshold values for reclassification by calculating the relationship between avalanche occurrence parameters and documented avalanche occurrence data.

2.6.2 Geospatial modelling and mapping

A. Frequency ratio model:

- a. Calculation of FR coefficients of each class of avalanche occurrence thematic layers
- b. Assign FR coefficients to each class of avalanche occurrence thematic layers
- c. Spatial overlay analysis of avalanche occurrence thematic layers to generate avalanche susceptibility index
- d. Generation of avalanche susceptibility map (zone-wise) by the reclassification of the avalanche index by applying (Jenks, 1967) natural break method

B. Multi-Criteria Decision Analysis-Analytical Hierarchy Process (MCDA-AHP) Model:

- a. Assign ratings to each class of the avalanche occurrence thematic layers
- b. Construction of pairwise comparison matrix
- c. Calculation of weight values and consistency ratio
- d. Assignment of weight value to each class of the avalanche occurrence thematic layers
- e. Spatial overlay analysis of avalanche occurrence thematic layers to generate avalanche susceptibility index
- f. Generation of avalanche susceptibility map (zone-wise) by the reclassification of the avalanche index by applying (Jenks, 1967) natural break method

C. Fuzzy Frequency Ratio (Fuzzy-FR) Model:

- a. Calculation of FR coefficients of each class of avalanche occurrence thematic layers
- b. Calculate the fuzzy membership value of each class of the avalanche occurrence thematic layers
- c. Representation of fuzzy membership values into each class of the avalanche occurrence thematic layers
- d. Fuzzification of each raster avalanche occurrence factor
- e. Fuzzy overlay analysis [Fuzzy OR (Max) Operator] of avalanche occurrence thematic layers to generate avalanche susceptibility index
- f. Generation of avalanche susceptibility map (zone-wise) by the reclassification of the avalanche index by applying (Jenks, 1967) natural break method

2.6.3 Evaluating the models' performance in the most appropriate fashion using GIS in combination with a statistical tool

- A. ROC-AUC Technique: Application of the area under the receiver operating characteristics (ROC-AUC) analysis for validation of the avalanche susceptibility maps generated from Probabilistic Frequency

Ratio Model, Multi-Criteria Decision Analysis-Analytical Hierarchy
Process (MCDA-AHP) Model and Fuzzy Frequency Ratio (Fuzzy-FR)
Model

3. STUDY AREA AND DATA SET

3.1 Study Area

Lahaul-Spiti region of Himachal Pradesh, Indian Himalaya, is selected for implementation of the proposed geospatial models because this region is frequently affected by avalanche activities and documented avalanche locations dataset is available for a few parts of this region. The study area is among the high avalanche prone regions in the Western Himalaya and most parts of the Lahaul region are prone to avalanche. The study area's spatial extent is $76^{\circ} 21' 29.73''$ to $77^{\circ} 47' 57.44''$ East Longitude and $32^{\circ} 05' 30.09''$ to $33^{\circ} 15' 20.85''$ North Latitude of highly complex mountainous zone having a mean altitude of 4701 m (Figure 3.1).

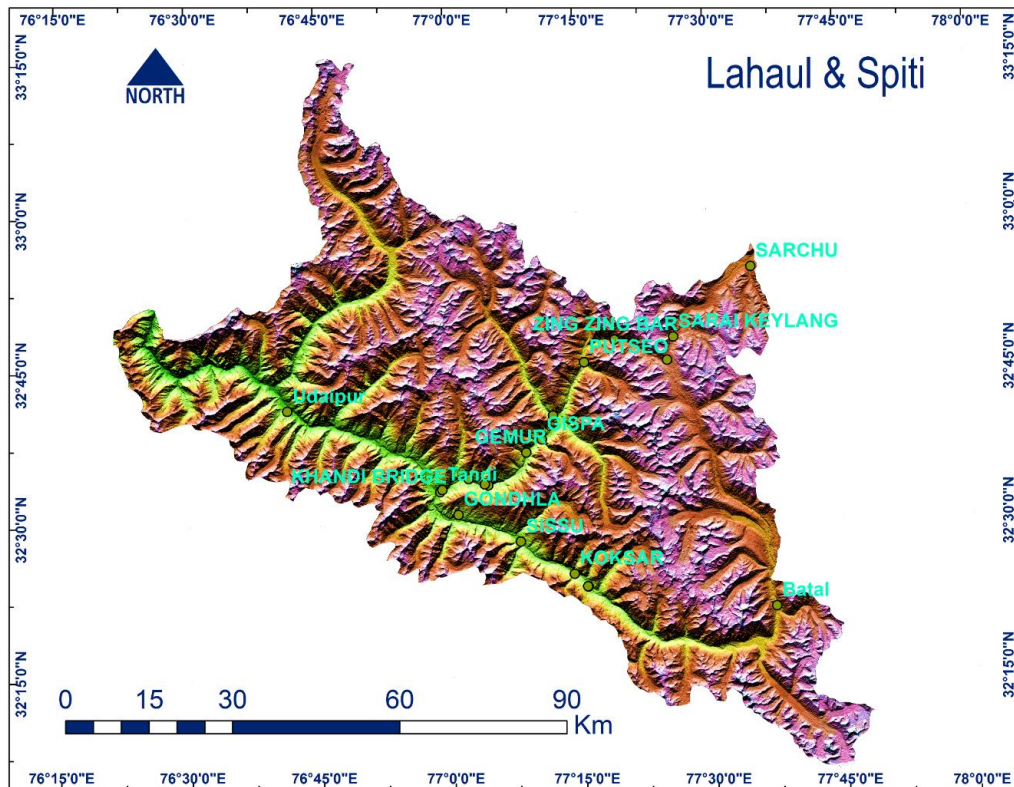


Figure 3.1: Location map of the study area.

An area of approximately 6651.17 Km² covers and encloses the Lahaul Spiti district. The study area is mostly covered by the snow in late winter season. In late summer, all the seasonal snow melted and the ground features are exposed with permanent snow or ice cover areas. An overview map of the area affected in

the western Himalayan region is presented in [figure 3.2](#). Topographical attributes of the study area are given in [table 3.1](#).

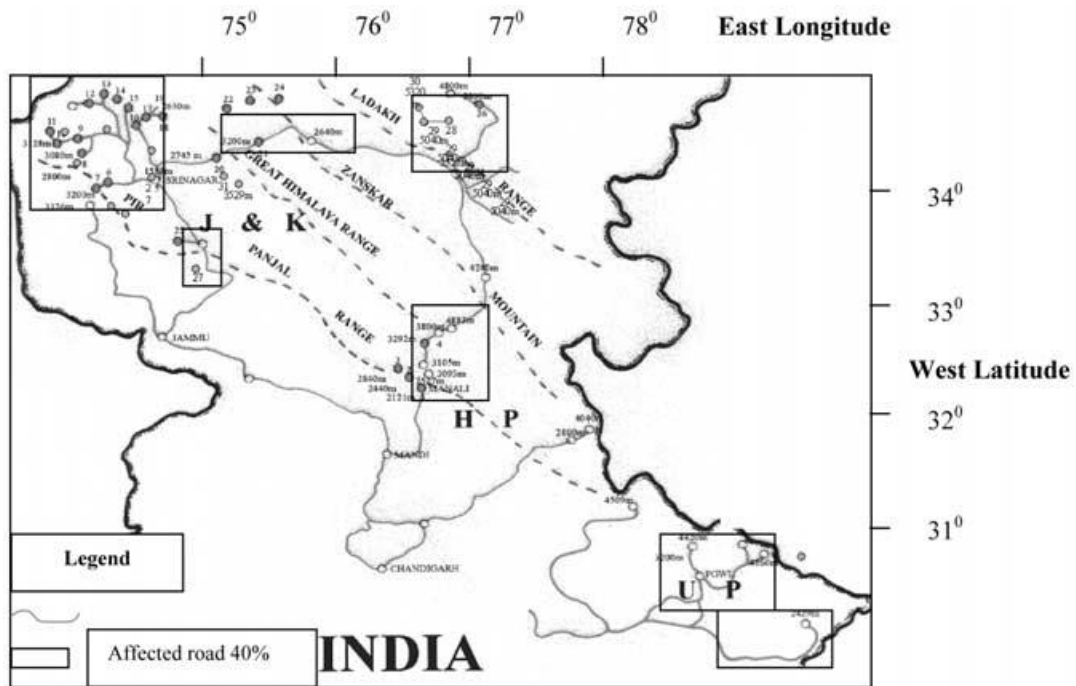


Figure 3.2: Avalanche affects 40 percent of various road axes in the western Himalayan region.

Table 3.1: Geographical attributes of the study area.

Geographic information	Study area
Topography	Very high complex and rugged mountainous terrain in NW Himalaya
Location	Longitude :76° 21' 29.73" to 77° 47' 57.44" E Latitude :32° 05' 30.09" to 33° 15' 20.85" N
Area	6651.17 Km ²
Elevation	
1. Range	2302 m – 6443 m
2. Mean	4701.8 m
3. Standard deviation	694.6 m
Slope	
1. Range	0° – 83.05°
2. Mean	28.83°
3. Standard deviation	14.31°

3.2 Data Used

Development of a model for avalanche susceptibility mapping required the identification of most prominent avalanche occurrence factors and collection of the related dataset. The analysis of avalanche susceptibility areas requires data of known avalanche locations and conditions (Pistocchi and Notarnicola 2013). Factually, the region based avalanche susceptibility mapping should be practical and appropriate. Snowpack data is sometimes essential to understand the snowpack stress for avalanche modelling (McClung and Schaerer 2006). But, the regular snowpack data of large area is generally not available because the conditions of snowpack vary significantly with time. In geospatial modelling, the snowpack may be used as an indicator of avalanche mapping. Otherwise, snow conditions are generally dependent on the morphological parameters of avalanche release areas. Various morphological parameters are elevation, slope, aspect, curvature, terrain roughness and vegetation cover. Therefore, we limited our consideration of these six parameters (Table 3.2).

Schweizer et al. (2003) stated three types of parameters (1. Terrain, 2. Meteorological, and 3. Snowpack) on which avalanche occurrence depends. Amongst these three parameters, Terrain is the most influencing parameter, and easier to map due to its temporal stability (Snehmani et al. 2013). In this study, ASTER GDEM V2 (30m spatial resolution) has been utilized for the extraction of terrain parameters because as per the recent studies by Singh et al. (2016a and 2016b) ASTER GDEM V2 is the most accurate DEM amongst all the freely available moderate resolution DEMs for this region.

3.2.1 Terrain data

The six avalanche occurrence parameters: elevation, slope, aspect, curvature, terrain roughness and vegetation-cover (NDVI) were obtained from the ASTER GDEM V2 (30 m) (Table 3.2) and Landsat 8 OLI imagery (30 m × 30 m). The attributes of Landsat 8 OLI bands are shown in Table 3.3.

Table 3.2: Occurrence parameters used in geospatial modelling of avalanche susceptibility, spatial resolution, and data sources.

No.	Parameter	Spatial resolution	Source
1	Slope	30 m × 30 m	ASTER GDEM
2	Aspect	30 m × 30 m	ASTER GDEM
3	Curvature	30 m × 30 m	ASTER GDEM
4	Elevation	30 m × 30 m	ASTER GDEM
5	Terrain roughness	30 m × 30 m	ASTER GDEM
6	Vegetation	30 m × 30 m	LANDSAT 8 OLI IMAGE

Table 3.3: Specifications of Landsat 8 OLI data

No.	Band	Spatial resolution (m)	Wavelength (μm)
1	Band 1-Blue	30	0.43-0.45
2	Band 2-Blue	30	0.45-0.51
3	Band 3-Green	30	0.53-0.59
4	Band 4-Red	30	0.64-0.67
5	Band 5-Near-infrared (NIR)	30	0.85-0.88
6	Band 6-Shortwave infrared (SWIR)	30	1.57-1.65
7	Band 7-Shortwave infrared (SWIR)	30	2.11-2.29
8	Band 8-Panchromatic (PAN)	15	0.50-0.68
9	Band 9-Cirrus	30	1.36-1.38
10	Band 10-Thermal infrared (TIR)	100	10.60-11.19
11	Band 11-Thermal infrared (TIR)	100	11.50-12.51

3.2.2 Meteorological data

Snow meteorological data (ambient temperature, wind speed, relative humidity and snow depth) were collected from three observatory sites - Manali, Dhundi (located in the Pir Panjal range) and Patsio (located in great Himalayan range) and also from two AWS (Patsio and Beaskund). Upper Air station (RadioSonde) temperature profile data of Manali station was used for the computation of the average lapse rate during the study period. Wind data has been used for wind speed/direction map generation. Extensive field data of avalanche occurrence of the registered avalanche sites of study area of 25 years have been used for analysis weights and rating of causative factors.

A detailed description of terrain and meteorological dataset and factors affecting the avalanche occurrence is presented in next chapter 4

4. INFLUENCE OF TERRAIN AND METEOROLOGICAL PARAMETERS IN AVALANCHE OCCURRENCE

4.1 Analysis of avalanche occurrence terrain parameters

Susceptibility mapping of avalanche is very difficult and complex because several factors are influencing an avalanche. The factors influencing the avalanche behaviour including meteorological, snowpack, terrain attributes, natural triggers, and social activity (Selçuk, 2013; Bühler et al., 2013). Some of the various meteorological factors contributing to avalanche hazard as snowfall, snowpack, wind, temperature, raining, and precipitation intensity. Snowpack structure is the result of succeeding snowfall events and its stability depends upon the cohesion and bonds between snow layers (Schweizer et al., 2003), vibrations and noise due to anthropogenic activity. The meteorological factors and snowpack structure are dynamic in nature and easily influenced by frequently changing weather conditions. However, the terrain factors are constant and suitable for avalanche susceptibility mapping for a long duration. These factors include elevation, slope, aspect, and curvature. In order to prepare an avalanche susceptibility map, the FR model incorporates terrain factors and vegetation cover. The following subsections provide the details of each factor.

4.1.1 Slope

Terrain slope is an essential factor affecting avalanche occurrence (Maggioni and Gruber 2003; Ghinoi and Chung, 2005). Statistically, it is generally accepted that most of avalanches activities occurred in a region where the slope angle ranges from 25° to 45° and rarely at the slope angle less than 25° (McClung and Schaerer, 2006; Selçuk, 2013). In Indian Himalaya, the majority of avalanche accidents took place in slopes angle between 30° and 45° (Ganju et. al., 2002). In common weather conditions, the snowpack below 25° slope angle remains stable and shear stress instigated by gravity is not sufficient to the occurrence of an avalanche (Ancy 2009). The avalanche activity on the slope angle of more than 45° is minor because snow accumulation on steep slopes is very limited and not well anchored to slide. The slope of the study has been extracted from the ASTER GDEM V2. Subsequently, extracted slope values were grouped

into 4 categories, such as 0° - 12°, 12° - 28°, 28° - 45° and above 45° (Figure 5.2). While choosing the four slope classes, statistics presented in Table 5.1 was considered to modify the classes given by Albrecht et al. (1994) and adopted by Selçuk (2013). As in present study, none of the avalanche accident was observed in the area where the slope angle is less than 12° (Table 5.1), so instead of using 0°-10° threshold as considered by Selçuk (2013) for no avalanche class, threshold limit 0° - 12° was used. Threshold limits for the rest of the slope classes were taken as considered by Selçuk (2013). The slope category ranges from 28° - 45° has a 78% documented avalanche slope, followed by 18% for 12° - 28°. The slope class less than 12° shows no avalanche clues in the past.

$$Slope = ATAN(\sqrt{[(dz/dx)^2 + (dz/dy)^2]}) \times 57.29578$$

$$Aspect = 57.29578 \times ATAN^2\left(\left[\frac{dz}{dy}\right] - \left[\frac{dz}{dx}\right]\right)$$

$$Curvature = -2(D + E) \times 100$$

$$roughness = 1 - \frac{\sqrt{(\sum x)^2 + (\sum y)^2 + (\sum z)^2}}{n}$$

4.1.2 Aspect

Aspect is a principal factor in avalanche occurrence (Ghinoi and Chung, 2005). Aspect direction in snow-covered terrain is direct, influenced by the heat radiation and contributed a significant effect on the stability of the snowpack. Aspect with respect to wind and sun is a significant factor in the release of avalanches. While sunny slopes stabilize faster after brief instability, the shady ones remain in instability for a longer duration. Similarly, leeward slopes become dangerous, with the loading of additional snow and windward slopes stabilize fast with the depletion of snow. The past avalanche accidents in Indian Himalaya have shown that northern, eastern and southern slopes contribute almost equally in the release of avalanches (Ganju et. al., 2002). Since the dominant wind, direction during winter is western; as a result, southern, eastern and northern slopes get additional drift snow. The past avalanche accidents revealed that NE-SE aspects had produced maximum avalanche accidents contributing by about 35% of the total avalanche accidents reported so far in Indian Himalaya (Ganju et. al, 2002). In the

present aspect values were extracted from ASTER GDEM V2 and further reclassified into nine principal categories (Figure 5.2). Six out of nine aspect categories showed significant association with avalanche occurrence locations such as north, northeast, south, east, southeast and southwest, respectively (Table 5.1).

4.1.3 Elevation

The elevation is an important terrain factor in avalanche occurrence because snowpack varies with the elevation due to varying snowfall, wind and temperature (Guy and Birkeland, 2013; Selçuk, 2013). The wind speed increases at high elevation and helps in increasing the snow sliding. Higher elevation area receives heavy snowfall most of the time in the winter season and thus increasing the avalanche activity. The conditions on higher elevation areas are suitable for avalanche occurrence because this area is generally exposed to wind, sun, different snowpack conditions and minimum forest/vegetation cover (McClung and Schaerer, 2006). The avalanche activity at a lower elevation is minor because the snow at minor elevation often melts and changes to rain. The topographical characteristics of the Lahaul & Spiti region are seemingly favorable for avalanches occurrence. Lahaul & Spiti region has a complex topography. The elevation of Lahaul & Spiti region ranges from 2302 m to 6443 m. In Western Indian Himalaya, most of the avalanches generally start at the elevation ranges from 2700 m and terminate at about 6000 m. In Lahaul & Spiti region, 98% of total documented avalanche sites have existed between the elevation ranges from 3200 m to 5800 m. The elevation values were reclassified into 8 categories as shown in Figure 5.2. Table 5.1 contains attributes of all the elevation classes. The elevation classes of less than 2800 m and above 5800 m showed no documented avalanche occurrence/activity over the study area in the past. While the elevation class of 3800 m to 4300 m has a maximum number of avalanche activities.

4.1.4 Curvature

Curvature has deemed an important terrain factor in avalanche occurrence (Ghinoi and Chung, 2005). Generally, the convex slope is highly contributing to the avalanche release area than flat and concave (Yilmaz, 2007; Nefeslioglu et al., 2013). The areas of a sudden change in the curvature also contribute to the release

of avalanches. A bowl-shaped formation zone holds more snow before releasing it, thus causing more destruction downhill than a flat open slope. Similarly, the shape of the crest line determines the pattern of snow accumulation at the avalanche formation zone. The curvature values were derived using ASTER GDEM V2 and reclassified into three categories, such as concave, convex and flat (Figure 5.2). Convex curvature showed a maximum relationship with documented avalanche locations (43.78%) than concave (33.48%) and flat (22.75%) curvature (Table 5.1).

4.1.5 Vegetation cover

Vegetation cover is also significant avalanche occurrence factor. Avalanches generally get released over barren slopes. Dense trees coverage holds the snow and protects against snow avalanches (Selçuk, 2013). In general, vegetation cannot stop the snow avalanches, but highly vegetation coverage controls the volume of snow contribution to the release of an avalanche. Grassy slopes release avalanches differently than those with shrubs. Landsat 8 images have been utilized for the preparation of a vegetation cover map. NDVI method was used for the extraction of vegetation cover values. The NDVI values were further reclassified into 4 categories such as <0.1, 0.1-0.2, 0.2-0.3 and >0.4 (Figure 5.2). The vegetation cover increases with the increase in the values of NDVI. The vegetation-cover is dense when the NDVI values are greater than 0.2. Snow avalanches showed a significant relationship with <0.1 NDVI values because maximum avalanches have occurred (83.26%) in this category (Table 5.1).

4.1.6 Terrain roughness

Terrain roughness is a significant avalanche occurrence component. Terrain roughness reports a rugged and sporadic surface, which blocks the snowpack in the downward movement and prevents the formation of a consistent weak layer, important for fracture in the snowpack (McClung, 2001; Schweizer et al., 2003). The terrain roughness is calculated using the ruggedness method of Sappington (2007). The study area with ruggedness values are classified into three classes of roughness (Figure 5.2). The spatial relationship between each class of terrain roughness with avalanche occurrences is shown in Table 5.1.

4.2 Analysis of avalanche occurrence meteorological parameters

4.2.1 Air Temperature Map

(a) Lapse rate (λ) calculation

Upper air data from three stations was used to calculate the temperature lapse rate in the study area for the same day. RadioSonde data gives the vertical profile of air temperature (t °c) in the atmosphere with height (z km). So, the lapse rate can be determined by this equation ($\lambda = dt/dz$, °c/km). Figure 4.1. Shows a typical vertical profile.

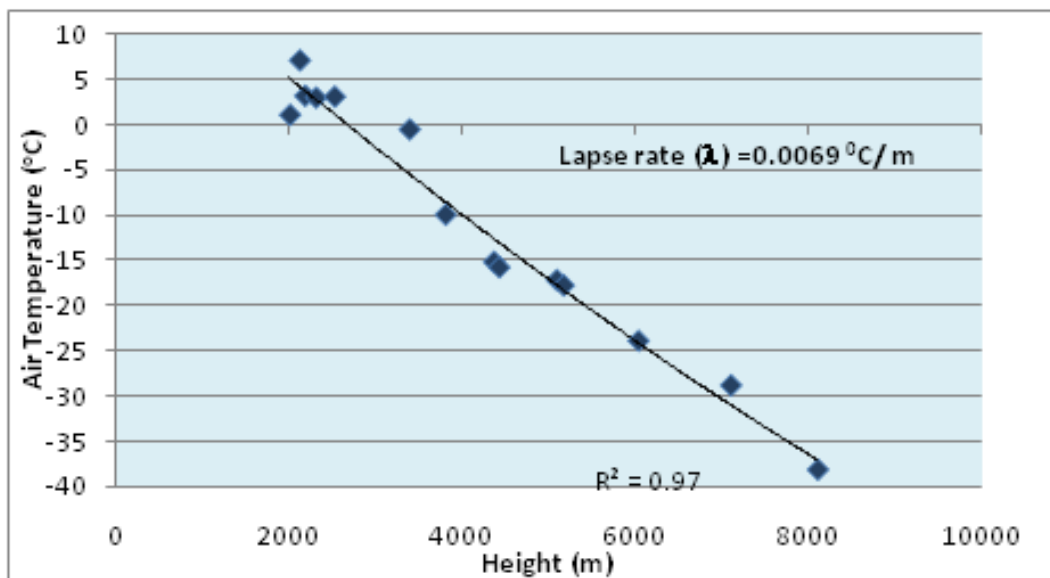


Figure 4.1: Profile of air-temperature of 25-January-2018.

(b) Generation of Temperature Map Using Single Point Interpolation Technique

Variation of temperature with the altitude (one point temperature map) of the study area was calculated from the data of each station separately using the lapse rate equation, $T_p = T_0 + \lambda(h_p - h_0)$, where T_0 and T_p are the known temperature at an altitude of h_0 and derived temperature at an altitude of h_p respectively. This equation makes the use of λ calculated in the previous step and a high-resolution DEM was to calculate elevation variation ($h_p - h_0$), where T_0 and T_p are the known temperature at an altitude of h_0 and derived temperature at an altitude of h_p respectively.

(c) Calculating the Distances and Inverse Distance Weights

The euclidean distance of all the pixels from each station is calculated. If the coordinates of a pixel are (x, y, z) and the coordinates of the station as (x_s, y_s, z_s) then Euclidean distance between these two is computed using the equation, $\sqrt{((x_s - x)^2 + (y_s - y)^2 + (z_s - z)^2)}$. The above equation is used while generating the distance maps for each station. These distances were normalized in the range of 0.0 – 1.0 in such a way that the sum of all three distances (distance of any pixel or point from all three field station) is 1.0. These normalized distance maps were finally converted into the inverse distance weights ranging from 1.0 - 0.0. All three distances weight maps are shown in [figure 4.2](#).

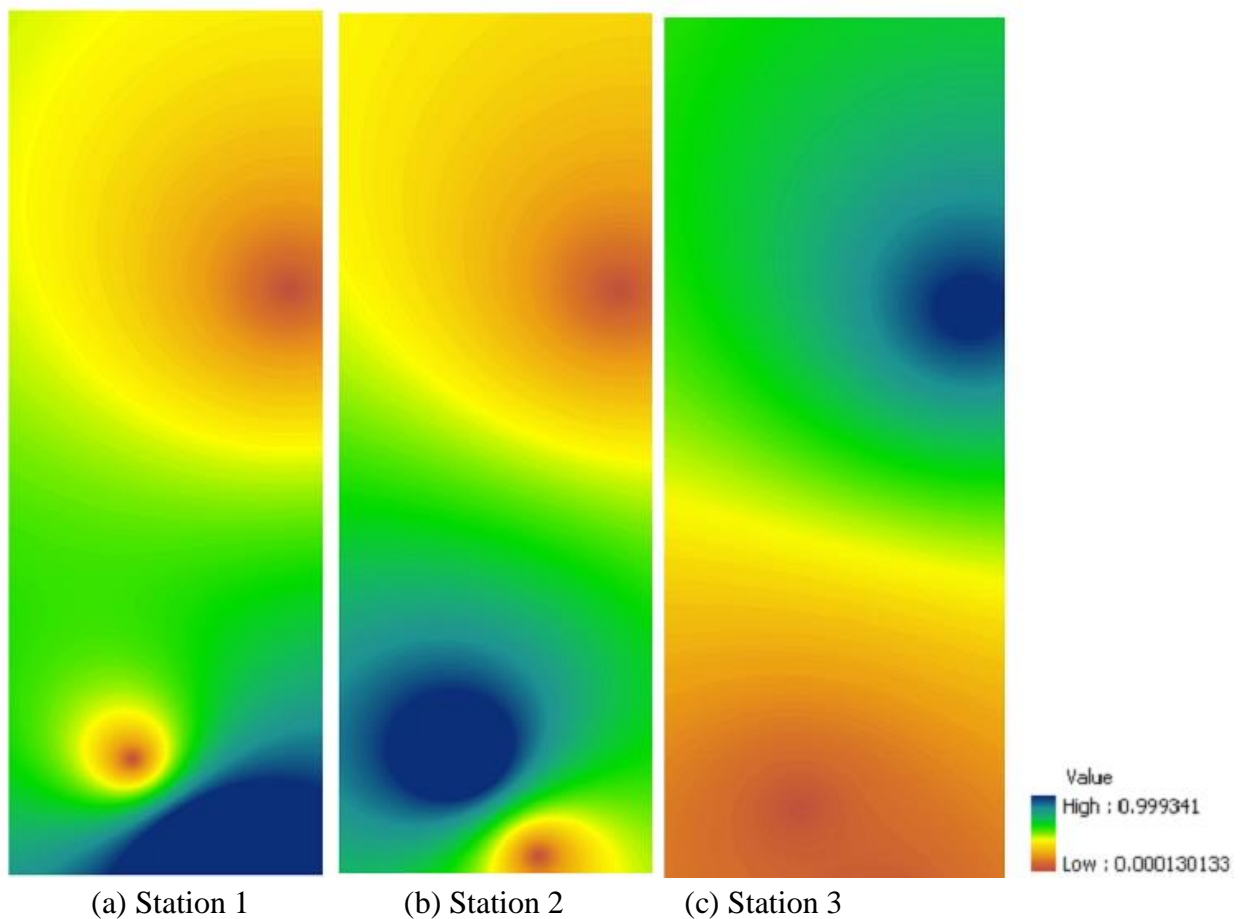


Figure 4.2: Distance weights of the different stations

(d) Generating Weighted Temperature Map

Weighted temperature map was generated by the following equation.

$$T_{\text{weightedmap}} = T_{\text{map1}} * W_{\text{map1}} + T_{\text{map2}} * W_{\text{map2}} + T_{\text{map3}} * W_{\text{map3}}$$

This is the sum of the product of one point temperature map and inverse distance weights for all three stations. Where $T_{\text{weightedmap}}$ is final temperature map and T_{map1} , T_{map2} and T_{map3} are one point temperature map of three stations and W_{map1} , W_{map2} and W_{map3} are weight maps for these stations respectively. Weights at any point must satisfy the condition; $W_{\text{map1}} + W_{\text{map2}} + W_{\text{map3}} = 1.0$.

The flow chart of the methodology adopted is shown in [figure 4.3](#). The air temperature map of the 25 January 2018 generated using this model is shown in [figure 4.6 \(a\)](#).

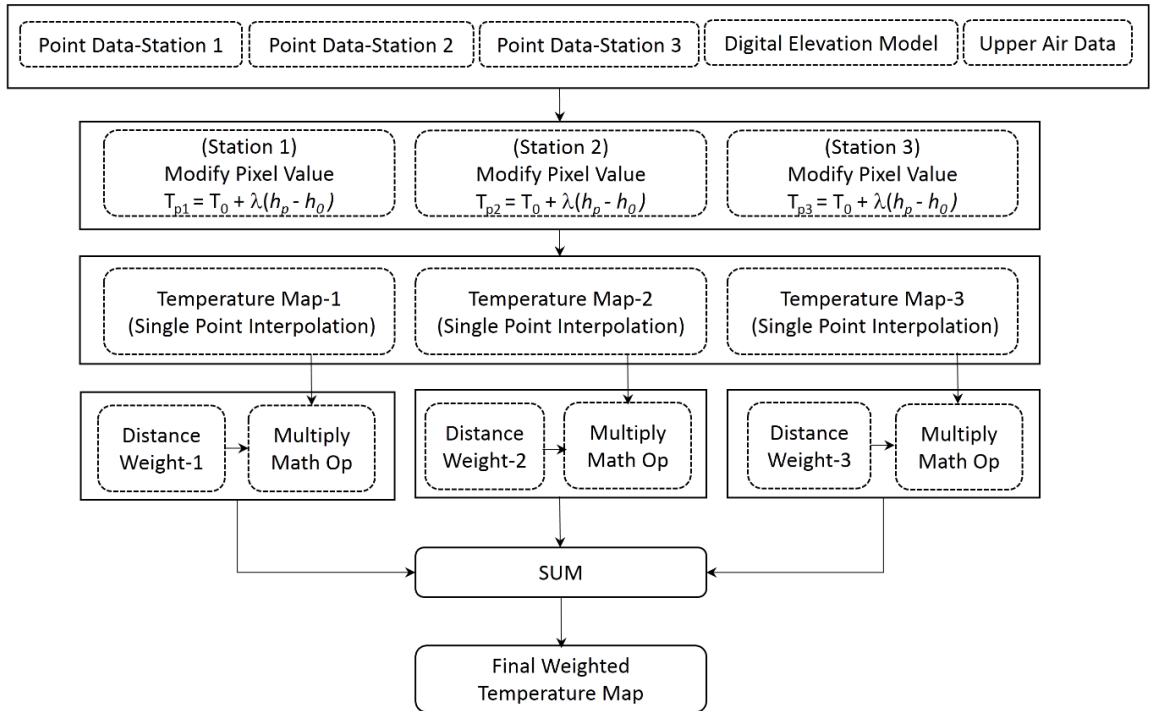


[Figure 4.3](#): Flow chart of the temperature map generation

4.2.2 Relative Humidity Map

(a) Calculating dew-point temperature:

The elevation adjustment has been taken place by converting the relative humidity ($RH\%$) into dew-point temperature Td ($^{\circ}\text{C}$) due to the linear variation of

dew-point temperature with elevation. Various steps followed for calculating the dew-point temperature as:

Step 1. Calculated saturation vapor pressure ($e_s(Pa) = a \exp\left[\frac{bT}{c+T}\right]$) by using air-temperature T ($^{\circ}\text{C}$) for water $a = 611.21 \text{ Pa}$; $b = 17.502$; $c = 240.97 \text{ }^{\circ}\text{C}$ and for ice $a = 611.15 \text{ Pa}$; $b = 22.452$; $c = 272.55 \text{ }^{\circ}\text{C}$ (Buck 1981).

Step 2. The vapor pressure [e (Pa)] was calculated by using ($\text{RH}\%$) of the station, where $\text{RH}(\%) = 100 \left[\frac{e}{e_s}\right]$

Step 3. The dew-point temperature is finally calculated as $T_d = \left[\frac{c \ln(e/a)}{b - \ln(e/a)}\right]$.

(b) Lapse rate (λ) calculation

The lapse rate λ_d ($^{\circ}\text{C m}^{-1}$) of dew-point temperature was calculated as $\lambda_d = \lambda_0 \left[\frac{c}{b}\right]$, where (λ_0) is the vapor pressure coefficient. The vapor pressure coefficient is changing every month (Kunkel 1989). The vapor pressure coefficients for the months of January and February are reported as 0.41 and 0.42.

(c) Dew-point temperature map by using single-point interpolation

A single-point interpolation technique was used to obtain a dew-point temperature map. The same procedure followed, which was applied in the generation of the air-temperature map in section 4.2.1 (b). At here, the temperature was dew-point temperature and the lapse rate was dew-point lapse rate.

(d) Weighted Dew-point Temperature Map

The same procedure has been applied to generate the air-temperature map. The figure 4.4 represents the methodology and figure 4.6 (b) is the model output for the date 25-January-2018.

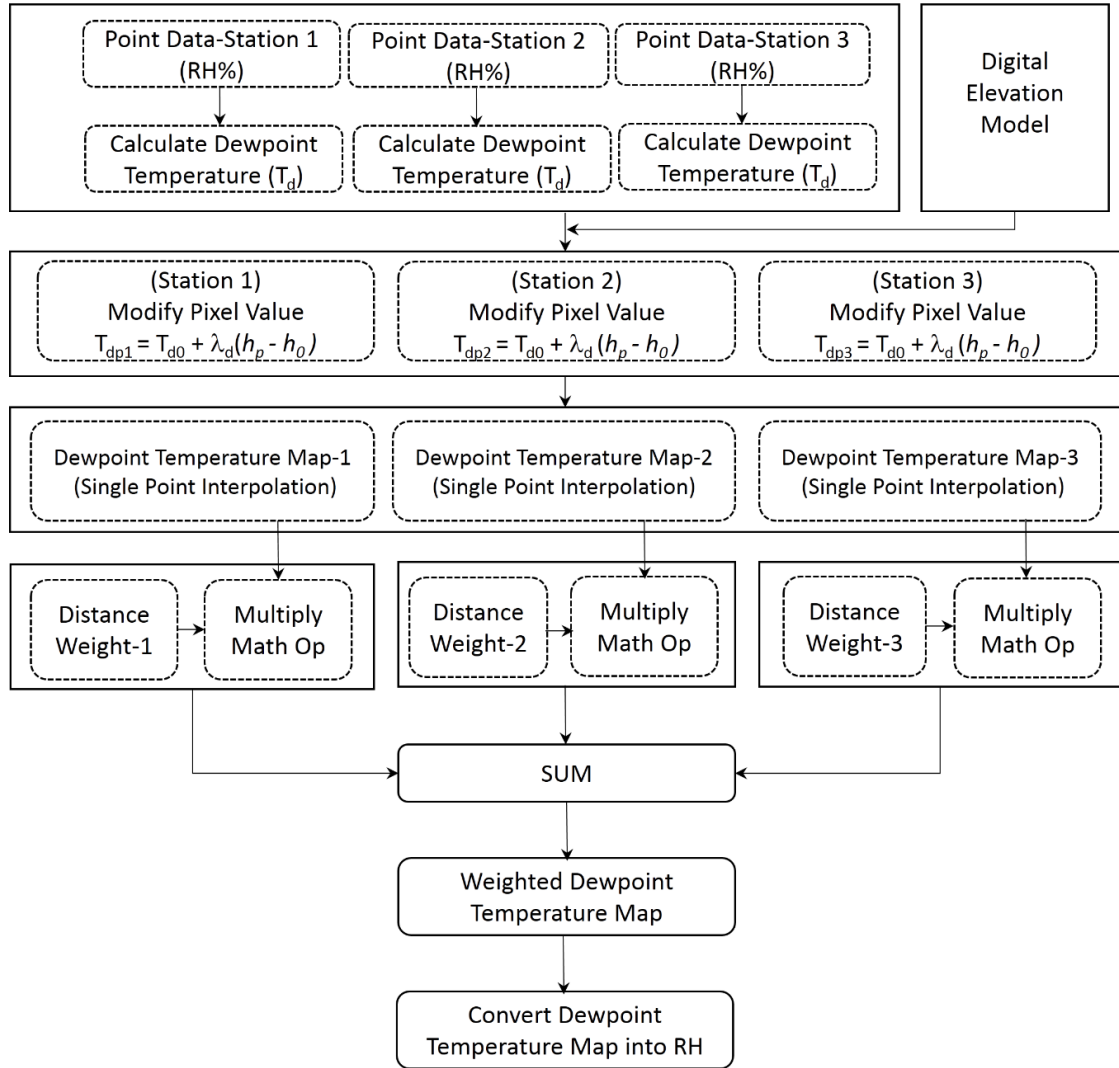


Figure 4.4: Flow chart to generate RH map

4.2.3 Snow Depth Map

(a) Snow depth map by using single-point interpolation

Snow depth, P_p (cm) at an elevation of h_p , is computed from $H_p = H_0 \left[\frac{1+\mu(h_p-h_0)}{1-\mu(h_p-h_0)} \right]$, where P_0 is the station snow depth, h_0 is the station elevation, and μ (km^{-1}) is a snow depth adjustment factor. The value of the μ was found 0.65 for the Pir Panjal range and for the greater Himalayan range, it was 0.52 (January and February) and 0.32 (March). These values of the μ were calculated from the snow depth data of the previous six years.

(b) Weighted Dewpoint snow depth Maps

The same procedure has been applied to generate the air-temperature map. The methodology for generation of snow-depth map is given in figure 4.5 and the snow-depth map of 25 January 2018 is given in figure 4.6 (c).

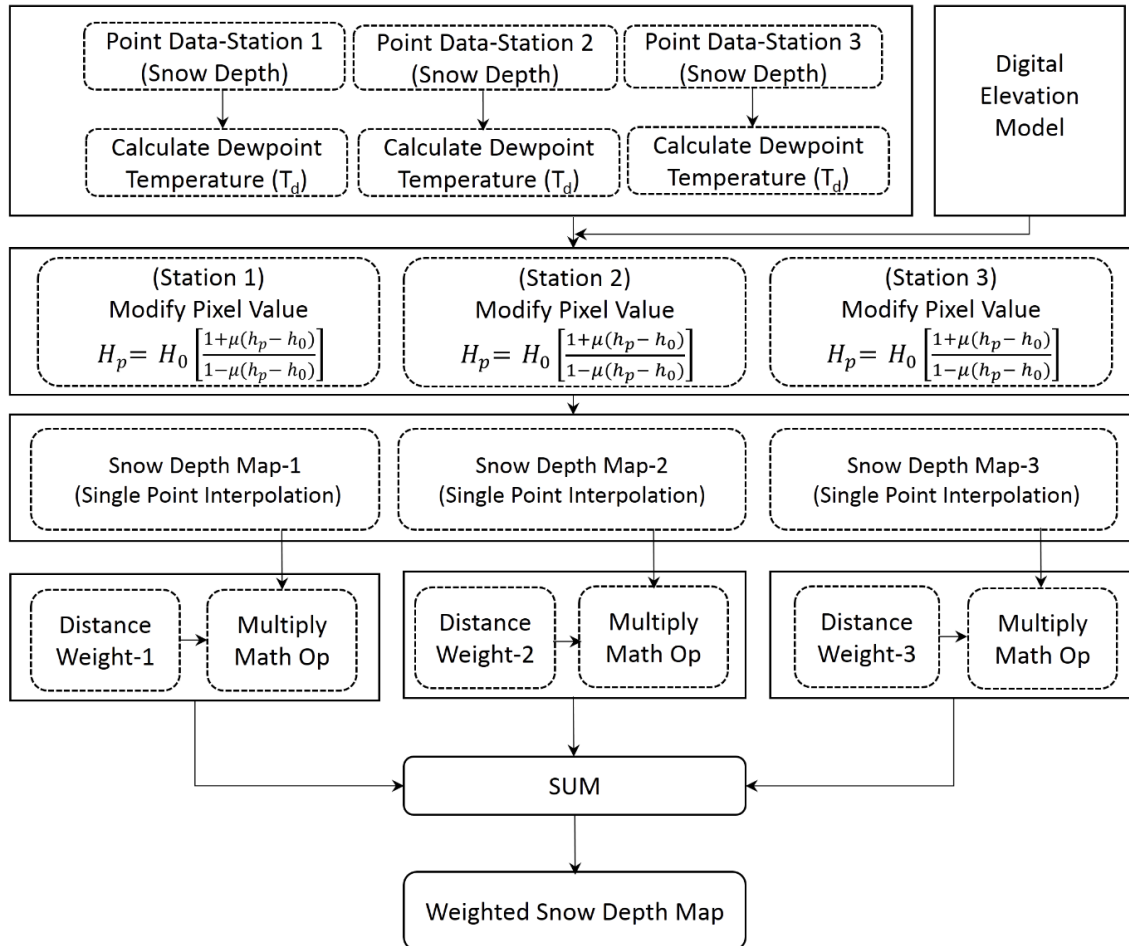


Figure 4.5: Snow depth map preparation workflow

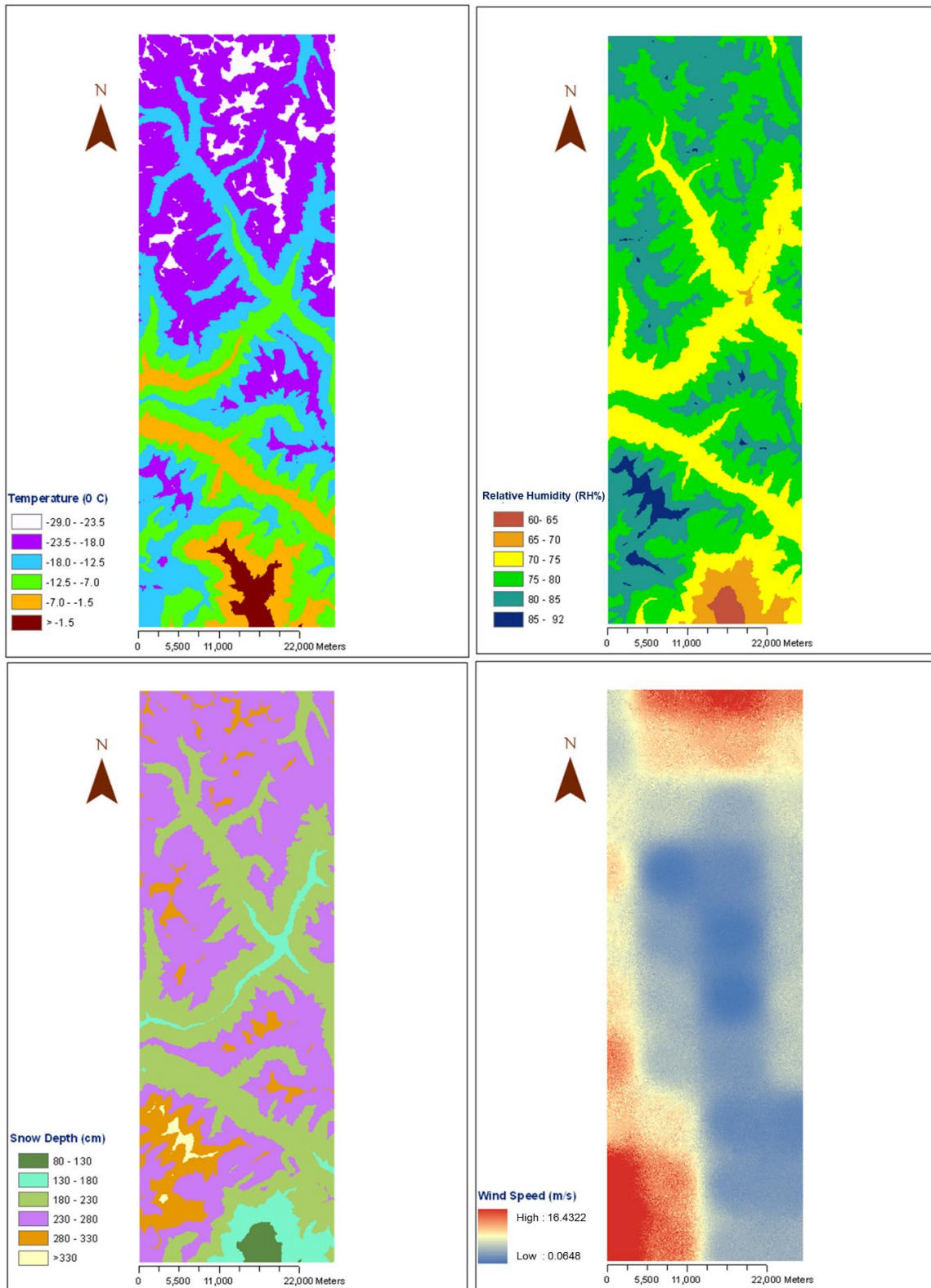


Figure 4.6: (a) Air-Temperature (b) Relative-Humidity (c) Snow-Depth and (d) Wind-Speed maps

4.2.4 Wind Speed and Direction Map

(a) Generating interpolated wind speed/direction map

To map the wind over a domain, the spatially distributed values of the wind components (u , and v) at the grid of 7 km X 7 km from the automatic weather stations (AWS) have been used. These u and v components were then independently interpolated using IDW. The interpolated values of u and v were converted into speed and direction using the following equations as:

$$w = \sqrt{[u^2 + v^2]} \text{ and } \theta = \frac{3\pi}{2} - \tan^{-1}(v/u) \text{ respectively.}$$

(b) Topographic correction of wind data:

Wind data is topographically modified using slope, aspect and curvature to adjust the wind speed and direction. Terrain parameters such as slope (β), curvature (Ω_c) and aspect (ξ) data was used for topographical correction.

The slope in wind direction is defined as:

$$\Omega_s = \beta \cos(\theta - \xi)$$

Slope (Ω_s) and curvature (Ω_c) are scaled by simulation for topographic correction of wind as $-0.5 \leq \Omega_s \leq 0.5$ and $-0.5 \leq \Omega_c \leq 0.5$

Modification of the wind speed has been done by a weighting factor W_w as:

$$W_w = 1 + \gamma_s \Omega_s + \gamma_c \Omega_c$$

Where, γ_s is a slope and γ_c is a curvature weight. The value of weights is ranging from 0 to 1.

The value of Ω_s and Ω_c have to establish as:

$$\Omega_s + \Omega_c = 1$$

The γ_s and γ_c weights are used as:

$$\gamma_s = \gamma_c = 0.5$$

Finally, the terrain modified wind speed is calculated using the equation

$$W_t(ms^{-1}) = W_w \times W.$$

Diverting factor θ_d for modification of wind direction is as:

$$\theta_d = -0.5\Omega_s \sin[2(\xi - \theta)]$$

The topographic modification of the wind direction is done by adding the diverting factor as:

$$\theta_t = \theta + \theta_d$$

At last, the modified wind direction and wind speed are converted into u and v components. The workflow of the process is given in figure 4.6. Wind rose of all three stations are presented in figure 4.8. Wind maps of wind speed and direction presented in figures 4.6 (d) and 4.8.

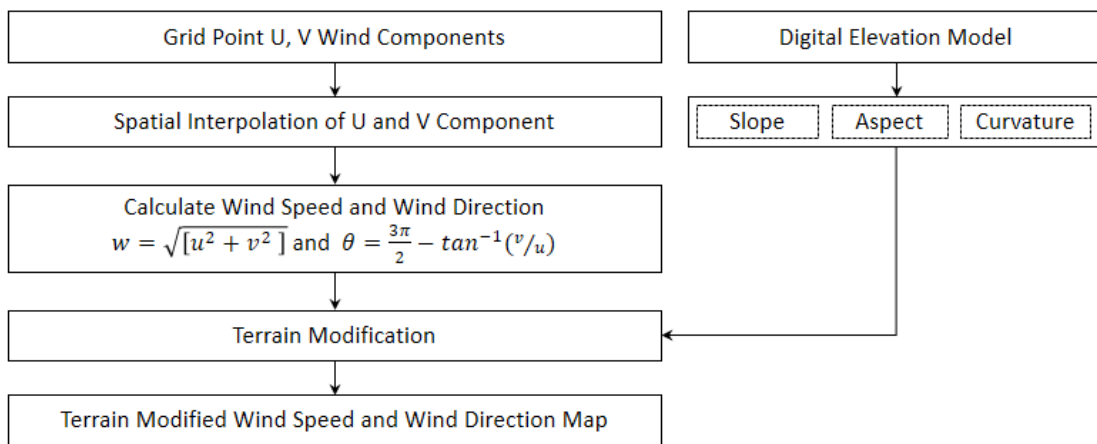


Figure 4.7: Process to generate terrain modified wind speed and direction

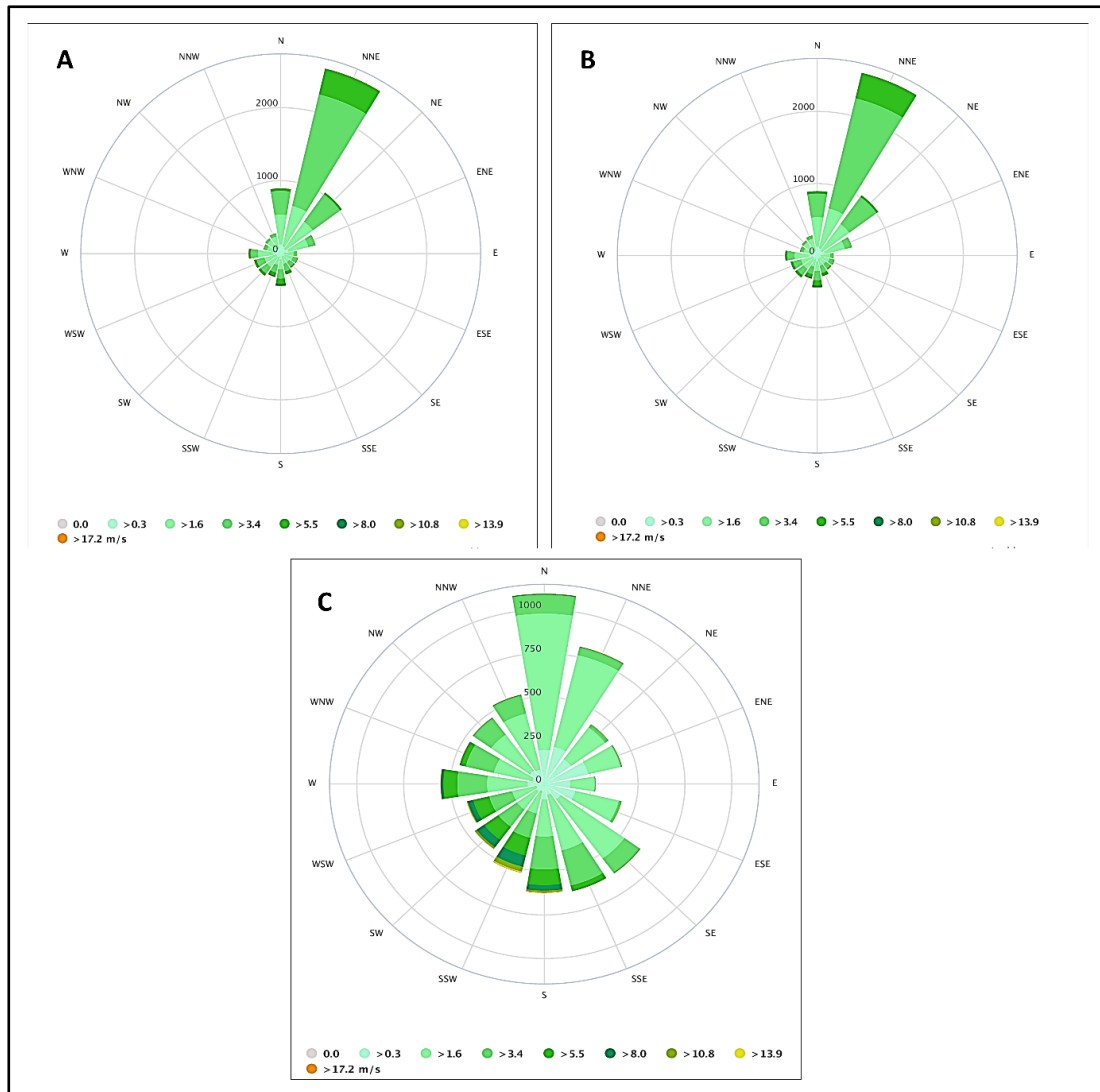


Figure 4.8: Wind rose of three automatic weather stations (AWS)

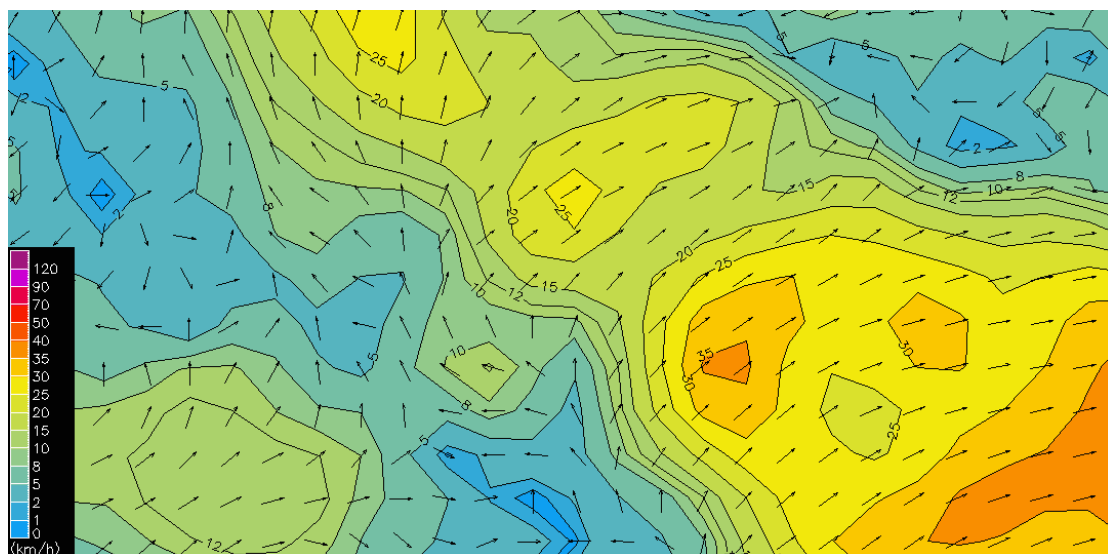


Figure 4.9: Terrain-modified wind speed/direction

Assessment of observed and terrain modified wind speed at stations 1 and 3 is given in figure 4.10

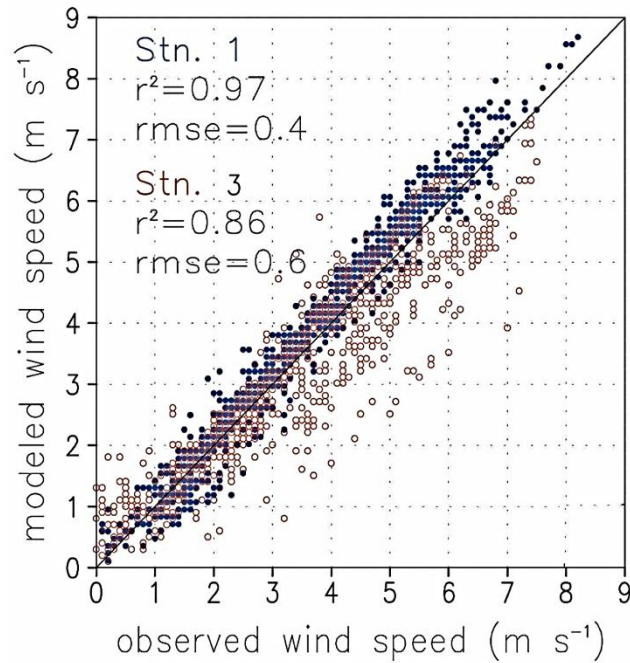


Figure 4.10: Assessment of observed and terrain modified wind speed at stations 1 and 3 with respect to RMSE, r^2 , and correlation coefficient

Frequency distribution of avalanche occurrence with respect to meteorological parameters is given in figure 4.11.

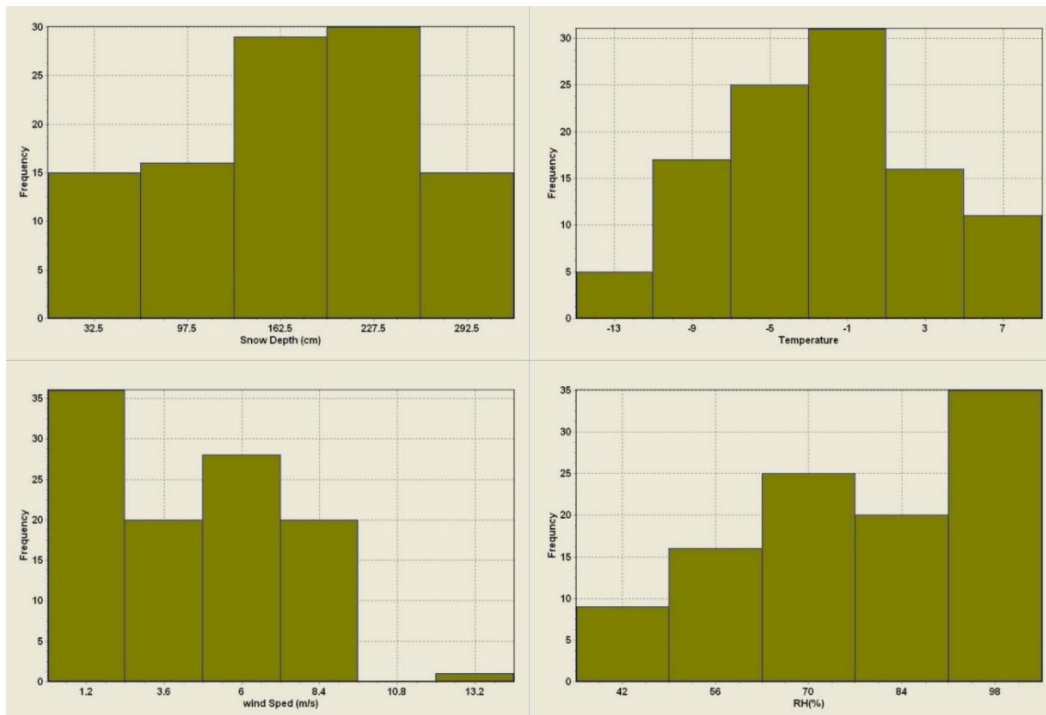


Figure 4.11: Frequency-distribution of avalanche occurrence with respect to meteorological parameters

5. GEOSPATIAL MODELLING AND MAPPING OF AVALANCHE HAZARD

5.1 Rationale

In chapter 4, the influence of terrain and meteorological parameters in avalanche occurrence was highlighted. Geospatial models for potential release area mapping of avalanches which integrates the terrain and meteorological parameters for generation of avalanche hazards map are presented in this chapter. Various terrain parameters such as slope, aspect, curvature, elevation, terrain roughness, and ground cover with additional meteorological parameters such as snow depth, air temperature, wind speed/direction and relative humidity are used for integration in the geospatial models. The detailed methodology design, modelling and the workflow for the mapping of avalanche hazard are explained. The detailed methodologies adopted for the modelling and mapping of the avalanche hazard are given in the next sections. In the first part of the methodology, snow avalanche occurrence related datasets have been gathered and transformed into a database including topographical factors and documented data of past avalanche events. An avalanche inventory map was prepared; subsequently, the avalanche affecting factors were analyzed and reclassified into categories as per the required specification of the proposed geospatial models. The proposed geospatial models for the avalanche hazard mapping such as Probabilistic Frequency Ratio Model, Multi-Criteria Decision Analysis-Analytical Hierarchy Process (MCDA-AHP) Model and Fuzzy Frequency Ratio (Fuzzy-FR) Model are developed applied and discussed in the present study. This chapter is dividing into the sections as: preparation of avalanche inventory map, analysis of avalanche occurrence factors & generation of thematic GIS layers, avalanche susceptibility mapping, validation, results & discussion.

5.2 Preparation of Avalanche inventory map

The first and main fundamental part of the avalanche susceptibility mapping is to acquire the avalanche occurrence data. The scenario of avalanche occurrence in the past and present is the source to the prediction of avalanches, an avalanche inventory map plays an important part in such a study. Furthermore, the

mapping of documented avalanche locations is essential to define the correlation between avalanche and occurrence factor. An avalanche inventory map gives the essential information for assessing avalanche susceptibility. Precise recognition of the location of snow avalanches is imperative for avalanche susceptibility mapping.

To obtain comprehensive and detailed avalanche inventory map, exhaustive field surveys and interpretations are accomplished in the avalanche-prone regions with well supported high-resolution satellite imagery and Survey of India (SoI) map sheets. A total number of 292 avalanche locations were demarcated in the avalanche inventory map. Afterward, the avalanche inventory map was categorized into two categories: (i) training dataset and (ii) validation dataset. In training data, 233 (80%) numbers for avalanche sites were selected at random and utilized to train the model. For validation of data, the remaining 59 (20%) number of avalanche locations were kept and used for the purpose of testing and validation of the results, respectively.

5.3 Analysis of avalanche occurrence factors and generation of thematic GIS layers

Avalanche formation conditions are crucial for the analysis of avalanche occurrence factors. Various significant avalanche occurrence conditions including meteorological, snowpack stability, topographical, natural triggers and anthropogenic activities. Understanding the snowpack stability is significant for avalanche susceptibility modelling, but the data is not thoroughly available for the present study area. The frequency of naturally triggered avalanches is more strongly correlated to topographical factors than meteorological factors (Smith and McClung, 1997). Moreover, meteorological factors and snowpack stability depend on the weather condition, which keeps on changing continuously. Topographical factors are only constant factors in the avalanche susceptibility mapping. Six most prominent avalanche occurrence topographical factors such as slope, aspect, curvature, elevation, terrain roughness, ground cover and four meteorological parameters such as air temperature, snow depth, wind speed/direction and relative humidity are used for avalanche susceptibility mapping and summarized as following:

The slope is an important and the primary avalanche occurrence factor ((Bühler et al., 2013; Ghinoi and Chung 2005; Snehmani et al., 2014). Statistically, it is generally accepted that most of avalanches activities occurred in a region where the slope angle ranges from 25° to 45° and rarely at the slope angle less than 25° (McClung and Schaerer, 2006, Selçuk, 2013). The ASTER GDEM V2 was used to generate slope values using the maximum transformation in neighbor cell values technique (Burrough and McDonell, 1998). Subsequently, the reclassification method was used to discriminate the slope values into 4 categories, such as slope angle below 12° , $12^{\circ} - 28^{\circ}$, $28^{\circ} - 45^{\circ}$ and above 45° (Figure 5.2). While choosing the four slope classes, statistics presented in Table 5.1 were considered to modify the classes given by Albrecht et al. (1994) and adopted by Selçuk (2013). As in the present study, none of the avalanche accidents were observed in the area where the slope angle is less than 12° (Table 5.1), so instead of using 0° - 10° threshold as considered by Selçuk (2013) for no avalanche class, threshold limit $0^{\circ} - 12^{\circ}$ was used. Threshold limits for the rest of the slope classes were taken as considered by Selçuk (2013). In the present study area, the slope angle ranges from 0° to 83° . The slope category ranges from $28^{\circ} - 45^{\circ}$ has a 78% documented avalanche slope followed by 18% in $12^{\circ} - 28^{\circ}$. The slope class less than 12° showed no avalanche clues in the past. The attributes of all slope categories are mentioned in Table 5.1.

Aspect is a principal parameter related to the avalanche occurrence (Ghinoi and Chung, 2005; Selçuk, 2013). The past avalanche accidents in Indian Himalaya have shown (Ganju et. al., 2002) that northern, eastern and southern slopes contribute almost equally in the release of avalanches. Since the dominant wind direction during winter months is westerly, as a result, southerly, easterly and northerly slopes get additional drift snow. The ASTER GDEM V2 was used to generate aspect values applying the algorithm which incorporating the values of the cell's eight neighbors (Burrough and McDonell, 1998) and further reclassified into nine principal categories (Figure 5.2). Six out of nine aspect categories showed significant association with avalanche occurrence locations such as north, northeast, south, east, southeast and southwest, respectively (Table 5.1).

The curvature has been deemed as an important terrain factor in the release of avalanches (Maggioni and Gruber, 2003; Ghinoi and Chung, 2005; Snehmani et al., 2014). Generally, convex slopes are more avalanche susceptible than flat and concave slopes (Nefeslioglu et al., 2013). The areas of a sudden change in the curvature also contribute to the release of avalanches. In the present study, the curvature values have been derived from ASTER GDEM using the second derivative value of the input cell \times cell of surface (Moore et al., 1991) and reclassified into 3 principal categories such as concave, convex and flat (Figure 5.2).

Convex curvature showed a maximum relationship with documented avalanche locations (43.78%) than concave (33.48%) and flat (22.75%) curvature (Table 5.1).

The elevation is a crucial terrain factor involved in the snow avalanche occurrence because snowpack frequently varies due to varying snowfall, wind and temperature at different elevations (McClung and Schaerer, 2006; Guy and Birkeland, 2013; Selçuk, 2013). The wind speed increases at high elevation and helps in increasing the snow sliding. Higher elevation area receives heavy snowfall most of the time in the winter season and thus increasing the avalanche activity. The conditions on higher elevation areas are suitable for avalanche occurrence because this area is generally exposed by wind, sun, different snowpack conditions and minimum forest/vegetation cover (McClung and Schaerer, 2006). In general, the avalanche activity at a lower elevation is minor because the snow at minor elevation often melts and changes to rain. The topographical characteristics of the Lahaul region are seemingly favorable for avalanche occurrence. The study area has complex terrain, with the altitude ranging from 2302 m to 6443 m. In Western Indian Himalaya, maximum avalanches generally start at the elevation ranges from 2700 m and terminate at about 6000 m. All slopes beyond 5500 m elevation are generally glaciated. In the Lahaul region, 98% of total documented avalanche sites have existed between the elevation ranges from 3200 m to 5800 m. In the present study, the elevation range was reclassified into 8 categories as shown in Figure 5.2. The attributes of all elevation categories are mentioned in Table 5.1. The elevation class of 3800 m to 4300 m has a maximum number of avalanche activities, which was followed by the elevation class of 4300 m to 4800 m. The elevation classes of less

than 2800 m and above 5800 m showed no avalanche occurrence/activity in the past.

Vegetation cover is also significant factor in the assessment of avalanche susceptibility. Avalanches generally released on barren slopes. Dense trees coverage holds the snow and protects against snow avalanches (Selçuk, 2013). In general, vegetation cannot stop the snow avalanches, but highly vegetation coverage controls the volume of snow that contributes to the release of an avalanche. Grassy slopes release avalanches differently than those with shrubs. Based on the experienced judgment in Indian Himalaya, the forested areas would contribute to about only by 10% towards avalanche initiation. Shrubs, tall grass would contribute to about 30% towards avalanche initiation and the maximum of 60% is from barren slopes. The application of vegetation cover in the preparation of the GIS-based map was achieved with the help of Landsat 8 OLI satellite image. The NDVI method was used for the extraction of vegetation cover values.

The NDVI values were calculated using the formula from the equation (5.1) (Ke et al., 2015)

$$NDVI = \frac{NIR - R}{NIR + R} \quad (5.1)$$

Where, *NIR* and *R* are the energy reflected in the near infrared and red portions of the electromagnetic spectrum.

The values of NDVI are further reclassified into 4 categories, such as <0.1, 0.1-0.2, 0.2-0.3 and >0.4 (Figure 5.2). The vegetation cover increases with the increase in the NDVI values. The vegetation cover is dense with the NDVI values > 0.2. Snow avalanches showed a significant relationship with <0.1 NDVI values because maximum avalanches have occurred (83.26%) in this category of NDVI (Table 5.1).

Terrain roughness is a significant avalanche occurrence component. Terrain roughness reports a rugged and sporadic surface, which blocks the snowpack in the downward movement and prevents the formation of a consistent weak layer, which is crucial for fracture in the snowpack (McClung, 2001; Schweizer et al., 2003). In the present study, the terrain roughness is calculated using the ruggedness method of Sappington (2007). The study area with ruggedness values are classified

into three classes of roughness (Figure 5.2). The spatial relationship between each class of terrain roughness with avalanche occurrences is shown in Table 5.1.

The Root Mean Square Error (RMSE) method was applied for calculation of errors in the reclassified avalanche occurrence parameters, which measure how accurate different calculated classes match with the real data. A variation was computed between the actual observation and the calculated value for each observation of a phenomenon. Then, each variation is squared up. The values calculated from sum of square was then divided by number of observations. Finally, a square root was calculated.

The root mean square error values i.e., RMSE of the avalanche occurrence parameters were calculated using the following equation as:

$$RMSE = \sqrt{\frac{1}{N} \sum_{i=1}^N (x_i - x_j)^2} \quad (5.2)$$

Where, x_i is the value in reclassified avalanche occurrence parameters and x_j is the real value of the of the avalanche occurrence parameters. A total number of 233 points were considered for error calculation of all avalanche occurrence parameters. An average RMSE of all avalanche occurrence parameters is calculated as ± 0.71 . An RMSE value of nearly ± 0.5 indicates acceptable results.

Snow-depth is considered as the most prominent meteorological parameter which influences avalanche occurrence. The downhill gravity increases with increasing the snow depth. With an increase in downhill gravity, the snowpack structure may fail and cause instability of snowpack. The histogram of snow-depth shows that maximum avalanche activities from 130 cm to 260 cm snow depth (figure 4.11a). The frequency of avalanche activity in snow-depth more than 260 cm is low because snow height remains for a short duration in winter. However, high weight is assigned in this category of snow-depth for hazard mapping. Air-temperature is considered as the second most prominent meteorological parameter. The morphological condition of the snow depends upon the air-temperature. The metamorphic process is slow with decreasing the air temperature and weak snowpack structure may remain for a long time. Therefore, low air-temperature

continue for a long time, which remains a snow instability situation. Whereas, high air-temperature melts the snow to a large extent and reduce the snowpack stability. Relative-humidity causes an indirect effect on snowpack stability. Weak snow surface layers also cause due to higher humidity with low wind. These conditions affect the snowpack stability. Winds conditions are also responsible for the avalanche occurrence. High wind also affects the snowpack stability.

Various kinds of GIS-based models developed and implemented in the present study for avalanche hazard mapping are given as follows:

1. Probabilistic frequency ratio model
2. Multi-Criteria Decision Analysis-Analytical Hierarchy Process (MCDA-AHP) Model
3. Fuzzy Frequency Ratio (Fuzzy-FR) Model

5.4 Probabilistic frequency ratio model for avalanche susceptibility mapping

Figure 5.1 showing the detailed flow chart of the methodology adopted for this study. The methodology is followed as: (a) gathering and transformation of the data including topographic, meteorological factors and avalanche occurrence data into a database; (b) formulation of the inventory map; (c) generation and reclassification of avalanche occurrence factors; (d) calculation of FR coefficients of all categories of factors; (e) generation of release area map of avalanches based on the FR coefficients of all categories of factors. Finally, the results are evaluated using R_A -index and ROC-AUC techniques.

The probabilistic FR model is a bivariate statistical model, that can provide the capability for calculating the relationships between the dependent and independent variables (Oh et al, 2011). The FR model still not used and tested for avalanche susceptibility mapping. Therefore, using the assumption of Oh et al., (2011), the level of relation between dependent and independent variables was calculated. The avalanche occurrences dataset was set as dependent variables and avalanche occurrence factors are set as independent variables. Hence, the more FR value, the higher relationship between avalanches and their occurrence factor's categories. Similarly lesser the FR value, weaker the relationship between avalanches and their occurrence factor's categories.

Equation (5.3) can express the probabilistic FR model for avalanche hazard index (AHI):

$$AHI = \sum (FR)_i \quad (i = 1, 2, 3, \dots \dots n) \quad (5.3)$$

Where, AHI is the avalanche hazard index, FR is the frequency ratio values of each class of an occurrence factor and n is the total number of input factors.

Using Equation (5.4), the FR value of each factor was calculated:

$$FR = \frac{N_p(SX_i) / \sum_{i=1}^m SX_i}{N_p(SX_j) / \sum_{j=1}^n SX_j} \quad (5.4)$$

Where, $N_p(SX_i)$ is the number of avalanches pixels in class i of factor (X), $N_p(SX_j)$ is the total number of pixels in that particular factor (X_j), m is the number of classes in the factor X_i and n is the total number of factors.

Figure 5.3 presents the example for calculating the FR values of each class of the factor. Figure 5.3a representing the total number of avalanche location pixels in an image, Figure 5.3b representing the total number of pixels for class 1 of factor A and Figure 5.3c representing the total number of avalanche location pixels for class 1 of factor A. In present study, avalanche occurrence locations are considered as dependent variables and terrain factors with vegetation cover values, which influencing the avalanche occurrence are considered as independent variables.

Avalanche occurrence data was considered as a dependent variable. While, terrain, meteorological factors and vegetation cover values were considered as independent variables. The level of correlation between the avalanche occurrences and each class of the avalanche occurrence factors were calculated. Table 5.1 describes the calculated FR values for each class of the avalanche occurrences

factor. Using these values, the thematic layers were reclassified and added in GIS to obtain the avalanche susceptibility map ([Figure 5.4](#)).

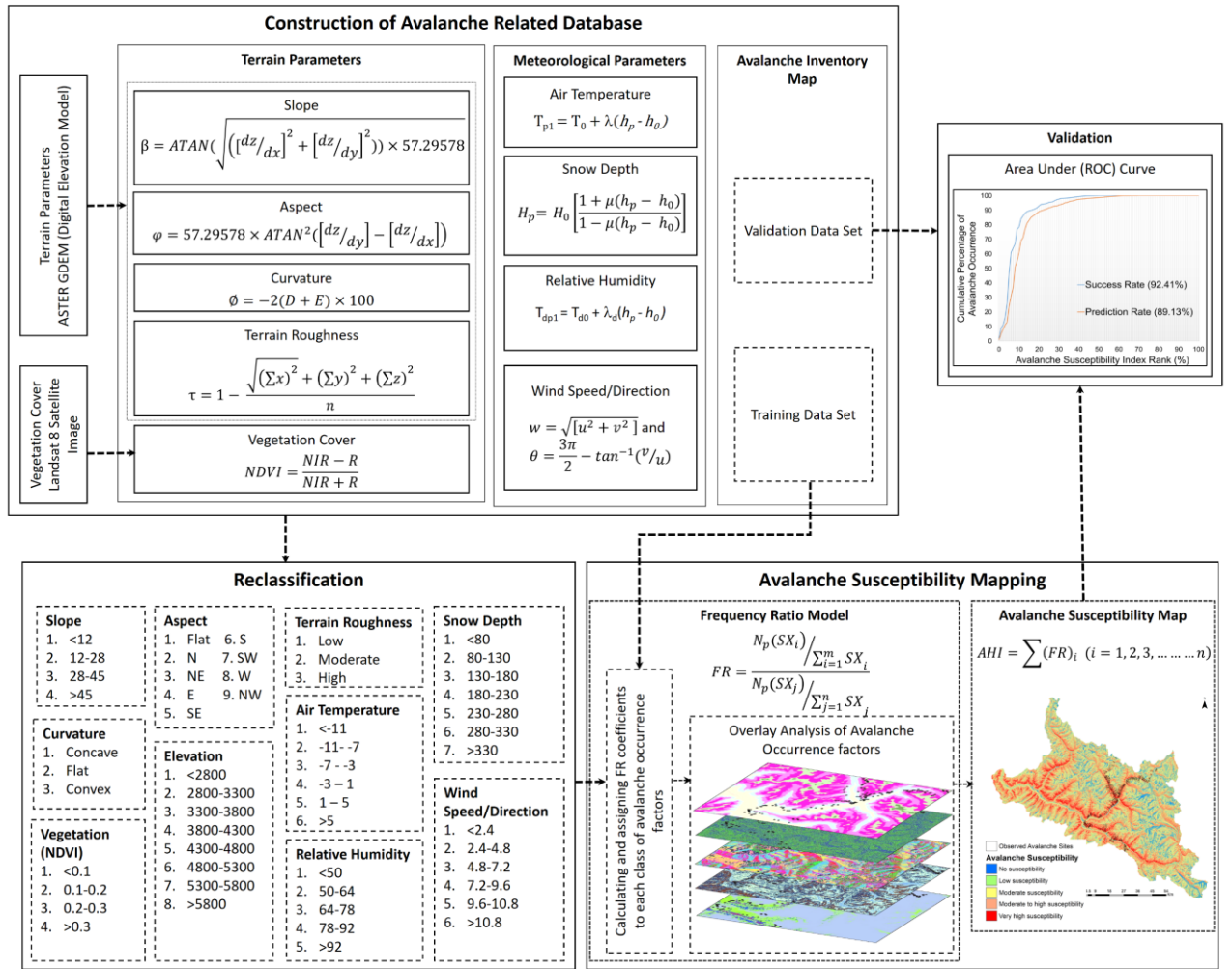


Figure 5.1: Flow chart of frequency ratio modelling for avalanche susceptibility mapping

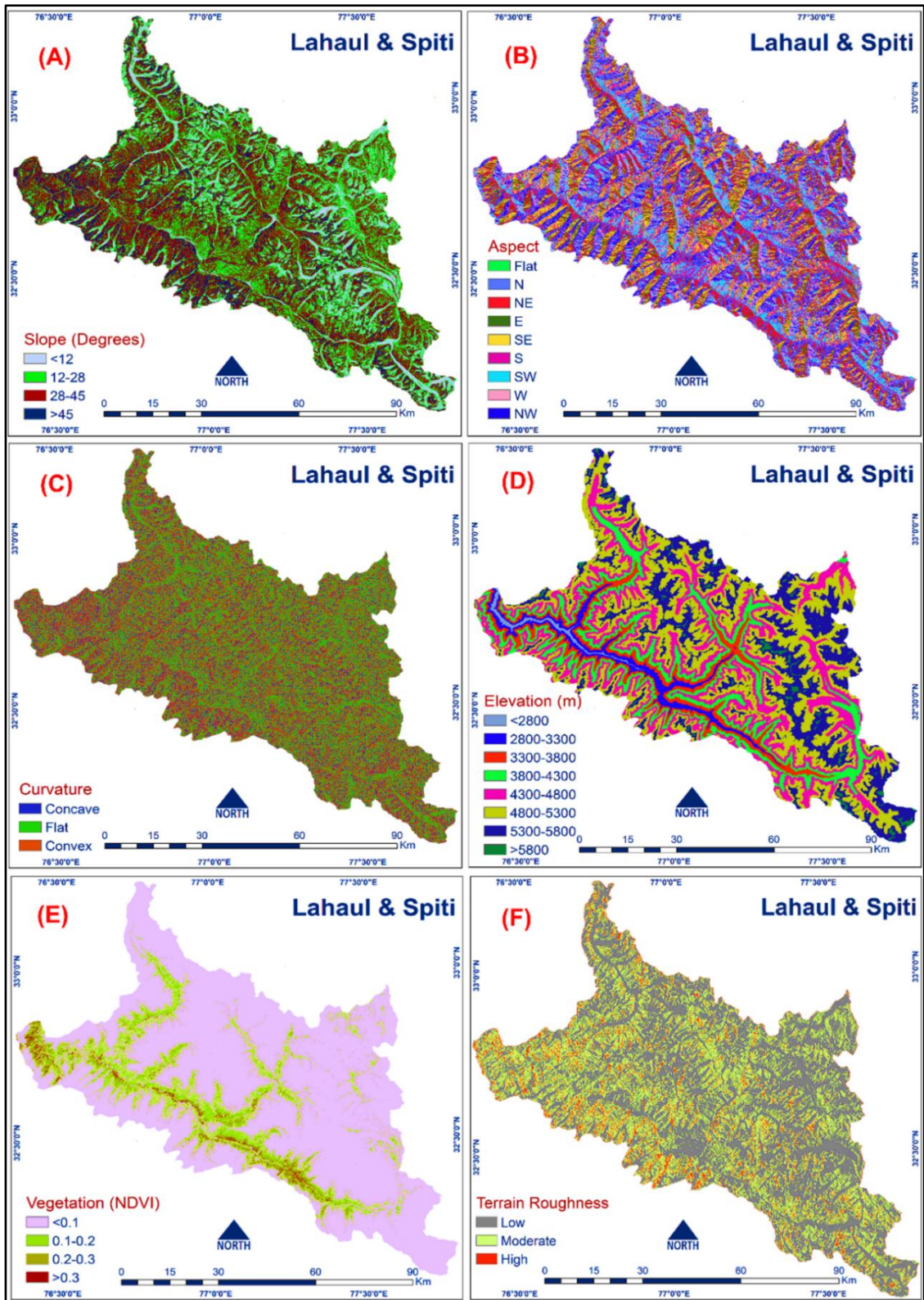


Figure 5.2: Avalanche occurrence terrain parameters: (A) Slope, (B) Aspect, (C) Curvature, (D) Elevation, (E) Vegetation, and (F) Terrain Roughness

Table 5.1: FR values in the each class of avalanche occurrence terrain factors.

Factor	Class	No. of Pixels in Class	% of Pixels in Class	Avalanche occurrence in class		FR
				<i>Number</i>	<i>%</i>	
Slope	0-12	1063674	14.5	0	0.0	0.0
	12-28	2424234	32.9	44	18.9	0.6
	28-45	2820771	38.3	182	78.1	2.0
	>45	1053553	14.3	7	3.0	0.2
Aspect	Flat	394	0.0	0	0.00	0.0
	N	885958	12.0	38	16.3	1.4
	NE	866318	11.8	30	12.9	1.1
	E	974675	13.2	38	16.3	1.2
	SE	972011	13.2	35	15.0	1.1
	S	872758	11.9	34	14.6	1.2
	SW	933351	12.7	26	11.2	0.9
	W	940738	12.8	16	6.9	0.5
Curvature	Concave	2529797	34.4	78	33.5	1.0
	Flat	2170362	29.5	53	22.8	0.8
	Convex	2662073	36.2	102	43.8	1.2
Elevation	<2800	54807	0.7	0	0.00	0.0
	2800-3300	284256	3.9	4	1.7	0.4
	3300-3800	553951	7.5	36	15.5	2.1
	3800-4300	1004255	13.6	60	25.8	1.9
	4300-4800	1641751	22.3	52	22.3	1.0
	4800-5300	2318163	31.5	48	20.6	0.7
	5300-5800	1399584	19.0	33	14.2	0.8
	>5800	105465	1.4	0	0.0	0.0
NDVI	<0.1	6035049	82.0	194	83.3	1.0
	0.1-0.2	997811	13.6	31	13.3	1.0
	0.2-0.3	277598	3.8	7	3.00	0.8
	>0.3	51774	0.7	1	0.4	0.6

Table 5.2: FR values in the each class of avalanche occurrence meteorological factors

Factor	Class	No. of Pixels in Class	% of Pixels in Class	Avalanche occurrence in class		FR
				<i>Number</i>	<i>%</i>	
Temperature	< -11	501316	6.8	14	6.0	0.9
	-11 - -7	859463	11.7	57	24.5	2.1
	-7 - -3	1265073	17.2	56	24.0	1.4
	-3 - 1	1610167	21.9	41	17.6	0.8
	1 -5	1880392	25.5	35	15.0	0.6
	>5	1245821	16.9	30	12.9	0.8
Snow Depth	< 80	376697	5.1	6	2.6	0.5
	80-130	626978	8.5	47	20.2	2.4
	130-180	938779	12.8	49	21.0	1.6
	180-230	1247037	16.9	39	16.7	1.0
	230-280	1526098	20.7	37	15.9	0.8
	280-330	1661993	22.6	32	13.7	0.6
	>330	984650	13.4	23	9.9	0.7
Wind Speed and Direction	< 2.4	506316	6.9	7	3.0	0.4
	2.4 - 4.8	866763	11.8	18	7.7	0.7
	4.8 - 7.2	1259973	17.1	35	15.0	0.9
	7.2 - 9.6	1606267	21.8	54	23.2	1.1
	9.6 - 10.8	1873492	25.4	77	33.0	1.3
	>10.8	1249421	17.0	42	18.1	1.1
Relative Humidity (RH%)	< 50	1723495	23.4	38	16.3	0.7
	50 - 64	2197610	29.8	48	20.6	0.7
	64 - 78	1701125	23.1	52	22.3	1.0
	78 - 92	615215	8.4	19	8.2	1.0
	>92	1124787	15.3	76	32.6	2.1

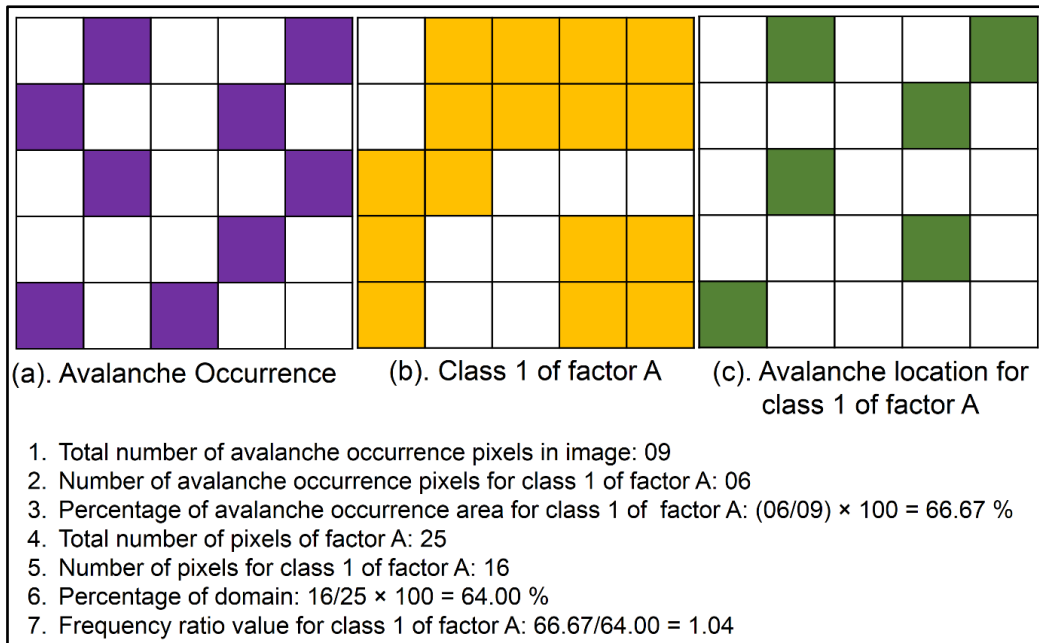


Figure 5.3: Diagram showing the example process for calculating the FR value of each class of the avalanche occurrence factor

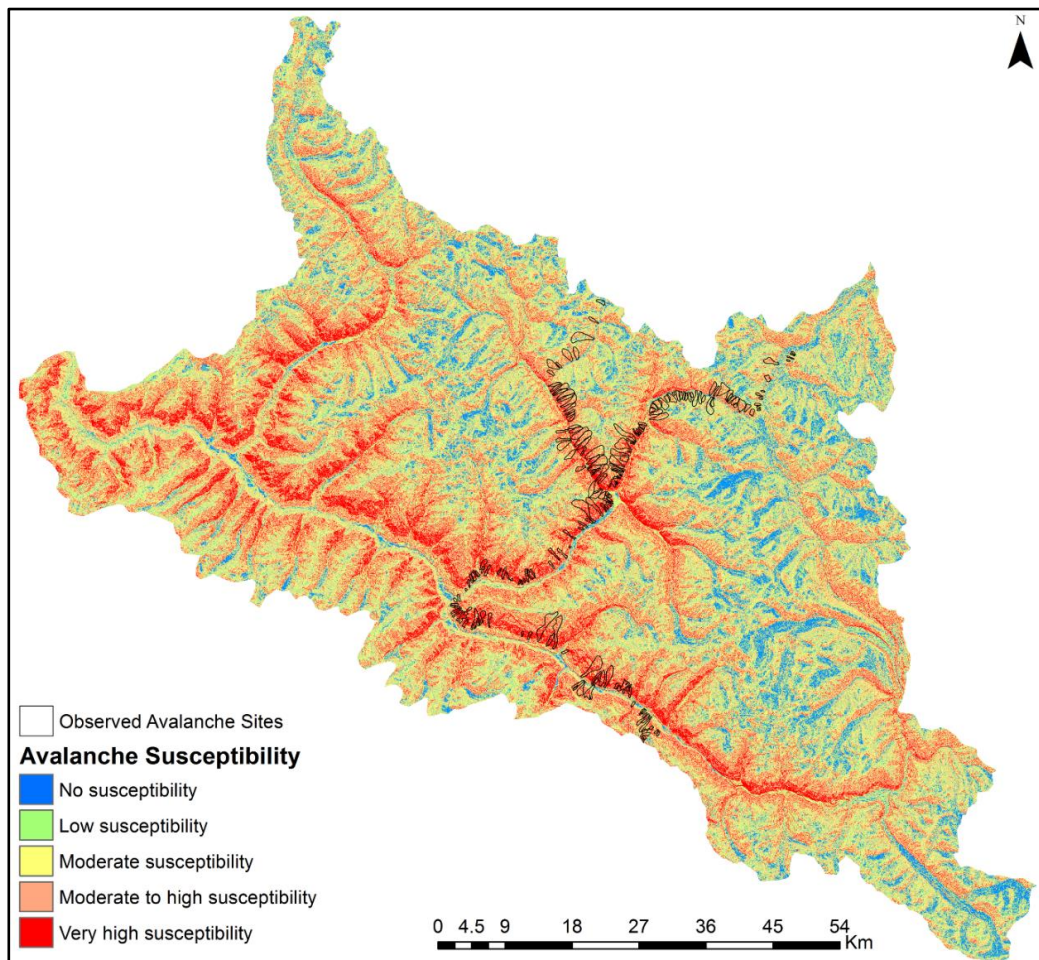


Figure 5.4: Avalanche susceptibility map of the study area generated using the FR model

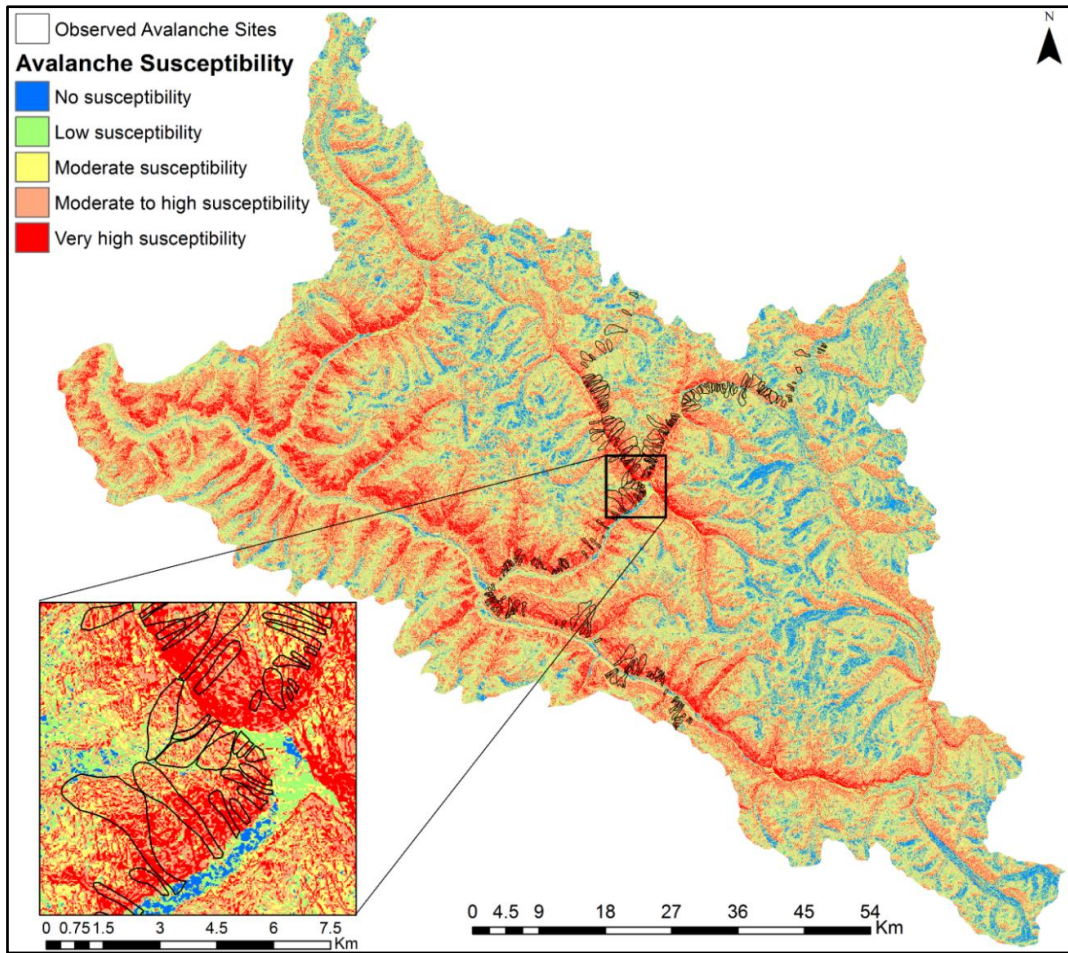


Figure 5.5: Avalanche susceptibility map of the study area obtained using FR model with observed avalanche polygons overlaid

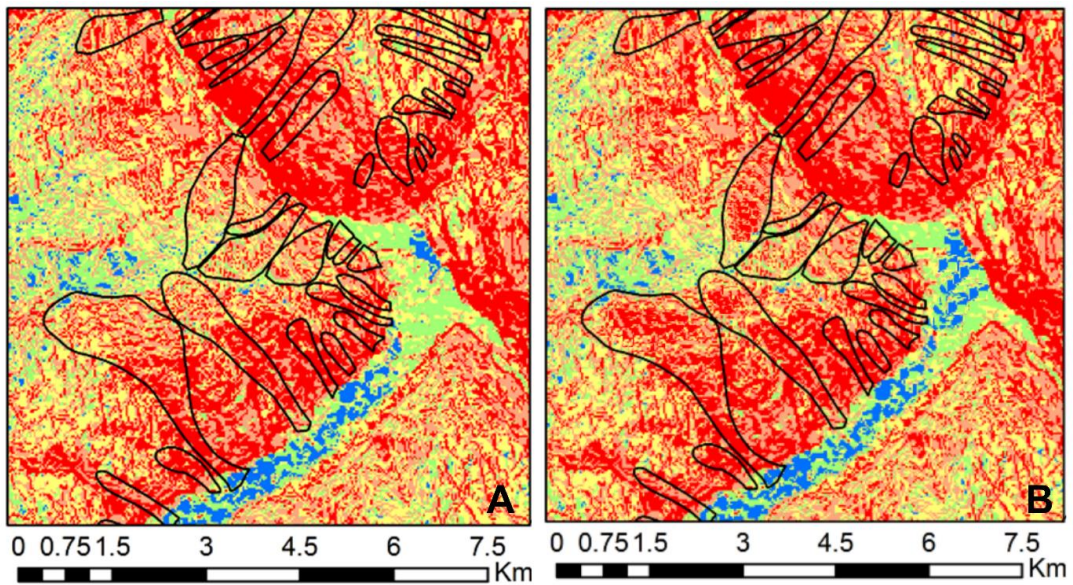


Figure 5.6: Partly comparison of avalanche susceptibility maps of terrain and meteorological-based parameters (A: Terrain-based avalanche hazard map; B: Hybrid (Terrain + Meteorological)-based avalanche hazard map)

5.5 Multi-Criteria Decision Analysis-Analytical Hierarchy Process (MCDA-AHP) Model

5.5.1 MCDA-AHP Model

Multi criteria decision analysis (MCDA) is a commonly applied model in GIS-based decision making problems (Jiang & Eastman 2000). However, the AHP model developed by Saaty (1980) is most popular among several numbers of models suggested for MCDA problems. A notable characteristic of the AHP model is the ability to assess both qualitative and quantitative parameters and possible alternatives on an equitable basis of preference scale. This model is used extensively and efficiently in numerous applications including natural hazard assessment (Nefeslioglu et al. 2013; Selçuk 2013; Snehmani et al. 2014), debris flow vulnerability assessment (Yang et al., 2011; Chen et al., 2015), landslide susceptibility mapping (Kayastha et al. 2013; Shahabi et al. 2015), suitability assessment and modelling (Zhang et al. 2015; Qaddah & Abdelwahed 2015). The AHP model solves the decision making problems by arranging the problems in a hierarchy. The AHP model is utilized for assigning the ratings a set of criteria. This model is also useful in selecting the best from a range of alternatives. The criteria rating and weighting of each criteria is carried in the entire objective (Boroushaki & Malczewski 2008). The theoretical background of the AHP model has been presented in Nefeslioglu (2013). The approach to use the AHP model usually outlined in the steps as: The first step of the approach is to define the unstructured problem and conclude the type of information required. In the second step, develop the decision hierarchy from the top, with the objective and splitting down through the intermediate levels to the lowest level. In the third step, construct a pairwise comparison matrix of a set of criteria using Saaty's importance or preference value scale (Table 5.2) and estimate the relative weight value of each criterion by calculating eigenvalues and eigenvectors. A pairwise comparison matrix is defined by Saaty (1987) as equation (5.5):

$$A = \begin{bmatrix} a_{11} & a_{12} & \cdots & a_{1n} \\ a_{21} & a_{22} & \cdots & a_{2n} \\ a_{31} & a_{32} & \cdots & a_{3n} \\ \vdots & \vdots & \vdots & \vdots \\ a_{n1} & a_{n2} & \cdots & a_{nn} \end{bmatrix} = \begin{bmatrix} 1 & w_1/w_2 & \cdots & w_1/w_n \\ w_2/w_1 & 1 & \cdots & w_2/w_n \\ w_3/w_1 & w_3/w_2 & \cdots & w_3/w_n \\ \vdots & \vdots & \vdots & \vdots \\ w_n/w_1 & w_n/w_2 & \cdots & 1 \end{bmatrix} \quad (5.5)$$

Where, A is the pairwise comparison matrix, which entry a_{ij} expressing how much the criteria x_i is preferring with criteria x_j . When all criteria are already known, each comparison value a_{ij} equals to w_i/w_j . The upper located entries used for comparison with reference to the diagonal of the pairwise comparison matrix.

Table 5.3: The importance value scale (Saaty, 1980).

Importance	Definition	Explanation
1	Equal importance	Contribution to objective is equal
3	Moderate importance	Attribute is slightly favoured over another
5	Strong importance	Attribute is strongly favoured over another
7	Very strong importance	Attribute is very strongly favoured over another
9	Extreme importance	Evidence favouring one attribute is of the highest possible order of affirmation
2,4,6,8	Intermediate values	When compromise is needed

The lower located entries are determined by calculating and implementing a reciprocal operation using equation (5.6).

$$a_{ji} = \frac{1}{a_{ij}} \quad (5.6)$$

In the fourth step, check the consistency ratio (CR) of the judgments. The CR should be calculated for evaluating the consistency with the pairwise comparison matrix. The CR value should be less than 0.1. Saaty (1987) defined a formula to determine the CR is given in equation (5.7) as:

$$CR = \frac{CI}{RI} \quad (5.7)$$

Where, CI is the consistency index and RI is the random consistency index. The consistency index measures the deviation from consistency and defined as (Saaty 1987) in equation (5.8):

$$CI = \frac{\lambda_{max} - N}{N - 1} \quad (5.8)$$

Where, λ_{max} is the largest eigenvalue and N is the order of the comparison matrix.

The random consistency index (Saaty 2000) is the index of randomly generated matrices and depends upon the number of elements being compared (Table 3). If CR exceeds a value of 0.1, the pairwise comparison matrix is recommended to be revised and reevaluate the judgments or preferences (Saaty & Vargas 1991).

Table 5.4: Random consistency index (Saaty, 2000); n = order of the matrix.

n	1	2	3	4	5	6	7	8	9	10	11	12	13	14	15
RI	0	0	0.58	0.90	1.12	1.24	1.32	1.41	1.45	1.49	1.51	1.53	1.56	1.57	1.59

In the fifth step, use the priorities calculated from the judgments to rating the priorities in the level below. Repeat this in the level below for each element, add its rating values and get its overall priority.

The final output is a summation of the product of factor weight values and factor's priority ratings. The factor weight values are calculated in the pairwise comparison matrix and the resulting indices is calculated using the equation (5.9) as follows:

$$Z = \sum_{i=1}^n (w_i x_i) \quad (5.9)$$

Where, Z denotes the summation of the product of criteria weight value w_i and factor's priority ratings x_i .

5.5.2 Avalanche susceptibility mapping using MCDA-AHP model

The MCDA-AHP model is implemented in GIS to generate avalanche susceptibility map of the Lahaul-Spiti. The reclassified thematic layers of avalanche occurrence terrain factors (Figure 5.2) are employed in GIS and ratings are assigned to each class or criteria of thematic layers using a scale from 1 to 9 (Table 5.5). The ratings assigned to each class of the factors are based on documented avalanche locations and expert's judgments of the study region. Subsequently, the weight values of each avalanche occurrence factor are calculated using a pairwise comparison matrix.

Table 5.5: Assignment of ratings for each terrain-based thematic layer/criteria.

Thematic Layer	Category	Rating	Weight
Slope	<12°	1	0.41
	12°-28°	3	
	28°-45°	9	
	>45°	5	
Elevation	< 2800	1	0.05
	2800-3300	3	
	3300-3800	7	
	3800-4300	5	
	4300-4800	5	
	4800-5300	3	
	5300-5800	1	
	>5800	2	
Aspect	Flat	1	0.14
	North	9	
	Northeast	9	
	East	3	
	Southeast	5	
	South	3	
	Southwest	2	
	West	2	
	Northwest	7	
Curvature	Concave	2	0.28
	Flat	3	
	Convex	5	
Terrain roughness	<0.001	2	0.09
	0.001-0.003	5	

	0.003-0.005	4	
	0.005-0.01	7	
	0.01-0.03	5	
	0.03-0.05	3	
	0.05-0.1	1	
	>0.1	1	
<hr/>			
NDVI	<0.1	5	0.03
	0.1-0.2	3	
	0.2-0.3	2	
	>0.3	2	
<hr/>			
Air Temperature	< -11	2	0.25
	-11 - -7	5	
	-7 - -3	7	
	-3 - 1	9	
	1 - 5	4	
	>5	3	
<hr/>			
Snow Depth	< 80	3	0.56
	80-130	5	
	130-180	8	
	180-230	9	
	230-280	7	
	280-330	5	
	>330	3	
<hr/>			
Wind speed and direction	< 2.4	9	0.13
	2.4 - 4.8	5	
	4.8 - 7.2	7	
	7.2 - 9.6	5	
	9.6 - 10.8	0	
	>10.8	0	
<hr/>			
Relative Humidity (RH%)	< 50	2	0.06
	50 - 64	4	
	64 - 78	6	
	78 - 92	5	
	>92	9	
<hr/>			

Table 5.6: Assignment of ratings for each meteorological-based thematic layer/criteria.

Thematic Layer	Category	Rating	Weight
Air Temperature	< -11	2	0.25
	-11 - -7	5	
	-7 - -3	7	
	-3 - 1	9	
	1 -5	4	
	>5	3	
Snow Depth	< 65	3	0.56
	65-130	5	
	130-195	8	
	195-260	9	
	>260	6	
Wind Speed and Direction	< 2.4	3	0.13
	2.4 - 4.8	5	
	4.8 - 7.2	6	
	7.2 - 9.6	7	
	9.6 - 10.8	9	
	>10.8	9	
Relative Humidity (RH%)	< 50	2	0.06
	50 - 64	4	
	64 - 78	6	
	78 - 92	5	
	>92	9	

In MCDA-AHP model, calculation of the avalanche occurrence factor weight values plays a crucial role for the generation of the avalanche susceptibility map. The eigenvector values are calculated in pairwise comparison and occurrence factors are ranked considering the importance ranging from 01 to 09. After computing the pairwise comparison matrix, the weight values of the factors are calculated (Table 5.5).

Table 5.7: Pairwise comparison matrix and weight values of each terrain-based layer using MCDA-AHP

Layer	S	C	A	TR	E	GC	Weight value
S	1	2	3	5	7	9	0.41
C	1/2	1	3	4	5	7	0.28
A	1/3	1/3	1	2	3	5	0.14
TR	1/5	1/4	1/2	1	2	3	0.09
E	1/7	1/5	1/3	1/2	1	2	0.05
GC	1/9	1/7	1/5	1/3	1/2	1	0.03
Consistency ratio (CR)							0.0118

S: Slope, C: Curvature, A: Aspect, TR: Terrain roughness, E: Elevation, GC: Ground cover

Table 5.8: Pairwise comparison matrix and weight values of each meteorological-based layer using MCDA-AHP

Layer	Snow Depth	Temperature	Wind Speed & Direction	Relative Humidity	Weight value
Snow Depth	1	3	7	9	0.56
Temperature	1/3	1	3	5	0.25
Wind Speed & Direction	1/7	1/3	1	2	0.13
Relative Humidity	1/9	1/7	1/3	1	0.06
Consistency ratio (CR)					0.0639

Slope factor is assigned the highest weight value. Curvature, aspect and terrain roughness are also found effective avalanche occurrence factors. Other factors, such as elevation and ground cover are identified as less important for avalanche susceptibility. In the MCDA-AHP model, the CR value indicates the consistency of the judgments in pairwise comparison matrix. The CR value should be less than 0.1. The CR value of the pairwise comparison matrix is calculated using equation (5.7) and estimated as 0.0118, far less than 0.1, confirming a valid consistency of judgments. Finally, the integration of the avalanche occurrence

factors and their classes in the avalanche susceptibility index (ASI) using equation (5.9) is given in equation (5.10) is:

$$ASI_{terrain} = \sum_{i=1}^n (0.41 * S + 0.28 * C + 0.14 * A + 0.09 * TR + 0.05 * E + 0.03 * GC) \quad (5.10)$$

$$ASI_{met} = \sum_{i=1}^n (0.56 * SD + 0.25 * T + 0.13 * W + 0.06 * RH) \quad (5.11)$$

Where, $ASI_{terrain}$ is terrain-based avalanche susceptibility index S, C, A, TR, E and GC are slope, curvature, aspect, terrain roughness, elevation and ground cover factors thematic layers with a rating score of factor's each class.

Where, ASI_{met} is meteorology-based avalanche susceptibility index SD, T, W and RH are snow depth, air temperature, wind, and relative humidity thematic layers with a rating score of each factor class

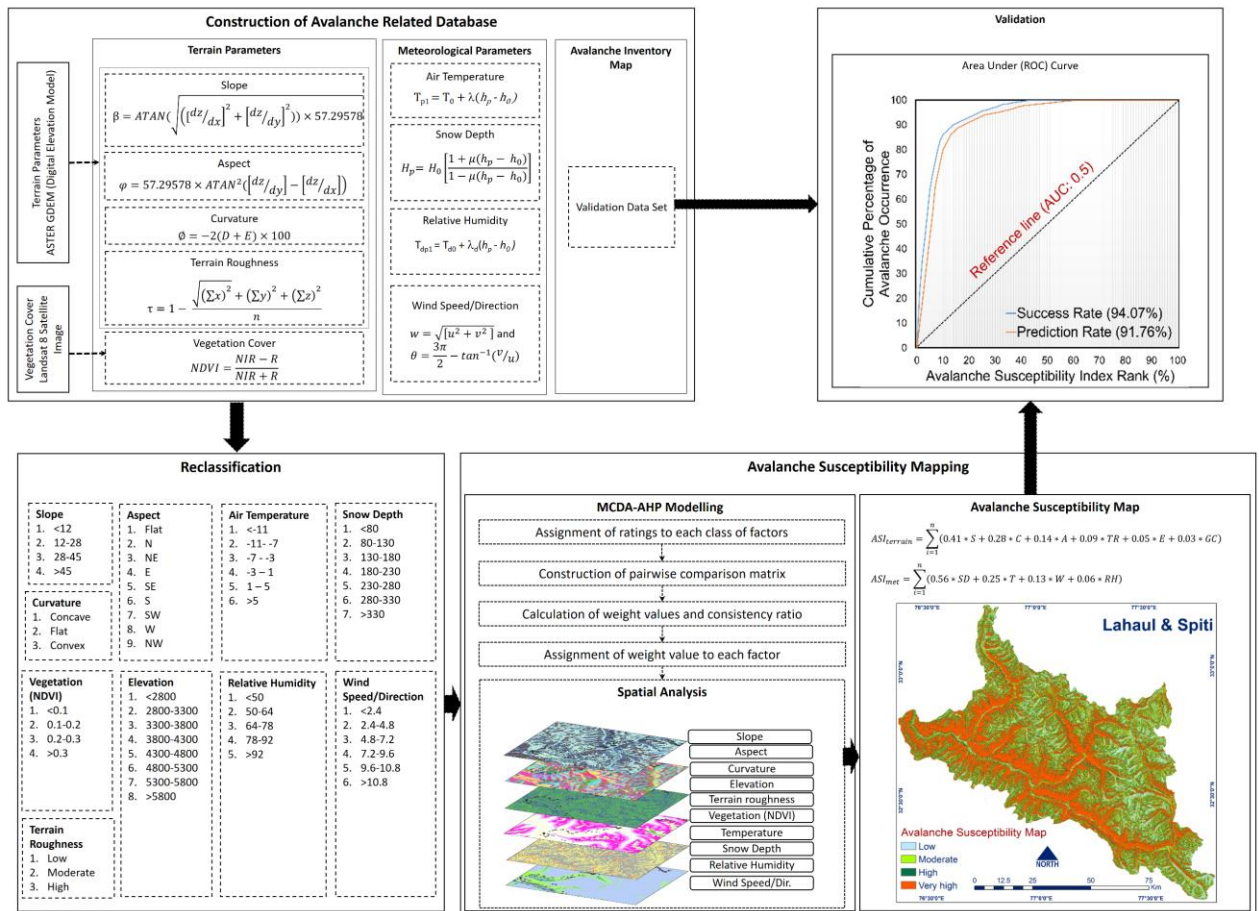


Figure 5.7: Flow chart of MCDA-AHP modelling for avalanche susceptibility mapping

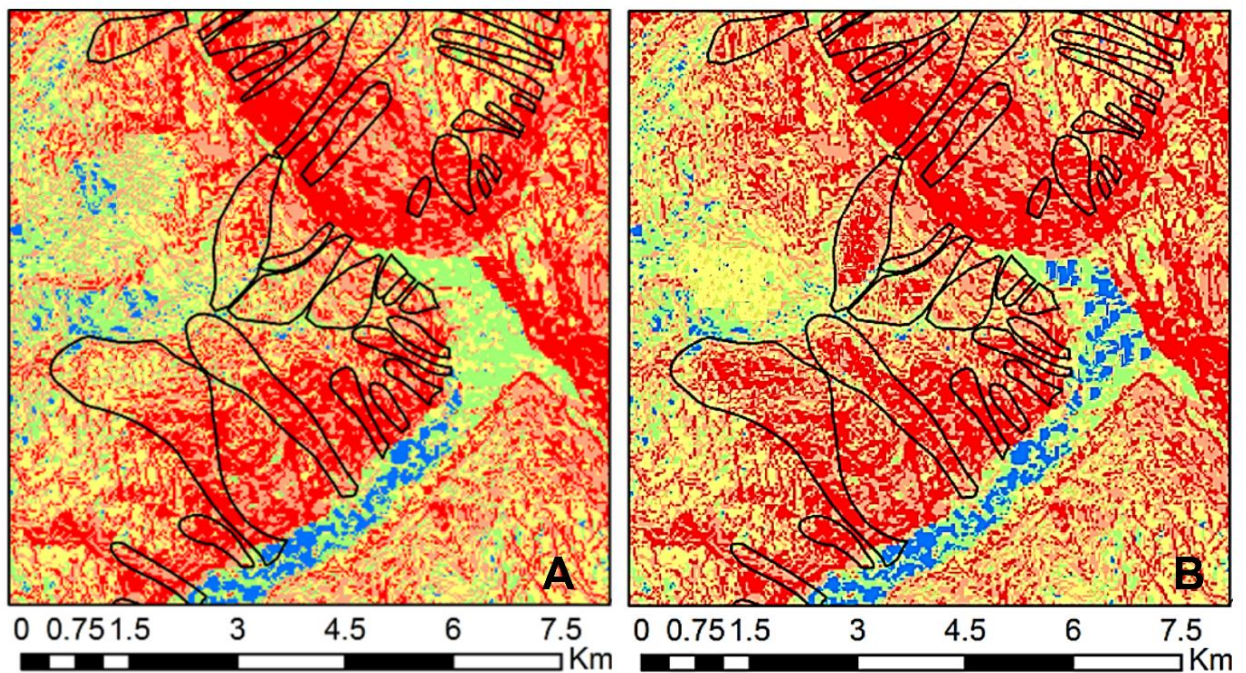


Figure 5.8: Partly comparison of avalanche susceptibility maps of terrain and meteorological-based parameters (A: Terrain-based avalanche hazard map; B: Hybrid (Terrain + Meteorological)-based avalanche hazard map)

5.6 Fuzzy Frequency Ratio (Fuzzy-FR) Model for Avalanche Susceptibility Mapping

5.6.1 Theoretical background of fuzzy set theory and frequency ratio method

(a) Fuzzy set theory

The fuzzy set theory (Zadeh, 1965) is extensively applied to complex problems, which are difficult to state precisely in crisp values. It is also capable of permitting the vague information (Feizizadeh et al., 2014). Fuzzy logic allows to handle the notion of partial truth in which the factors can be characterized with the degrees of truth and false (Barpi, 2004). The fuzzy logic is helpful in the development of expert knowledge-based and naturally vague large complex systems. In the geospatial mapping and management process, the fuzzy logic is capable of utilizing the spatial entities on a map as memberships of a spatial entity or a crisp set (Feizizadeh et al., 2014). However, a spatial object of the set can assign to membership values between 0 and 1, which defines a degree of membership.

A fuzzy set is defined as a set of systematic pairs in equation (5.11) (Feizizadeh et al., 2014):

$$A\{z, MF(z)\}, z \in Z \quad (5.11)$$

$MF(z)$ is a membership function (MF) of the set A , Z indicates a space of entities. Figure 5.9 shows a linear membership function (LMF), which comprises the basis for the MFs. This function has four parameters, such as a , b , c , and d that determine the shape of the function. These parameters signify the smallest, the most promising and the largest favorable values to define a fuzzy entity (Kahraman et al., 2003). The LMF is defined using this concept is given in equation (5.12):

$$\mu_A(x) = \begin{cases} 0 & x < a \\ \frac{x-a}{b-a} & a \leq x \leq b \\ 1 & b < x < c \\ \frac{d-x}{d-c} & c \leq x \leq d \\ 0 & x > d \end{cases} \quad (5.12) \text{(Kainz, 2008)}$$

The different shaped membership functions such as the trapezoidal, S & L-shaped and triangular can also be created for the appropriate purpose by using the proper values of a , b , c , and d respectively (Kainz, 2008).

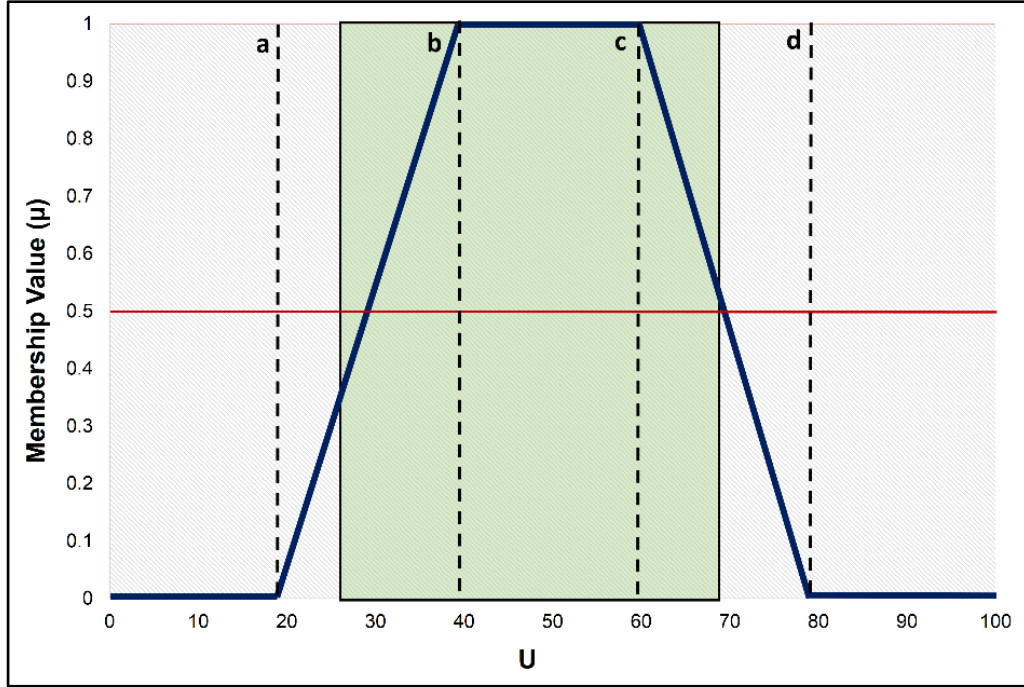


Figure 5.9: Linear membership function

(b) Frequency ratio method

FR represents the probability of the occurrence of a particular event (Bonham-Carter, 1994). In avalanche susceptibility mapping, this method is based on the calculation of the relationship between observed avalanche occurrences and each avalanche occurrence factor. Suppose, for an event X and related event factors attributed to Y , the frequency ratio of Y is given in equation (5.13) (Oh et al., 2011):

$$P\{X|Y\} = \frac{P\{X \cap Y\}}{P\{Y\}} \quad (5.13)$$

The formula behind FR can also be expressed by the given equation (5.14):

$$FR_{ij} = \frac{N_p(SX_i) / \sum_{i=1}^m SX_i}{N_p(SX_j) / \sum_{j=1}^n SX_j} \quad (5.14)$$

Where, $N_p(SX_i)$ denotes the total number of avalanche occurrence pixels in class i of avalanche occurrence factor X ; $N_p(SX_j)$ denotes the total number of pixels in the avalanche occurrence factor X_j ; m is the number of classes in the avalanche occurrence factor X_i ; n is the number of avalanche occurrence factors.

In the present study, avalanche occurrence locations are considered as dependent variables and terrain factors with vegetation cover values, which influence the avalanche occurrence, are considered as independent variables.

5.6.2 Methodology for fuzzy-frequency ratio modelling

The overall methodology is summarized in the flow chart presented in [Figure 5.10](#). The flow chart shows the construction of avalanche related database and procession stages of avalanche susceptibility mapping using the Fuzzy-FR model. In the first part of the methodology, the snow avalanche occurrence related datasets were gathered and transformed into a database, including topographical factors and documented data of past avalanche events. An avalanche inventory map was prepared; subsequently, the avalanche occurrence factors were analysed and reclassified. FR coefficients for each of these factor categories are computed and normalized in $[0, 1]$ to express their FM degrees and termed as “Fuzzy membership functions” ([Bonham-Carter, 1994](#)). Finally, the fuzzy overlay analysis combines the avalanche occurrence factors to obtain an avalanche susceptibility map using the Fuzzy OR operator. The results of avalanche susceptibility mapping using the Fuzzy-FR model were compared with documented avalanche occurrence locations by calculating the area under the ROC curve analysis technique. The detailed methodology is presented in [the next subsections](#).

5.6.3 Fuzzy-Frequency Ratio Modelling for avalanche susceptibility mapping

In Fuzzy-Frequency Ratio modelling for avalanche susceptibility mapping, the pixel of the GIS layer of the avalanche occurrence factor is considered as susceptible to avalanches. The pixel values are ranges from 0 to 1. The value 0 signifies ‘not susceptible to avalanche,’ and the value 1 signifies ‘highly susceptible to avalanche’. The values range from 0 to 1 can be chosen with the degree of membership of an entity set. The values of the degree of membership of an entity set can be derived on the basis of subjective judgment ([Bonham-Carter, 1994](#)). These values can also be obtained from frequency ratio or

multi criteria decision analysis methods, such as an analytical hierarchy process (AHP). Herein, the FR method is applied to derive the FM values.

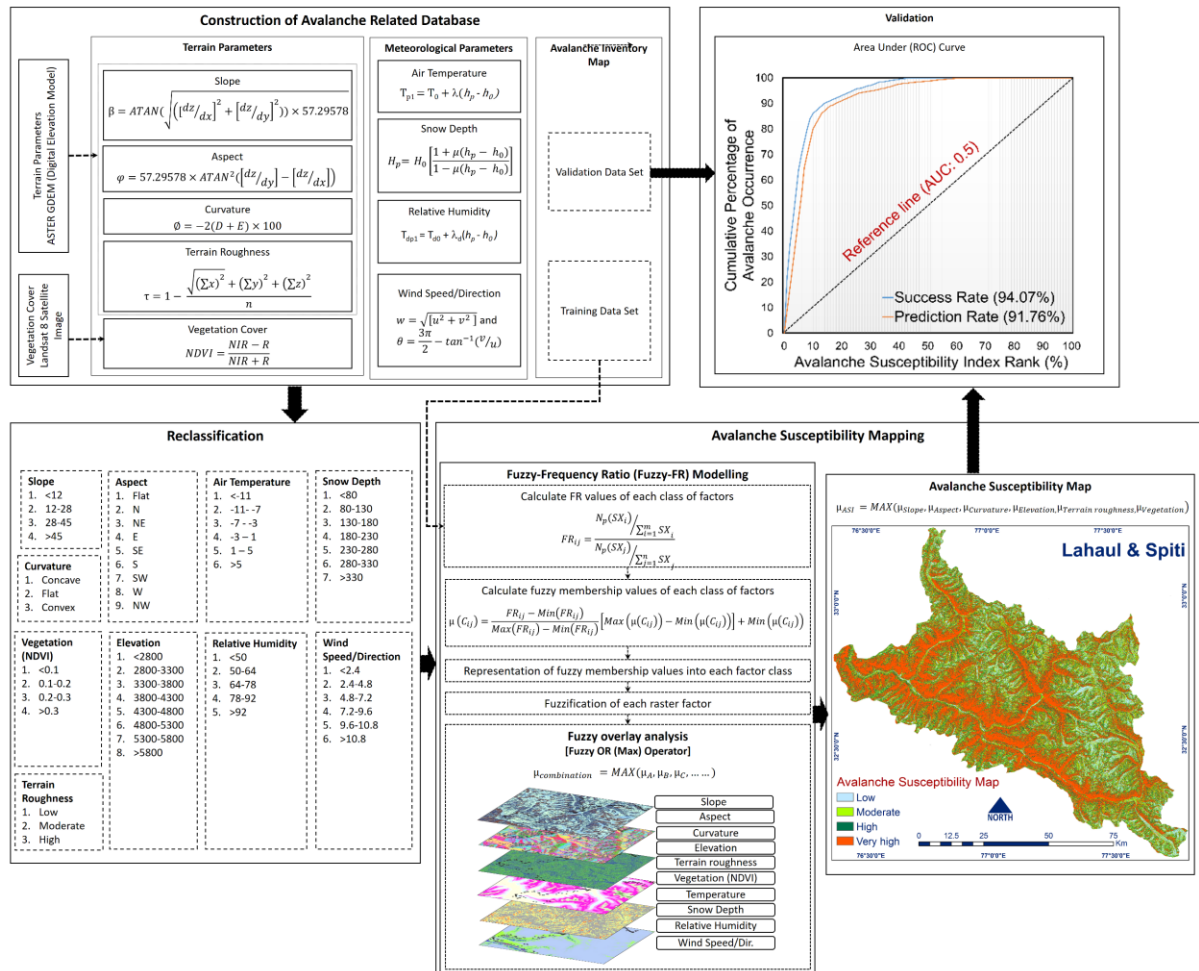


Figure 5.10: Flow chart of fuzzy-FR modelling for avalanche susceptibility mapping

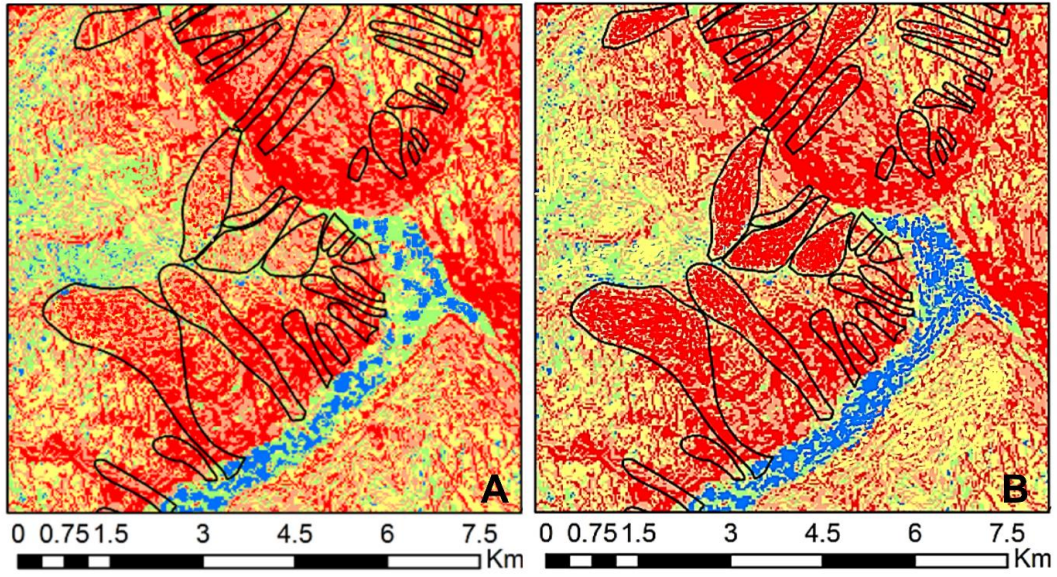


Figure 5.11: Partly comparison of avalanche susceptibility maps of terrain and meteorological-based parameters (A: Terrain-based avalanche hazard map; B: Hybrid (Terrain + Meteorological)-based avalanche hazard map)

5.6.3.1 Frequency ratio values for each class of avalanche occurrence factors

The FR values for each class of the factor are calculated by using the formula in equation (5.14), respectively. The avalanche occurrence location dataset was considered as dependent variables and terrain factors with vegetation cover values, which influence the avalanche occurrence, were considered as independent variables. Using the FR method, the relationship between avalanche occurrence locations and each class of the occurrence factors were calculated and shown in Table 5.6.

5.6.3.2 Fuzzification of FR based avalanche occurrence factors

To fuzzify the avalanche occurrence factors, the FR values for each class of avalanche occurrence factor are normalized in [0, 1] to express their membership degrees using the formula given in equation (5.15):

$$\mu(C_{ij}) = \frac{FR_{ij} - \text{Min}(FR_{ij})}{\text{Max}(FR_{ij}) - \text{Min}(FR_{ij})} [\text{Max}(\mu(C_{ij})) - \text{Min}(\mu(C_{ij}))] + \text{Min}(\mu(C_{ij})) \quad (5.15)$$

Where, $\mu(C_{ij})$ is the FM value; FR_{ij} is the FR value of a class of avalanche occurrence factor; $\text{Min}(FR_{ij})$ is the minimum FR value of an occurrence factor;

$Max(FR_{ij})$ is the maximum FR value of an occurrence factor; $Max(\mu(C_{ij}))$ and $Min(\mu(C_{ij}))$ are the maximum and minimum normalization limits.

Therefore, for all factors, the membership functions are obtained and each class of avalanche occurrence factor was assigned a membership function. The membership functions were used to create a relationship between the selected factors and the degree of the membership of avalanche and no-avalanche locations. The membership function layers for avalanche susceptibility are generated using the fuzzy linear membership function i.e. “FuzzyLinear ({min}, {max})” for avalanche occurrence factor maps (Figure 5.2).

5.6.3.3 Fuzzy overlay analysis to obtain fuzzified avalanche susceptibility index

Fuzzy overlay analysis has the capability to combine various reclassified occurrence factors to calculate the natural hazard (Kirschbaum et al., 2015). Bonham-Carter (1994) described five fuzzy operators for combining the occurrence factors such as “Fuzzy OR”, “Fuzzy AND”, “Fuzzy Product”, “Fuzzy Sum” and “Fuzzy Gamma”. The “Fuzzy OR” operator functions was used to combine the membership functions of the occurrence factors to obtain the fuzzified index to express the possibility of belonging to avalanche or not. The reason for using the “Fuzzy OR” operator to combine the membership functions was to take the maximum value at each point to estimate the effectiveness factors representing the possibility of the avalanche occurrence. The remaining operators such as: “Fuzzy AND”, “Fuzzy Product”, “Fuzzy Sum” and “Fuzzy Gamma” can also be utilized to combine the membership functions of the occurrence factors to generate the avalanche susceptibility map. In this study, all the membership functions of the avalanche occurrence factors are combined using the “Fuzzy OR” operator given in equation (5.16):

$$\mu_{combination} = MAX(\mu_A, \mu_B, \mu_C, \dots \dots) \quad (5.16)$$

Where, $\mu_{combination}$ is the combination of the maximum values of each membership function of the factor, μ_A is the membership function for factor A at a

particular location, μ_B is the membership function for factor B, μ_C is the membership function for factor C, and so on.

The final fuzzified avalanche susceptibility index was obtained using equation (5.16) and expressed in equation (5.17):

$$\mu_{ASI} = MAX(\mu_{Slope}, \mu_{Aspect}, \mu_{Curvature}, \mu_{Elevation}, \mu_{Terrain\ roughness}, \mu_{Vegetation}) \quad (5.17)$$

Where, μ_{ASI} the calculated avalanche susceptibility index and $\mu_{Slope}, \mu_{Aspect}, \mu_{Curvature}, \mu_{Elevation}, \mu_{Terrain\ roughness}, \mu_{Vegetation}$ are the membership values for slope, aspect, curvature, elevation, terrain roughness, vegetation.

Subsequently, the performance of the avalanche susceptibility map is discussed in the next section.

Table 5.9: Spatial relationship between each terrain-based avalanche conditioning factor, avalanche occurrence and fuzzy membership values

Factor	Class	Class no.	No. of pixels in class		Avalanche occurrence		FR	Fuzzy membership function
			<i>Number</i>	<i>%</i>	<i>Number</i>	<i>%</i>		
Slope	0-12	1	1063674	14.45	0	0.00	0.00	0.00
	12-28	2	2424234	32.93	44	18.88	0.57	0.28
	28-45	3	2820771	38.31	182	78.11	2.04	1.00
	>45	4	1053553	14.31	7	3.00	0.21	0.10
Aspect	Flat	1	394	0.01	0	0.00	0.00	0.00
	N	2	885958	12.03	38	16.31	1.36	1.00
	NE	3	866318	11.77	30	12.88	1.09	0.80
	E	4	974675	13.24	38	16.31	1.23	0.91
	SE	5	972011	13.20	35	15.02	1.14	0.84
	S	6	872758	11.85	34	14.59	1.23	0.91
	SW	7	933351	12.68	26	11.16	0.88	0.65
	W	8	940738	12.78	16	6.87	0.54	0.40
	NW	9	916029	12.44	16	6.87	0.55	0.41

Factor	Class	Class no.	No. of pixels in class		Avalanche occurrence		FR	Fuzzy membership function
			<i>Number</i>	<i>%</i>	<i>Number</i>	<i>%</i>		
Curvature	Concave	1	2529797	34.36	78	33.48	0.97	0.46
	Flat	2	2170362	29.48	53	22.75	0.77	0.00
	Convex	3	2662073	36.16	102	43.78	1.21	1.00
Elevation	<2800	1	54807	0.74	0	0.00	0.00	0.00
	2800-3300	2	284256	3.86	4	1.72	0.44	0.22
	3300-3800	3	553951	7.52	36	15.45	2.05	1.00
	3800-4300	4	1004255	13.64	60	25.75	1.89	0.92
	4300-4800	5	1641751	22.30	52	22.32	1.00	0.49
	4800-5300	6	2318163	31.49	48	20.60	0.65	0.32
	5300-5800	7	1399584	19.01	33	14.16	0.75	0.36
	>5800	8	105465	1.43	0	0.00	0.00	0.00
NDVI	<0.1	1	6035049	81.97	194	83.26	1.02	1.00
	0.1-0.2	2	997811	13.55	31	13.30	0.98	0.92
	0.2-0.3	3	277598	3.77	7	3.00	0.80	0.46
	>0.3	4	51774	0.70	1	0.43	0.61	0.00
Terrain Roughness	Low	1	4854080	65.93	148	63.52	0.96	0.65
	Moderate	2	2011430	27.32	77	33.05	1.21	1.00
	High	3	496722	6.75	8	3.43	0.51	0.00

Table 5.10: Spatial relationship between each meteorological-based avalanche conditioning factor, avalanche occurrence and fuzzy membership values

Factor	Class	Class no.	No. of pixels in class		Avalanche occurrence		FR	Fuzzy membership function
			<i>Number</i>	<i>%</i>	<i>Number</i>	<i>%</i>		
Temperature	< -11	1	501316	6.8	14	6.0	0.9	0.20
	-11 - -7	2	859463	11.7	57	24.5	2.1	1.00
	-7 - -3	3	1265073	17.2	56	24.0	1.4	0.53
	-3 - 1	4	1610167	21.9	41	17.6	0.8	0.13
	1 -5	5	1880392	25.5	35	15.0	0.6	0.00
	>5	6	1245821	16.9	30	12.9	0.8	0.13
Snow Depth	< 80	1	376697	5.1	6	2.6	0.5	0.00
	80-130	2	626978	8.5	47	20.2	2.4	1.00
	130-180	3	938779	12.8	49	21.0	1.6	0.58
	180-230	4	1247037	16.9	39	16.7	1.0	0.26
	230-280	5	1526098	20.7	37	15.9	0.8	0.16
	280-330	6	1661993	22.6	32	13.7	0.6	0.05
	>330	7	984650	13.4	23	9.9	0.7	0.11
Wind Speed and Direction	< 2.4	1	506316	6.9	7	3.0	0.4	0.00
	2.4 - 4.8	2	866763	11.8	18	7.7	0.7	0.33
	4.8 - 7.2	3	1259973	17.1	35	15.0	0.9	0.56
	7.2 - 9.6	4	1606267	21.8	54	23.2	1.1	0.78
	9.6 - 10.8	5	1873492	25.4	77	33.0	1.3	1.00
	>10.8	6	1249421	17.0	42	18.1	1.1	0.78

Factor	Class	Class no.	No. of pixels in class		Avalanche occurrence		FR	Fuzzy membership function
			<i>Number</i>	<i>%</i>	<i>Number</i>	<i>%</i>		
Relative Humidity (RH%)	< 50	1	1723495	23.4	38	16.3	0.7	0.00
	50 - 64	2	2197610	29.8	48	20.6	0.7	0.00
	64 - 78	3	1701125	23.1	52	22.3	1.0	0.21
	78 - 92	4	615215	8.4	19	8.2	1.0	0.21
	>92	5	1124787	15.3	76	32.6	2.1	1.00

6. RESULTS AND DISCUSSION

6.1 Probabilistic Frequency Ratio Model

The level of relationship between avalanches occurrence and their factors was calculated using the FR model. Various avalanche occurrence factors considered are topographical, vegetation cover and meteorological. The relationship between avalanche occurrences and slope ([Table 5.1](#)) shows that a slope angle of 28° to 45° has higher avalanche probabilities. For slope values below 12°, the FR value was 0, which indicated a lesser probability of avalanche occurrence. The slope values from 12° to 28°, the ratio was 0.57, which indicated a moderate probability of avalanche occurrence. While in the aspect, avalanches are abundant on north and east facing slopes. Lowest FR values were observed on the west facing slopes. The curvature values represent the topographical morphology and ranges from negative to positive. A positive value signifies convex curvature. Whereas, the negative and zero values represent the concave and flat surfaces. Convex curvature has a higher probability of avalanche occurrence ([Table 5.1](#)).

Concave curvature has a moderate probability of avalanches and flat has a low FR value of 0.77 ([Table 5.1](#)), which means a low probability of avalanches in that class of curvature. In elevation, the FR value of elevation below 2800 m and above 5800 m was 0, which indicates a lesser probability of avalanche occurrence. The FR values in elevation ranges from 3300m to 3800 m and 3800 m to 4300 m were 2.05 and 1.89, which indicated a higher probability of avalanche occurrence. In the vegetation index, the FR value for NDVI below 0.1 was 1.02, which indicated a high probability of avalanche occurrence. The FR value above 0.3 was 0.61, which indicated a low probability of avalanche occurrence in NDVI. With decreases in the NDVI values, the probability of avalanche increases.

Similarly, the FR values/coefficients of correlation between avalanche occurrence and meteorological parameters are presented in [table 5.2](#).

Based upon the FR coefficients, all the considered and above discussed factors were reclassified and subsequently utilized in GIS using the spatial overlaying technique to generate a release area map of the avalanche. The final

release area map of avalanches was further reclassified into 5 relative susceptibility zones based on the Jenks (Jenks, 1967) natural break method as: (i) No, (ii) Low, (iii) Moderate, (iv) Moderate to high, and (v) Very high susceptibility. Figures 5.5 and 5.6 present the contribution of various avalanche susceptibility classes in the study area. Two types of avalanche release area maps were generated (i) based on terrain parameters and (ii) hybrid (terrain + meteorological) parameters. Partly maps of both types are shown in figure 5.6. Initially, the scenario-based comparison has been made between terrain and hybrid parameter based avalanche release area. In hybrid parameters based avalanche release area map, the pixels are better classified in particular avalanche release zones than a terrain-based map. A statistical assessment technique ROC-AUC was also used to compare the results from both types of parameters.

The ROC-AUC technique determines the correlation between the avalanche susceptibility map and the avalanche inventory map of the documented avalanche occurrence locations. Popularly, ROC-AUC values ranging from 0.5 to 1.0 is used for estimating the prediction accuracy (Yesilnacar and Topal, 2005). The ROC-AUC value ranges from 0.9 to 1.0 is the ideal situation for prediction accuracy (Regmi et al., 2014). The ROC-AUC value of the avalanche susceptibility index was calculated by 100 subdivisions of the total number of pixels in the study area and the cumulative percentage of documented avalanche occurrences.

Validation of the release area map has been performed by calculating success and prediction rates. The training data has been applied for the calculation of the success rate. While, the validation data has been applied for calculation of prediction rate. The values of success rate help to define the correlation of avalanche susceptibility map with the documented avalanche locations. The value of the prediction rate determines the accuracy of the model predicting the avalanches. For validation, 233 i.e. 80% avalanche occurrence data, has been applied for training the model. While, the remained 59 i.e., 20% are employed for validation.

The success rate and prediction rate are calculated for verification and validation of the results. The success rates of the probabilistic FR model of terrain

and hybrid (terrain+ meteorological) parameters are calculated as 0.9241 and 0.9321. Therefore, success accuracies of the probabilistic FR model for terrain and hybrid parameters are demonstrated as 92.41% and 93.21%. The prediction rate of the FR model of the terrain and hybrid parameters are calculated as 0.8913 and 0.8974. Hence, the prediction accuracies for terrain and hybrid parameters are demonstrated as 89.13% and 89.74%, respectively. Figures 6.1 and 6.2 present ROC-AUC of success and prediction rate of avalanche susceptibility index for both types of occurrence parameters. Through ROC-AUC analysis, the hybrid (terrain + meteorological)-based model demonstrated better results than terrain-based.

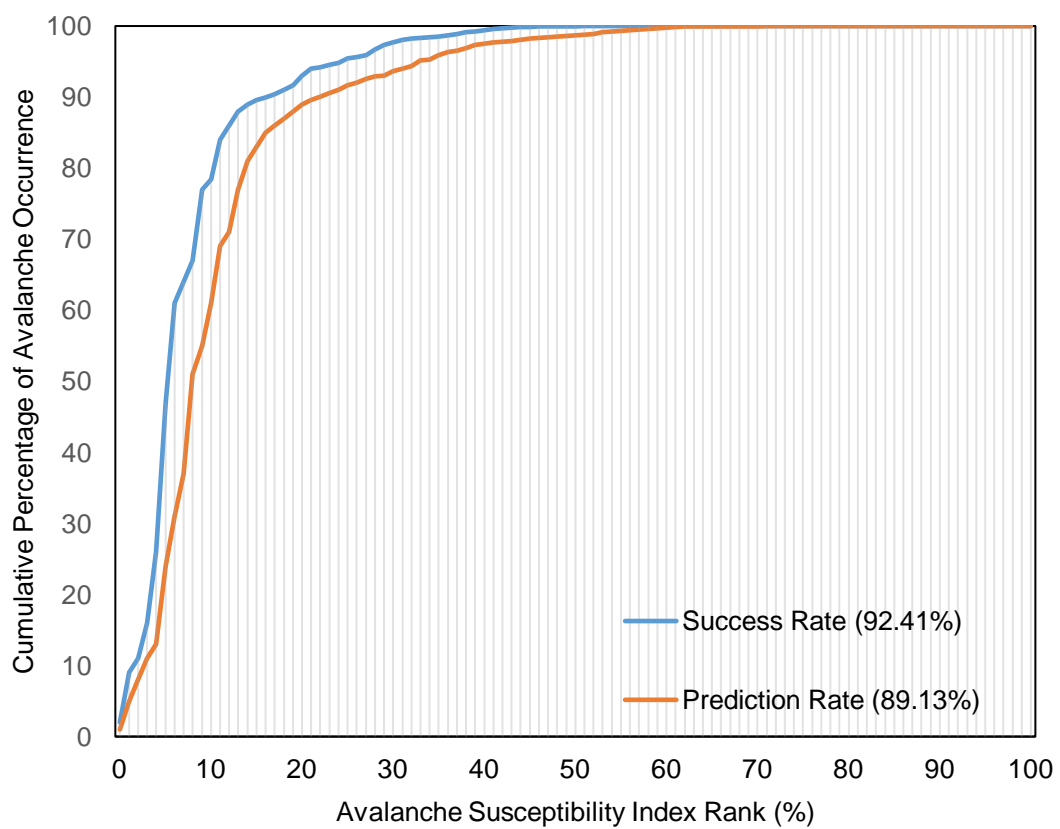


Figure 6.1: ROC curve for success rate and prediction rate of terrain-based avalanche susceptibility index

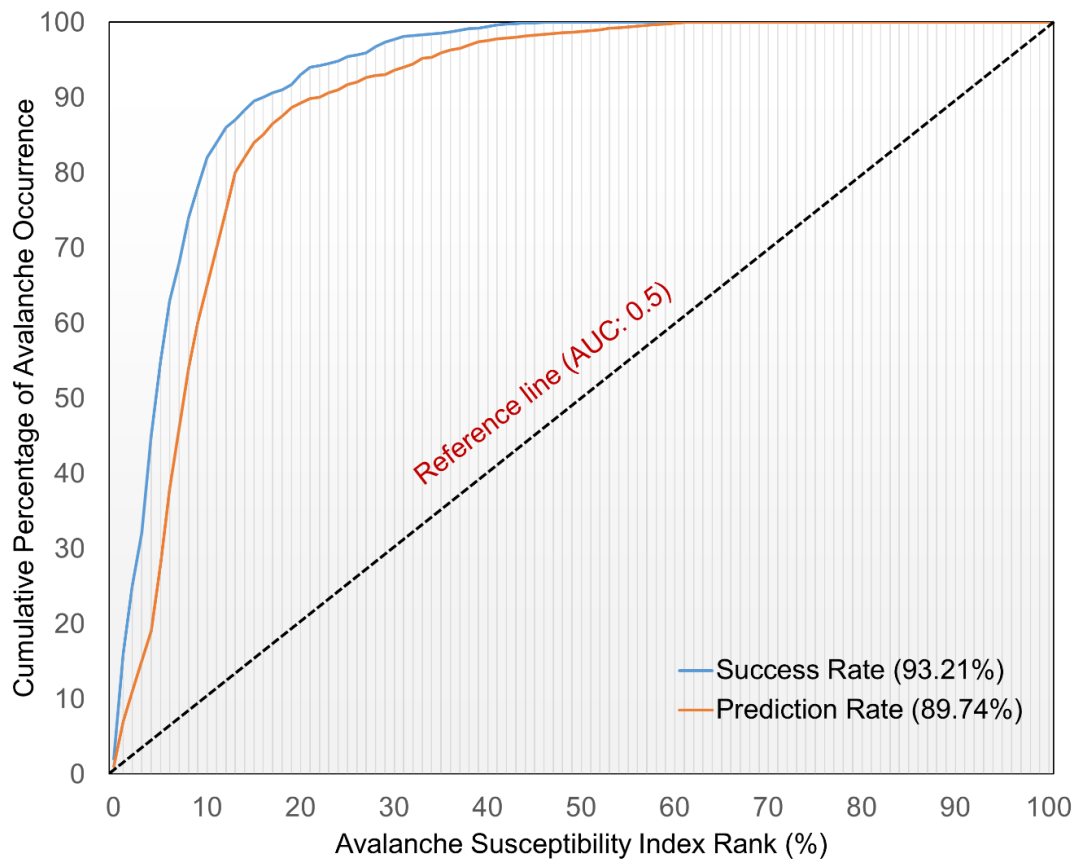


Figure 6.2: ROC curve for success rate and prediction rate of terrain and meteorological parameters based avalanche susceptibility index

6.2 Multi-Criteria Decision Analysis-Analytical Hierarchy Process (MCDA-AHP) Model

Avalanche susceptibility mapping requires analysis of the terrain and meteorological factors together. In this study, both terrain and meteorological factors are considered. Various input terrain factors such as slope, aspect, curvature, elevation, terrain roughness and ground cover for avalanche susceptibility mapping of the Lahaul region are derived from the ASTER GDEM V2 and Landsat 8 OLI imagery. An avalanche inventory map of documented avalanche locations is also compiled. The slope is considered as the primary and one of the most significant avalanche occurrence factors, which is reclassified into five classes, such as : <12, 12-28, 28-45, and >55 degrees. The ratings are assigned to these slope classes on the basis of documented avalanche locations and expert’s judgments.

The slope class with angle ranges from 28-45 degrees is found to be the most prominent and hence maximum rating is assigned to this class (Table 5.4). Aspect is classified into nine classes, such as: Flat, North, Northeast, East, Southeast, South, Southwest, West and Northwest, respectively. According to documented avalanche locations and field knowledge, northern slope classes are considered more important for avalanche occurrence and hence maximum ratings are assigned to these classes (Table 5.4).

Curvature values are reclassified into three classes such as: concave, flat and convex. As per the reference of documented avalanches, the convex curvature values have a high probability of avalanche occurrences than flat and concave. Hence, the convex curvature has assigned high ratings than flat and concave curvature (Table 5.4). The elevation is classified into six classes such as: <2800, 2800-3300, 3300-3800, 3800-4300, 4300-4800, 4800-5300, 5300-5800 and >5800 respectively. According to the documented avalanche locations, maximum avalanches have occurred in the elevation class of 3300-3800, 3800-4300, 4300-4800, 4800-5300 and 5300-5800. Hence, higher ratings are assigned to these classes than others (Table 5.4). Terrain roughness is reclassified into eight classes such as: <0.001, 0.001-0.003, 0.003-0.005, 0.005-0.01, 0.01-0.03, 0.03-0.05, 0.05-0.1 and >0.1. After correlating the terrain roughness classes with documented avalanche locations and an expert's knowledge, the roughness classes of 0.001-0.003, 0.005-0.01 and 0.01-0.03 are found more important in avalanche occurrence than other classes of this factor, hence, has assigned higher ratings than other classes of roughness (Table 5.4). The NDVI map generated from Landsat 8 OLI satellite image is reclassified into four classes as :< 0.1, 0.1-0.2, 0.2-0.3 and >0.3. As per the analysis of the document, the higher ratings are assigned to < 0.1 than other classes (Table 4).

The reclassification, rating and weight values of meteorological parameters are presented in table 5.6 and 5.8.

Subsequently, these reclassified factors layers are employed in MCDA-AHP model and weight values of each avalanche occurrence factor are calculated using pairwise comparison or preference matrix. The preference matrix is shown in Table 5.7 and 5.8, respectively. In the pairwise preference matrix, the

highest preference was given to the slope factor as compared to other factors. The preference for each factor is given on the basis of 1 to 9 scale (Saaty 1980) and is shown in Table 5.2. After computing the preference values in the matrix, the weight values assigned to the slope, aspect, curvature, elevation, terrain roughness and ground cover are given as: 0.41, 0.14, 0.28, 0.05, 0.09 and 0.03 (Table 5.7).

Similarly, the weight values assigned to meteorological parameters snow depth, air temperature, wind speed & direction and relative humidity as: 0.56, 0.25, 0.13 and 0.06 (Table 5.8). Hence, the highest weight value is assigned to the slope factor and lowest for ground cover in terrain-based. In meteorological-based, the highest value has been assigned to snow depth due to a high correlation with avalanche occurrence. The consistency ratio of the matrix is calculated as 0.0118, which confirmed as valid consistency of preferences or judgments. After incorporating these factor weight values and assigned a score to each class of the factors, these factor layers are integrated with GIS using equation (5.10) to obtain an avalanche susceptibility index.

The resulting avalanche susceptibility index is classified into five susceptibility zones or levels using the natural breaks (Jenks) method. The Jenks method is a data grouping scheme intended to determine the best organization of values by interactively comparing the sum of the squared difference between observed values within each class and class means (Jenks 1967). The Jenks method is also known as a Jenks optimization method. The avalanche susceptibility index is classified into five susceptibility zones or levels as: no, low, moderate, moderate to high and very high.

Although the MCDA-AHP model provides great benefits with respect to the complex decision problems and arrangement of spatial data, determination of prediction rate/accuracy is also crucial for validation of the model results. The validation process is performed to determine the prediction rate of the MCDA-AHP based avalanche susceptibility map. A popular statistical assessment technique, the area under the ROC curve is utilized in this process. This ROC-AUC method is one of the most popular methods for calculating the prediction rate (Yesilnacar & Topal 2005; Van Den Eeckhaut et al. 2006; Baeza et al. 2010). To generate the prediction rate curve or ROC curve, the cumulative percentage of

observed or documented avalanche locations are plotted against the obtained avalanche susceptibility index and the area under a ROC curve values are calculated (Figure 6.4). An ideal situation or result would have an area under the curve equal to 1. The area under a ROC curve ranging from 0.5 to 1 is a good fit and less than 0.5 indicates an irregular fit (Hanley & McNeil 1983). The value of the area under a ROC curve is calculated as 0.9097 for terrain-based and 0.9342 for hybrid based maps ((Figure 6.4). The validation results imply that the overall prediction rate of the avalanche susceptibility maps based on terrain and hybrid maps are 90.97% and 93.42, which means that the total avalanche pixels are properly categorized by the avalanche susceptibility mapping model and demonstrated the acceptable agreement relating to avalanche susceptibility map. However, as per the ROC-AUC technique, the hybrid parameters based map demonstrated better results than terrain-based.

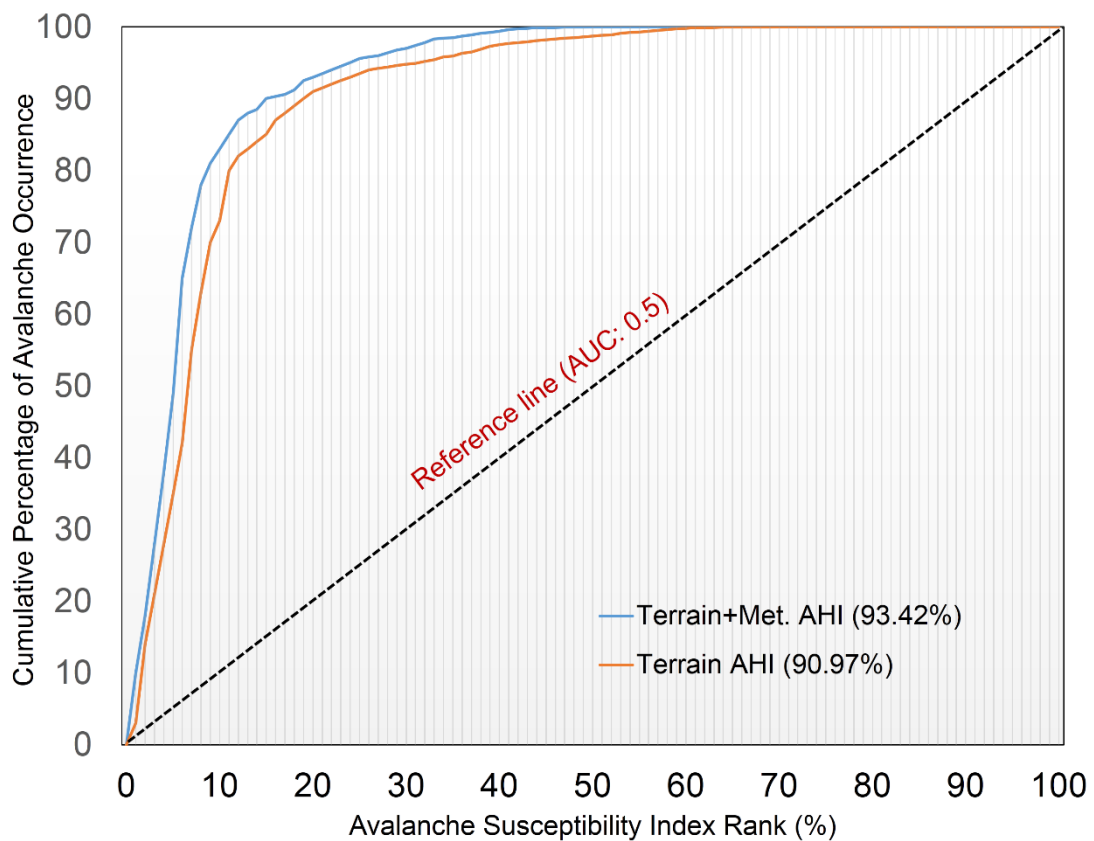


Figure 6.3: ROC curve analysis of prediction rate for avalanche hazard index based on terrain and meteorological parameters

6.3 Fuzzy Frequency Ratio (Fuzzy-FR) Model

To create the fuzzy membership functions of the avalanche occurrence factors, the FR values were calculated for each class of the factors on the basis of the equations (5.13) and (5.14). FR values calculated for each class of the avalanche occurrence factors are shown in Table 5.9 and 5.10. These FR values depict the spatial relationship between the avalanche occurrence and avalanche occurrence factors. In slope classes, the class of the angle ranges 28-45 degrees has the highest FR value of 2.04 than other slope classes (Table 5.9) and indicated a very high possibility of the avalanche. In the aspect factor, the avalanche activities were abundant in the north, northeast, east and southeast facing and lower in the case of west and northwest aspect angles (Table 5.9). The curvature factor represents the topographical morphology. A zero-curvature value indicates the flat surface. Negative curvature values indicate concave surface and positive curvature values indicate a convex surface. The FR value for flat curvature indicated the lowest probability of avalanches than the concave surface and convex surface (Table 5.9).

For elevation factor, the FR value of the elevation classes of the value below 2800 m and above 5800 m indicated a very low probability of avalanches. The FR values of the elevation classes 3300 m-3800 and 3800 m-4300 m indicated a very high probability of the avalanches. The FR values of classes for elevation ranges 4300-4800, 4800-5300 and 5300-5800 were calculated indicated high to moderate probability of the avalanches (Table 5.9). The FR value for NDVI indicated the probability of the avalanche occurrence increases with a decrease in the NDVI values (Table 5.9). In the case of the terrain ruggedness factor, the FR values for low and moderate ruggedness class indicated a high probability of the avalanches than high ruggedness class (Table 5.9). Similarly, the correlation of meteorological parameters with avalanche occurrences is also presented in table 5.10.

These FR values for each class of the occurrence factors were normalized to a scale from 0 to 1 to express their fuzzy membership functions using the formula given in equation (5.15). The fuzzy membership functions of each class of the occurrence factors are shown in the Table 5.9 and 5.10. The value 0 is allocated to the lowest observed avalanche occurrence classes and the value 1 allocated to the

highest observed avalanche occurrence classes of the factors. The representation of a fuzzy set for each avalanche occurrence factor was obtained and shown in [Table 6.3](#). Subsequently, the thematic GIS layers were created on the basis of the fuzzy set of the avalanche occurrence factors. To construct fuzzified index maps for each avalanche occurrence factors, a fuzzy linear membership “FuzzyLinear ($\{\min\}$, $\{\max\}$)” function was applied. A fuzzy overlay technique using a fuzzy OR (Max) operator in fuzzy mathematics was applied to combine all the fuzzified maps of the avalanche occurrence factors to create an avalanche susceptibility map.

The final release area map of avalanches was further reclassified into 5 relative susceptibility zones based on the Jenks ([Jenks, 1967](#)) natural break method as: (i) No, (ii) Low, (iii) Moderate, (iv) Moderate to high, and (v) Very high susceptibility. The Jenks method is a data grouping scheme intended to determine the best organization of values by interactively comparing the sum of the squared difference between observed values within each class and class means ([Jenks 1967](#)). The Jenks method is also known as a Jenks optimization method.

Table 6.1: Fuzzy set of avalanche occurrence factors

Occurrence factor	Fuzzy set
μ_s Slope	(0/1, 0.28/2, 1/3, 0.10/4)
μ_s Aspect	(0/1, 1/2, 0.80/3, 0.91/4, 0.84/5, 0.91/6, 0.65/7, 0.40/8, 0.41/9)
μ_s Curvature	(0.46/1, 0/2, 1/3)
μ_s Elevation	(0/1, 0.22/2, 1/3, 0.92/4, 0.49/5, 0.32/6, 0.36/7, 0/8)
μ_s Terrain roughness	(0.65/1, 1/2, 0/3)
μ_s Vegetation (NDVI)	(1/1, 0.92/2, 0.46/3, 0/4)
μ_s Snow depth	(0/1, 1.0/2, 0.58/3, 0.26/4, 0.16/5, 0.05/6, 0.11/7)
μ_s Air temperature	(0.20/1, 1.0/2, 0.53/3, 0.13/4, 0.0/5, 0.13/6)
μ_s Wind speed/direction	(0.0/1, 0.33/2, 0.56/3, 0.78/4, 1.0/5, 0.78/6)
μ_s Relative humidity	(0.0/1, 0.0/2, 0.21/3, 0.21/4, 1.0/5)

The final avalanche susceptibility map indicates that the north, northeast and northwest parts of the Lahaul-Spiti region have the highest avalanche risk. The higher susceptibility zones concentrate in the middle of the study area and along the River and its torrents. The moderate susceptibility zones are in the middle and

lower reaches and some in the upper reaches, most of which are located on both sides of high susceptibility zones.

The avalanche susceptibility map was evaluated by comparison of the map with both the training data of avalanche occurrence locations that were used for constructing the models and with the avalanche occurrence locations that were not used during the model construction phase from the avalanche inventory map.

A ROC-AUC analysis technique was used to validate the results. For validation of the results by the ROC-AUC technique, the success rate and the prediction rate were calculated. The training data of the documented avalanche occurrence locations was used to calculate the success rate of the avalanche susceptibility map. The validation data of the documented occurrence locations was used to calculate the prediction rate of the avalanche susceptibility map.

In this study, 233 (80%) of randomly selected avalanche locations from inventory maps used to train the model and the remaining 59 (20%) were used for validation of the model results. The success rate and prediction rate of the Fuzzy-FR model of terrain and hybrid parameters was calculated (Figure 6.4 and 6.5). The success rate of the Fuzzy-FR model based on terrain and hybrid parameters were calculated as 0.9407 and 0.9454. Hence, the success accuracy of the model based on terrain and hybrid parameters are determined as 94.07% and 94.54%. The prediction rate of the Fuzzy-FR model based on terrain and meteorological parameters are calculated as 0.9176 and 0.9201. Hence, the prediction accuracy of the Fuzzy-FR model based on terrain and hybrid parameters is determined as 91.76% and 92.01%, respectively.

The accuracy assessment of the model has been demonstrated that the hybrid parameters (terrain + meteorological) improved the results of the applied geospatial models for avalanche susceptibility mapping. The results from prediction rate directed to avoid any kind of activities in high potential avalanche release areas. The human activity should be avoided in the moderate avalanche potential areas to minimize the threat. A risk inspection should be carried out in the low susceptibility zones to ensure the no threat of avalanche occurrence to humankind and other related infrastructure. This is also suggested that the dynamic avalanche models should be further utilized to quantify the avalanche risk and run-

out areas of potential avalanche sites. The avalanche susceptibility map obtained can be a better reference for planners and engineers to design and develop control structures. This avalanche susceptibility map presents helpful information so that consciousness can be accorded to higher avalanche susceptibility zones for any kind of infrastructure development in the near future. The avalanche susceptibility map will be useful for concerned experts in disaster management, planning and mitigation purposes.

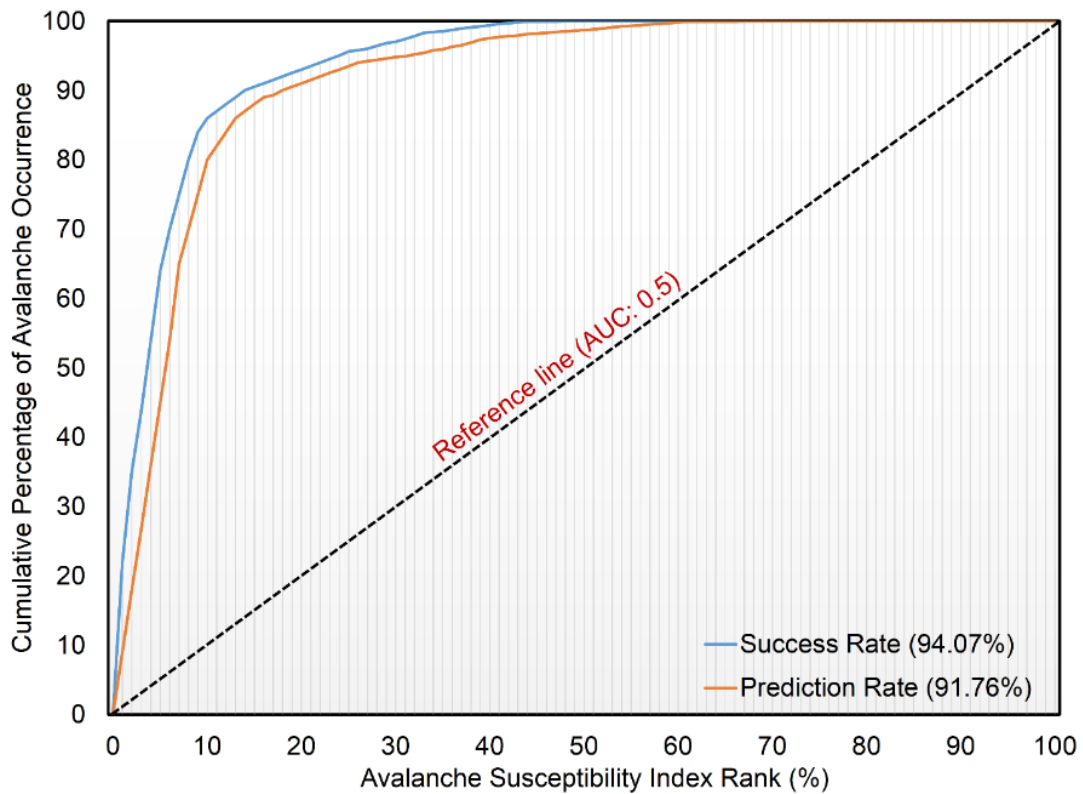


Figure 6.4: ROC curve for success rate and prediction rate of terrain-based avalanche susceptibility index

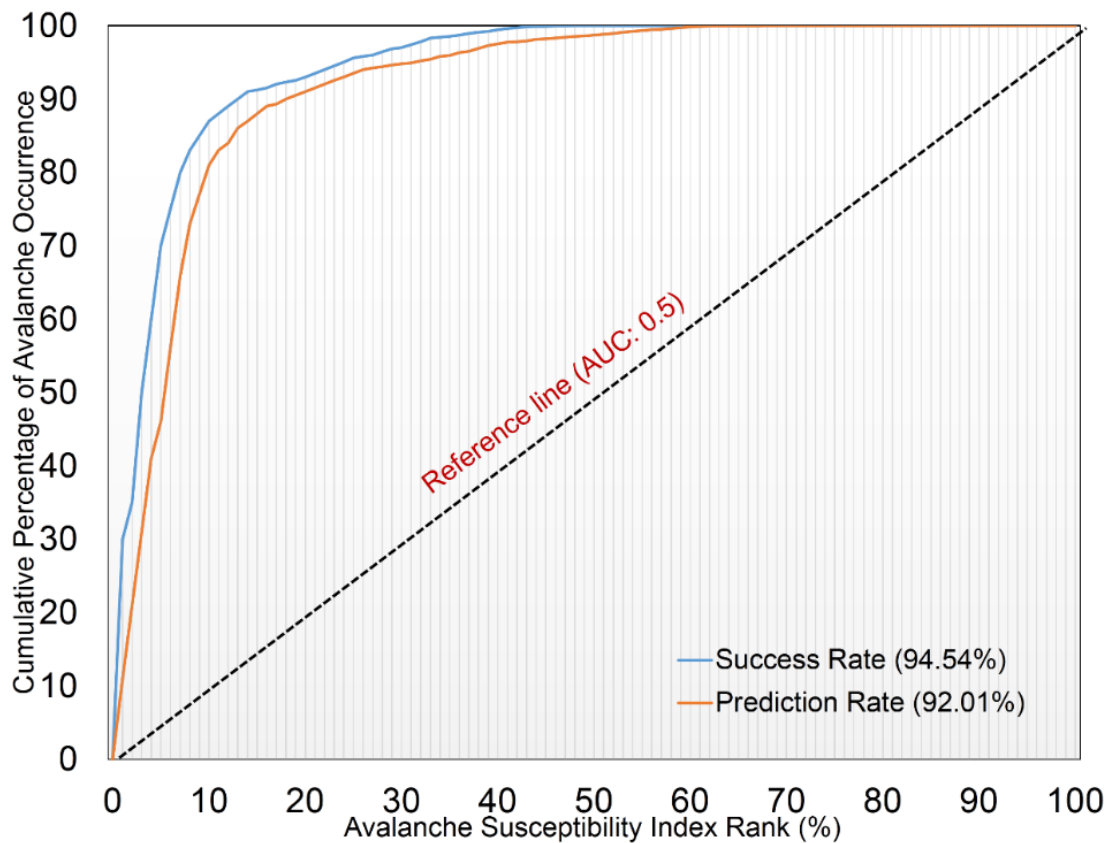


Figure 6.5: ROC curve for success rate and prediction rate of terrain and meteorological parameters based avalanche susceptibility index

6.4 Comparison of results between FR, MCDA-AHP and Fuzzy-FR models

The present research focused on three geospatial models such as frequency ratio, multi-criteria analytical hierarchy process and fuzzy-frequency ratio models for avalanche susceptibility mapping. Five terrain parameters such as slope, aspect, curvature, elevation and vegetation cover as constant parameters, whereas dynamic parameters i.e., meteorological parameters such as snow depth, air temperature, wind speed/direction and relative humidity are used in all geospatial models for avalanche susceptibility indexing. The generated avalanche susceptibility index are further reclassified into avalanche susceptibility zones by using Jenks (1967) natural break method.

Results from all three geospatial models are assessed using the most popular statistical assessment technique i.e., area under the receiver operating characteristics (ROC-AUC) technique. The ROC-AUC technique determines the correlation between the avalanche susceptibility map and the avalanche

inventory map of the documented avalanche occurrence locations. Popularly, ROC-AUC values ranging from 0.5 to 1.0 is used for estimating the prediction accuracy (Yesilnacar and Topal, 2005). The ROC-AUC value ranges from 0.9 to 1.0 is the ideal situation for prediction accuracy (Regmi et al., 2014). The ROC-AUC value of the avalanche susceptibility index was calculated by 100 subdivisions of the total number of pixels in the study area and the cumulative percentage of documented avalanche occurrences.

Validation of the release area map has been performed by calculating success and prediction rates. The training data has been applied for the calculation of the success rate. While, the validation data has been applied for calculation of prediction rate. The values of success rate help to define the correlation of avalanche susceptibility map with the documented avalanche locations. The value of the prediction rate determines the accuracy of the model predicting the avalanches. For validation, 233 i.e., 80% avalanche occurrence data has been applied for training the model. While, the remained 59 i.e. 20% are employed for validation.

The success rate and prediction rate are calculated for verification and validation of the results. The success rates of the probabilistic FR model of terrain and hybrid (terrain+ meteorological) parameters are calculated as 0.9241 and 0.9321. Therefore, success accuracies of the probabilistic FR model for terrain and hybrid parameters are demonstrated as 92.41% and 93.21%. The prediction rate of the FR model of the terrain and hybrid parameters are calculated as 0.8913 and 0.8974. Hence, the prediction accuracies for terrain and hybrid parameters are demonstrated as 89.13% and 89.74%, respectively.

Similarly, the prediction rates of the MCDA-AHP model of the terrain and hybrid parameters are calculated as 0.9097 and 0.9342. Therefore, the prediction accuracies of AHP model based on terrain and hybrid parameters are determined as 90.97% and 93.42%. For the MCDA-AHP model, only the prediction rate has been calculated because of only expert judgments and regional knowledge used for derivation of weight values for each avalanche occurrence parameter. There is no need to use a sample dataset for training the MCDA-AHP model. So, the success rate was not considered in the MCDA-AHP model.

Finally, the success rate and prediction rate of the Fuzzy-FR model of terrain and hybrid parameters was also calculated. The success rate of the Fuzzy-FR model based on terrain and hybrid parameters were calculated as 0.9407 and 0.9454. Hence, the success accuracy of the model based on terrain and hybrid parameters are determined as 94.07% and 94.54%. The prediction rate of the Fuzzy-FR model based on terrain and meteorological parameters are calculated as 0.9176 and 0.9201. Hence, the prediction accuracy of the Fuzzy-FR model based on terrain and hybrid parameters are determined as 91.76% and 92.01%, respectively.

The accuracy assessment of the three models has been demonstrated that the hybrid parameters (terrain + meteorological) improved the results of the applied geospatial models for avalanche susceptibility mapping. The ROC-AUC of success rate and prediction rate of FR model are presented in [figures 6.3 and 6.4](#). The ROC-AUC of the prediction rate of MCDA-AHP is shown in [figure 6.5](#). Finally, the ROC-AUC of success rate and prediction rate of Fuzzy-FR model are shown in [figures 6.6 and 6.7](#)

The accuracy assessment of these three models proves that the Fuzzy-FR model provides better results than the probabilistic FR model and MCDA-AHP model. However, the probabilistic FR model and MCDA-AHP model also shown acceptable results.

7. CONCLUSION AND FUTURE RESEARCH

7.1 Conclusion

A snow avalanche is a severe threat to life and property in the mountainous snow covered regions. Thus, avalanche release area mapping is one of the preliminary steps in the screening of hazardous area and minimizing the loss. GIS has become an important instrument in the last two decades for natural hazard assessment and susceptibility mapping. In the present research, a GIS-based FR, MCDA-AHP and Fuzzy-FR models were applied for release area mapping of the avalanche hazard of the study area (Lahaul region). Most prominent terrain and meteorological avalanche occurrence parameters were incorporated in GIS models for release area mapping of snow avalanches. These parameters were reclassified and utilized as per the configuration of GIS models. The generated release area maps of the avalanche were further reclassified into five zones, such as - no susceptibility, low susceptibility, moderate susceptibility, moderate to high susceptibility and very high susceptibility, respectively. ROC-AUC technique was used to evaluate the accuracy of the model results. The validation of the performance of the geospatial models such as the Probabilistic Frequency Ratio Model, Multi Criteria Decision Analysis-Analytical Hierarchy Process (MCDA-AHP) Model and Fuzzy-Frequency Ratio by utilizing the ROC-AUC technique was performed by utilizing the ROC-AUC technique.

The GIS models in present research may help in the early stages of avalanche risk mapping. These models may be considered as an enhancement of basic assessment approach based on morphological and meteorological parameters. The application of these models usually based on terrain and meteorological parameters to detect vulnerable site that works better than a basic slope, curvature and roughness threshold. It has been already recommended to test different parameter settings (Bühler et al., 2013). The study by Bühler et al. (2013) for avalanche release areas was only on the basis of thresholds values applied on three terrain parameters. The selection of threshold values were based on expert judgments. These authors suggest that the potential avalanche release areas (PARAs) usually detected by basic binary morphological criteria for

threshold values of slope between 30° and 60°, plan curvature values ≤ 5 and roughness values of ≤ 0.5 . The model was not trained for occurrence parameters using documented avalanche occurrence data of the Himalaya region. While, the present model is based on the data-driven approach and expert judgments. Training of the models has been done for occurrence parameters using documented avalanche data of the study area.

PARAs can usually be related to morphological analysis. This approach may be considered as relatively intuitive in the avalanche hazard assessment. The similar example of hazard assessment system was discussed by [Maggioni and Gruber \(2003\)](#). These authors suggest that the potential avalanche release areas (PARAs) usually detected by basic binary morphological criteria for threshold values of slope between 30° and 60°, plan curvature values ≤ 5 and roughness values of ≤ 0.5 . Their approach was commonly used as a screening criterion for the detection of PARAs ([Eckert et al. 2007a, b](#)). In a few cases, the approach was shown to conform to the observed avalanches. To the best of information, however, a thorough outcome of this basic threshold based approach against observed releases of avalanches has not been carried out.

As a result, the avalanche susceptibility maps show good prediction capacity, thus proving its usefulness for designing and development of future infrastructure by avoiding the highly susceptible zones. Direct recognition of avalanche location based on the avalanche inventory map of previously avalanche activities may be suitable where these are strongly indicative of avalanches that occurred throughout the time spent by the field surveyors. These hazardous locations need to be verified by field surveys. To quantify the risk for the settlements, infrastructures and delineations of run-out, the dynamic models may be further utilized.

As per the results of the prediction rate, it is proposed that anthropogenic and other related activities should be avoided in the high and very high susceptibility zones. This is further suggested to do not initiate development projects in these susceptibility zones. In the moderate susceptibility zones, human activity should avoid these zones. The standards for engineering controls should be implemented where possible. The risk assessment must also be performed in the low susceptibility zones to ensure the threat of avalanche occurrence to

humankind and other related infrastructure. This is also suggested that the dynamic avalanche models should be further utilized to quantify the avalanche risk and potential avalanche run-out areas. The avalanche susceptibility map obtained in this study can be a better reference for planners and engineers to design and develop control structures. This avalanche susceptibility map presents helpful information so that consciousness can be accorded to high and very high avalanche susceptibility zones of the study area for the high and very high susceptible zones for any kind of infrastructure development in the near future. The avalanche susceptibility map will be useful for concerned experts in disaster management, planning and mitigation purposes.

The fuzzy logic with frequency ratio method (Fuzzy-FR) is appropriate for avalanche susceptibility mapping, where documented avalanche locations data is limited or unavailable. This method is to be adopted when documented data is confined and experts could not go to the affected areas for detailed exploration of avalanche sites. Therefore, present approach is considered as very useful in inaccessible large areas for the initial screening of potential avalanche affected sites. The models results are assessed using ROC-AUC technique. It is found that the Fuzzy-FR model is applicable for avalanche susceptibility mapping over the mountainous region of Lahaul-Spiti. The resultant avalanche susceptibility map could be easily utilized efficiently to design control structures, prepare avalanche risk maps, planning and mitigation purposes. In such cases, the knowledge of the topographical and meteorology is beneficial.

The membership functions of avalanche occurrence factors used in the present model can also be inferred from expert judgment-based method i.e. analytical hierarchy process (AHP). In this approach, an expert knowledge can be easily included in the fuzzy approach.

Moreover, the model with fuzzy membership functions calculated in this study may be used in other study areas or valleys of Himachal Pradesh with similar geomorphological, meteorological and snowpack conditions, where documented avalanche occurrences data is limited or does not exist. The Fuzzy-FR model would need revision when applied in areas with different conditions. In such cases, the model could be easily revised by modifying the fuzzy membership functions.

7.2 Future research

As per the present research, it is found that the Fuzzy-FR model demonstrated the better results than probabilistic FR and MCDA-AHP models. Therefore, it is recommended to incorporate the model in a GIS environment to develop a geospatial tool to the automated mapping of the potential avalanche release areas of avalanche susceptibility in Western Indian Himalaya.

The automated tool may also be implemented and publish as a geospatial web service in a GIS server from geospatial models for automatic avalanche mapping susceptibility in the WebGIS environment.

The present research was focused on the utilization of the most prominent avalanche occurrence terrain, meteorological and snowpack parameters. A few numbers of distributed stations are available in the study area to collect meteorological data. In future, if number of stations increased then training the models using meteorological data from more distributed stations will be added advantage to obtain more precise results. In the future, if more meteorological parameters and highly densified data will available as covering the region may integrated in the Fuzzy-FR model which may become the integrated model for release area mapping of the avalanches for highly accurate results. Fuzzy-Analytical Hierarchy Process (Fuzzy-AHP) Model, Modified Analytical Hierarchy Process (M-AHP) Model may also be developed and utilized for avalanche susceptibility mapping by taking the reference of the present research.

This is also suggested that the dynamic avalanche models should be further utilized to quantify the avalanche risk and potential avalanche run-out areas. The avalanche susceptibility map obtained can be a better reference for planners and engineers to design and develop control structures. The avalanche susceptibility map will be useful for concerned experts in disaster management, planning and mitigation purposes.

8. REFERENCES

- Aksoy, B., Ercanoglu, M., 2012. Landslide identification and classification by object-based image analysis and fuzzy logic: An example from the Azdavay region (Kastamonu, Turkey). *Computers and Geosciences*, 38: 87-98
- Albrecht V.M., Jaeneke G., Sommerhoff W., Kellermann, 1994. *Wetter-Lawinen*, In: Deutscher, Osterreichischer A, herausgeber. *Alpin-Lehrplan 9*: 1–198
- Ancey, C., 2001. Snow avalanches. In: Balmforth, N., Provenzale, A. (Eds.), *Geomorphological Fluid Mechanics: Selected Topics in Geological and Geomorphological Fluid Mechanics*, 319 – 338.
- Ancey C., 2009. Snow avalanches. In: Delage P, Schrefler B, editors. Wiley & Sons, New York. Available online at <http://www.lhe.epfl.ch/articles/2009WILEY2.pdf>
- Baeza C, Lantada N, Moya J. 2010. Validation and evaluation of two multivariate statistical models for predictive shallow landslide susceptibility mapping of the Eastern Pyrenees (Spain). *Environ Earth Sci.* 61:507–523.
- Bahadur J., 2004. *Himalayan Snow and Glaciers: Associated Environmental Problems, Progress and Prospects*. Concept Publishing Company, New Delhi, India
- Barbolini M., Natale L., Tecilla G., Cordola M., 2001. Linee guida metodologiche per la perimetrazione delle aree esposte al pericolo di valanghe. AINEVA. Available online at http://www.aineva.it/pubblica/Quaderno_Finale.pdf
- Barbolini M., Pagliardi M., Ferro F., Corradeghini P., 2011. Avalanche hazard mapping over large undocumented areas. *Natural Hazards*, 56(2):451–464.
- Barpi F., 2004. Fuzzy modelling of powder snow avalanches. *Cold Region Science & Technology*, 40 (3): 213-227
- Bianchini, S., Solari, L., Del Soldato, M., Raspini, F., Montalti, R., Ciampalini, A. and Casagli, N., 2019. Ground subsidence susceptibility (gss) mapping in grosseto plain (tuscany, italy) based on satellite insar data using frequency ratio and fuzzy logic. *Remote Sensing*, 11(17), p.2015.

- Biskupic M., Barka I., 2010. Spatial modelling of snow avalanche run-outs using GIS. GIS Ostrava, 2010:1-11. Ostrava, Czech Republic. Available online at http://www.gis.vsb.cz/GIS_Ostrava/GIS_Ova_2010/sbornik/Lists/Papers/EN_3_4.pdf
- Bonham-Carter, G.F., 1994. Geographic Information Systems for Geoscientists: Modeling with GIS. Pergamon Press, Ottawa.
- Borouhaki S, Malczewski J. 2008. Implementing an extension of the analytical hierarchy process using ordered weighted averaging operators with fuzzy quantifiers in ArcGIS. *Comput Geosci*. 34:399–410.
- Brundl M., Etter H.J., Steiniger M., Klingler C., Rhyner J., Ammann W.J., 2004. IFKIS—a basis for managing avalanche risk in settlements and on roads in Switzerland. *Natural Hazards Earth System Sciences*, 4:257–262
- Buck A. L., 1981. New equations for computing vapor pressure and enhancement factor. *Journal of Applied Meteorology*, vol. 20, Issue 12, pp.1527-1532
- Bühler, Y., Hüni, A., Christen, M., Meister, R. and Kellenberger, T., 2009. Automated detection and mapping of avalanche deposits using airborne optical remote sensing data. *Cold Regions Science and Technology*, 57(2–3):99-106.doi: 10.1016/j.coldregions.2009.02.007
- Bühler Y., Kumar S., Veitinger J., Christen M., Stoffel A, Snehmani, 2013. *Nat. Hazards Earth Syst. Sci.*, 13: 1321–1335
- Bühler, Y., Bieler, C., Pielmeier, C., Wiesmann, A., Caduff, R., Frauenfelder, R., Jaedicke, C. and Bippus, G., 2014b. All-weather avalanche activity monitoring from space?, *Proceedings of the International Snow Science Workshop, 2014, Banff, Canada*, pp. 795-802.
- Bühler, Y., Meier, L. and Ginzler, C., 2015. Potential of operational, high spatial resolution near infrared remote sensing instruments for snow surface type mapping. *IEEE Geoscience and remote sensing letters*, 12(4): 821-825
- Bui, D.T., Pradhan, B., Lofman, O., Revhaug, I., Dick, O.B., 2012. Spatial prediction of landslide hazards in Hoa Binh province (Vietnam): a comparative assessment of the efficacy of evidential belief functions and fuzzy logic models. *Catena*, 96:28-40. doi:10.1016/j.catena.2012.04.001

- Burrough, P. A., and R. A. McDonell. 1998. Principles of Geographical Information Systems. New York: Oxford University Press.
- Caduff, R., Wiesmann, A., Bühler, Y., 2015. Continuous monitoring of snowpack displacement at high spatial and temporal resolution with terrestrial radar interferometry. *Geophys. Res. Lett.* 01. <http://dx.doi.org/10.1002/2014GL062442>.
- Campbell C., Gould B., Newby J., 2012. Zoning with the avalanche terrain exposure scale. Proceedings of 2012 International Snow Science Workshop. Anchorage, Alaska, 450–457. Available online at <http://www.arc.lib.montana.edu/snow-science/objects/issw-2012-450-457.pdf>
- Chen X., Chen H., You Y., and Liu J. 2015. Susceptibility assessment of debris flows using the analytic hierarchy process method - A case study in Subao river valley, China; *Journal of Rock Mechanics and Geotechnical Engineering*, 7 (4): 404-410
- Chang A.T., Foster, J.L., Hall, D.K., Rango, A. and Hartline, B.K., 1982. Snow water equivalent estimation by microwave radiometry. *Cold Regions Science and Technology*, 5: 259-267
- Choubin, B., Borji, M., Mosavi, A., Sajedi-Hosseini, F., Singh, V.P. and Shamshirband, S., 2019. Snow avalanche hazard prediction using machine learning methods. *Journal of Hydrology*, 577, p.123929.
- Christen M., Kowalski J., Bartlet P., 2010. RAMMS: Numerical simulation of dense snow avalanches in three-dimensional terrain. *Cold Regions Science and Technology*, 63:1-14
- Christiansen, H.H., 2001. Snow-cover depth, distribution and duration data from northeast Greenland obtained by continuous automatic digital camera. *Annals of Glaciology*, 32: 102-108.doi: 10.3189/172756401781819355
- Chrustek, P. and Wezyk, P., 2009. Using high resolution LiDAR data to estimate potential avalanche release areas on the example of Polish mountain regions, Proceedings of the International Snow Science Workshop, 2009, Davos, Switzerland, pp. 495-499.

- Chung C-J.F., Fabbri A.G., 1993. The representation of geoscience information for data integration. *Natural Resources Research*, 2(2):122–139. DOI: 10.1007/BF02272809
- Chung C.F., Fabbri A.G., 1999. Probabilistic prediction models for landslide hazard mapping. *Photogrammetric Engineering and Remote Sensing*, 65(12):1389–1399
- De Scally, F.A. & Gardner, J.S., 1994. Characteristics and mitigation of the snow avalanche hazard in Kaghan Valley, Pakistan Himalaya. *Natural Hazards*, 9(1-2):197-213
- Falah, F. and Zeinivand, H., 2019. GIS-based groundwater potential mapping in khorramabad in lorestan, Iran, using frequency ratio (FR) and weights of evidence (WoE) models. *Water Resources*, 46(5), pp.679-692.
- Deems, J.S., Gadomski, J., Vellone, D., Evanczyk, R., LeWinter, A., Birkeland, K. and Finnegan, D.C., 2014. Mapping starting zone snow depth with a groundbased Lidar to improve avalanche control and forecasting, *Proceedings of the International Snow Science Workshop, 2014, Banff, Canada*, pp. 101-108.
- Deems, J.S., Painter, T.H. and Finnegan, D.C., 2013. Lidar measurement of snow depth: a review. *Journal of Glaciology*, 59: 467-479.doi:10.3189/2013JoG12J154
- Delparte D., Jamieson B., Waters N., 2008. Statistical runout modeling of snow avalanches using GIS in Glacier National Park, Canada. *Cold Region Science and Technology*, 54:183-192
- DLR, 2014. E-SAR. The experimental airborne SAR system of DLR.
- Dong, C., 2018. Remote sensing, hydrological modeling and in situ observations in snow cover research: A review. *Journal of Hydrology*, 561, pp.573-583.
- Dozier J., 1989a. Remote sensing of snow in visible and near-infrared wavelengths. *Theory and Applications of Optical Remote Sensing*. John Wiley and Sons, New York.

- Dozier J., 1989b. Spectral signature of alpine snow cover from the landsat thematic mapper. *Remote Sensing of Environment*, 28(0): 9-22.doi: 10.1016/0034-4257(89)90101-6
- Eckerstorfer, M., Malnes, E., Frauenfelder, R., Domaas, U. and Brattlien, K., 2014. Avalanche debris detection using satellite-borne radar and optical remote sensing, *Proceedings of the International Snow Science Workshop 2014*, Banff, Canada, pp. 122-128.
- Eckerstorfer, M., Solbø, S.A. and Malnes, E., 2015. Using "structure-from-motion" photogrammetry in mapping snow avalanche debris. In: K. Kriz (Editor), *Wiener Schriften zur Geographie und Kartographie*. University of Vienna, Vienna, pp. 171-187.
- Eckerstorfer, M. and Malnes, E., 2015. Manual detection of snow avalanche debris using high-resolution Radarsat-2 SAR images. *Cold Regions Science and Technology*, 120, 205-218
- Eckerstorfer, M., Bühler, Y., Frauenfelder, R. and Malnes, E., 2016. Remote sensing of snow avalanches: Recent advances, potential, and limitations, 121, 126-140.
- Eckert N., Parent E., Bêlanger L., Garcia S., 2007. Hierarchical Bayesian modelling for spatial analysis of the number of avalanche occurrences at the scale of the township. *Cold Regions Science and Technology*, 50 (1–3): 97–112.
- Feick, S., Mitterer, C., Dreier, L., Harvey, S. and Schweizer, J., 2012. Automated detection and monitoring of glide-snow events using satellite-based optical remote sensing *Proceedings of the International Snow Science Workshop, 2012*, Anchorage, Alaska, pp. 603-609.
- Feizizadeh, B., M. S. Roodposhti, P. Jankowski, and T. Blaschke. 2014. "A GIS-based Extended Fuzzy Multi-criteria Evaluation for Landslide Susceptibility Mapping." *Computers and Geosciences* 73: 208–221. doi:10.1016/j.cageo.2014.08.001.

- Fuchs S., Bründl M., 2005. Damage Potential and Losses Resulting from Snow Avalanches in Settlements of the Canton of Grisons, Switzerland. *Natural Hazards*, 34: 53–69
- Fuchs S., Thöni M., McAlpin M.C., Gruber U., Bründl M., 2007. Avalanche Hazard Mitigation Strategies Assessed by Cost Effectiveness Analyses and Cost Benefit Analyses—evidence from Davos, Switzerland. *Natural Hazards*, 41(1):113-129
- Furdada G., Marti G., Oller P., Garcia C., Mases M., Vilaplana J.M., 1995. Avalanche mapping and related GIS applications in the Catalan Pyreness. *Surveys in Geophysics*, 16 (5-6): 681-693. DOI: 10.1007/BF00665748
- Ganju A., Thakur N.K., Rana V., 2002. Characteristics of avalanche accidents in western Himalayan region, India, *International Snow Science Workshop (2002: Penticton, B.C.)*, 200207
- Ganju A., Dimri A.P., 2004. Prevention and Mitigation of Avalanche Disasters in Western Himalayan Region. *Natural Hazards* 31: 357–371.
- Gardner J.S., Saczuk E., 2004. Systems for hazards identification in high mountain areas: an example from the Kullu District, Western Himalaya. *Journal of Mountain Science*, 1:115–127.
- Gauthier, D., Conlan, M. and Jamieson, B., 2014. Photogrammetry of fracture lines and avalanche terrain: Potential applications to research and hazard mitigation projects, *Proceedings of the International Snow Science Workshop, 2014, Banff, Canada*, pp. 109-115.
- Ghinoi A, Chung CJ, 2005. STARTER: a statistical GIS-based model for the prediction of snow avalanche susceptibility using terrain features’ application to Alta val Badia, Italian dolomites. *Geomorphology*, 66 (1–4):305–325.
- Gholami, M., Ghachkanlu, E.N., Khosravi, K. and Pirasteh, S., 2019. Landslide prediction capability by comparison of frequency ratio, fuzzy gamma and landslide index method. *Journal of Earth System Science*, 128(2), pp.1-22.
- Gilany, N. and Iqbal, J., 2019. Simulation of glacial avalanche hazards in Shyok Basin of Upper Indus. *Scientific reports*, 9(1), pp.1-14.

- Gleason J.A., 1994. Terrain parameters of avalanche starting zones and their effects on avalanche frequency. International Snow Science Workshop (ISSW), Snowbird, Utah, USA, 393-404. Available online at <http://www.arc.lib.montana.edu/snow-science/objects/issw-1994-393-404.pdf>
- Gruber U., Bartelt P., 2007. Snow avalanche hazard modelling of large areas using shallow water numerical methods and GIS, *Environmental Modelling and Software*, 22 (10): 1472–1481. DOI:10.1016/j.envsoft.2007.01.001
- Guy Z.M., Birkeland, K.W., 2013. Relating complex terrain to potential avalanche trigger locations. *Cold Regions Science and Technology*, 86: 1–13.
- Hall D.K., Riggs, G.A., Salomonson, V.V., DeGirolamo, N.E., Bayr, K.J. and Jin, J.M., 2002. MODIS snow-cover products. *Remote Sensing of Environment*, 83: 181-194
- Hanley JA, McNeil BJ. 1983. A method of comparing the areas under receiver operating characteristic curves derived from the same cases. *Radiology*. 148:839–843.
- Hebertson E.G., Jenkins M.J., 2003. Historic climate factors associated with major avalanche years on the Wasatch Plateau, Utah. *Cold Regions Science and Technology*, 37(3):315–332. DOI: 10.1016/S0165-232X(03)00073-9
- Hendrikx, J., Peitzsch, H.E. and Fagre, D.B., 2012. Time-lapse photography as an approach to understanding glide avalanche activity, *Proceedings of the International Snow Science Workshop, 2012, Anchorage, Alaska*, pp. 872-877.
- Hendrikx J., Owens I., Carran W., Carran A., 2004. Overview of the spatial distribution of avalanche activity in relation to meteorological and topographic variables in an extreme maritime environment. *Proceedings of the International Snow Science Workshop. Jackson Hole, Wyoming, USA*, 299-307. Available online at <http://www.arc.lib.montana.edu/snow-science/objects/issw-2004-299-307.pdf>
- Hervas J., 2003. Recommendations to deal with snow avalanches in Europe. EC-JRC

- Hines J.W., 1997. Fuzzy and neural approaches in engineering. Wiley, New York, NY
- Huang, S., Li, X., Wang, Y., 2012. A new model of geo-environmental impact assessment of mining: a multiple-criteria assessment method integrating Fuzzy-AHP with fuzzy synthetic ranking. *Environmental Earth Science* 66, 275–284.
- Instanes, A., Lønne, I. and Sandaker, K., 2004. Location of avalanche victims with ground-penetrating radar. *Cold Regions Science and Technology*, 38(1): 55-61
- Jaccard C., 1990. Fuzzy factorial analysis of snow avalanches. *Natural Hazards*, 3(4):329-340.
- Jarsve, K., Devoli, G. and Schuler, T.V., 2019, January. Uncertainties of Simulating Debris Avalanches Using RAMMS. In *Geophysical Research Abstracts (Vol. 21)*.
- Jenks G.F. 1967. The Data Model Concept in Statistical Mapping. *International Yearbook of Cartography* 7: 186–190.
- Jiang H, Eastman JR. 2000. Application of fuzzy measures in multi-criteria evaluation in GIS. *Int J Geog Inf Sci*. 14:173–184.
- Jomelli V., Delval C., Grancher D., Escande S., Brunstein D., Hetu B., Filion L., Pech P., 2007.
- Kahraman, C., U. Cebeci, and Z. Ulukan. 2003. “Multi-criteria Supplier Selection using Fuzzy AHP.” *Logistics Information Management* 16 (6): 382–394. doi:10.1108/09576050310503367.
- Kainz, W. 2008. *Fuzzy Logic and GIS*. Vienna: University of Vienna. http://homepage.univie.ac.at/wolfgang.kainz/Lehrveranstaltungen/ESRI_Fuzzy_Logic/File_2_Kainz_Text.pdf.
- Kavzoglu T., Sahin E.K., Colkesen I., 2014. Landslide susceptibility mapping using GIS-based multi-criteria decision analysis, support vector machines, and logistic regression. *Landslides*, 11(3):425-439

- Kayastha P, Dhital MR, Smedt FD. 2013. Application of the analytical hierarchy process (AHP) for landslide susceptibility mapping: a case study from the Tinau watershed, west Nepal. *Comput Geosci.* 52:398–408.
- Kim Ki-Dong., Lee S., Oh Hyun-Joo, Choi Jong-Kuk., Won Joong-Sun. 2006. Assessment of ground subsidence hazard near an abandoned underground coal mine using GIS. *Environ. Geol.* 50, 1183–1191. DOI: 10.1007/s00254-006-0290-5
- Kirschbaum, D., T. Stanley, and S. Yatheendradas. 2015. “Modeling Landslide Susceptibility over Large Regions with Fuzzy Overlay.” *Landslides* 1–12. doi:10.1007/s10346-015-0577-2.
- Koenderink, J.J. and van Doorn, A.J., 1991. Affine structure from motion. *Journal of the Optical Society of America. A, Optics and image science*, 8(2): 377-385
- Lato, M.J., Frauenfelder, R. and Bühler, Y., 2012. Automated detection of snow avalanche deposits: segmentation and classification of optical remote sensing imagery. *Nat. Hazards Earth Syst. Sci.*, 12(9): 2893-2906.10.5194/nhess-12-2893-2012
- Larsen, S.Ø., Salberg, A.-B. and Solberg, R., 2013. Automatic avalanche mapping using texture classification of optical satellite imagery, *EARSel*, pp. 399-410.
- Lee, S., Oh, H.J., and Kim, K.D. 2010. “Statistical spatial modeling of ground subsidence hazard near an abandoned underground coal mine.” *Disaster Advances* 3:11–23.
- Maggioni, M., Gruber, U., Stoffel, A. 2002. Definition and characterisation of potential avalanche release areas. 22nd Annual Esri International User Conference, San Diego Available online at <http://avalanchemapping.org/linksresearch.htm>
- Maggioni M., Gruber U., 2003. The influence of topographic parameters on avalanche release dimension and frequency. *Cold Regions Science and Technology*, 37 (3): 407–419. DOI: 10.1016/S0165-232X(03)00080-6

- Maggioni, M. 2004. Avalanche release areas and their influence on uncertainty in avalanche hazard mapping. Ph.D. thesis, University of Zürich, Zürich. Available online at http://www.geo.uzh.ch/fileadmin/files/content/abteilungen/gis/research/phd_theses/thesis_MargheritaMaggioni_2005.pdf
- Malnes, E., Eckerstorfer, M., Larsen, Y., Frauenfelder, R., Jonsson, A., Jaedicke, C. and Solbø, S.A., 2013. Remote sensing of avalanches in northern Norway using Synthetic Aperture Radar, Proceedings of the International Snow Science Workshop 2013, Grenoble - Chamonix, Mont Blanc, France, pp. 955-959.
- Malnes, E., Eckerstorfer, M. and Vickers, H., 2015. First Sentinel-1 detections of avalanche debris. *The Cryosphere Discuss.*, 9: 1943-1963. doi: 10.5194/tcd-9-1943-2015
- Martinez-Vazquez, A. and Fortuny-Guasch, J., 2008. A GB-SAR Processor for Snow Avalanche Identification. *Geoscience and Remote Sensing, IEEE Transactions on*, 46(11): 3948-3956. 10.1109/TGRS.2008.2001387
- McCammon I., Häegeli P., 2007. An evaluation of rule-based decision tools for travel in avalanche terrain. *Cold Region Science Technology*, 47(1–2):193–206
- McClung D.M., Mears A.I., 1995. Dry-flowing avalanche run-up and run-out. *Journal of Glaciology*, 41: 359-372
- McClung, D. M. 2001. “Characteristics of Terrain, Snow Supply and Forest Cover for Avalanche Initiation caused by Logging.” *Annals of Glaciology* 32: 223–229.
- McClung D.M, Schaerer P., 2006. *The avalanche handbook*, third edition. The Mountaineers Books, Seattle, WA, USA
- Mears A.I., 1992. *Snow-Avalanche hazard analysis for land-use planning and engineering*. Bulletin 49, Colorado Geological Survey, Denver
- Meer, M.S. and Mishra, A.K., 2020. Observational study of a severe snowfall avalanche over a state in North India in November 2019 using GIS. *Journal of Earth System Science*, 129(1), pp.1-5.

- Naghibi S.A, Pourghasemi H.R., Pourtaghi Z.S., Rezaei A., 2015. Groundwater qanat potential mapping using frequency ratio and Shannon's entropy models in the Moghan watershed, Iran. *Earth Science Informatics*. 8 (1): 171-186. DOI: 10.1007/s12145-014-0145-7
- Naaïm M., Faung T., Naaïm-Bouvet F., 2003. Dry granular flow modelling including erosion and deposition. *surveys in geophysics*, 24:569-585
- Naaïm M., Naaïm-Bouvet F., Faug T., Bouchet A., 2004. Dense snow avalanche modeling: flow, erosion, deposition and obstacle effects. *Cold Regions Science and Technology*, 39:193-204
- Nefeslioglu H.A., Sezer E.A., Gokceoglu C., Ayas Z., 2013. A modified analytical hierarchy process (M-AHP) approach for decision support systems in natural hazard assessments
- Nolin A.W., 2010. Recent advances in remote sensing of seasonal snow. *Journal of Glaciology*, 56(200): 1141-1150
- Norwegian Geotechnical Institute NGI, 2015. Towards an automated snow property and avalanche mapping system (ASAM) - Avalanche recognition and snow variable retrieval. version 2 (Technical report). NGI Report no. 20130092-04-R. 127.
- Oh, H.J., Kim, Y.S., Choi, J.K., Lee, S. 2011. "GIS mapping of regional probabilistic groundwater potential in the area of Pohang City, Korea." *Journal of Hydrology* 399(3-4): 158– 172. doi:10.1016/j.jhydrol.2010.12.027.
- Oller P. et al., 2010. Using AVAL-1D to simulate avalanches in the eastern Pyrenees. *Cold Regions Science and Technology*, 64:190-198
- Ozdemir A., 2011. GIS-based groundwater spring potential mapping in the Sultan Mountains (Konya, Turkey) using frequency ratio, weights of evidence and logistic regression methods and their comparison. *Journal of Hydrology*, 411 (3-4):290–308. DOI:10.1016/j.jhydrol.2011.10.010
- Ozdemir, A., 2020. A Comparative Study of the Frequency Ratio, Analytical Hierarchy Process, Artificial Neural Networks and Fuzzy Logic Methods for

- Landslide Susceptibility Mapping: Taşkent (Konya), Turkey. *Geotechnical and Geological Engineering*, pp.1-29.
- Peitzsch, H.E., Hendrikx, J., Fagre, B.D. and Reardon, B., 2010. Characterizing wet slab and glide slab avalanche occurrence along the Going-to-the-sun road, Glacier national park, Montana, USA, *Proceedings of the International Snow Science Workshop 2010, Squaw Valley*, pp. 651-659.
- Perla R., Cheng T.T., McClung D.M., 1980. Two-parameter model of snow-avalanche motion. *Journal of Glaciology*, 94:197-207
- Perla R., 1984. Particle simulation of snow avalanche motion. *Cold Regions Science and Technology*, 9:191-202
- Pistocchi A., Notarnicola C., 2013. Data-driven mapping of avalanche release areas: a case study in South Tyrol, Italy. *Natural Hazards*, 65(3): 1313-1330
- Pourghasemi H.R, Pradhan B., Gokceoglu C., Moezzi K.D., 2013. A comparative assessment of prediction capabilities of Dempster-Shafer and weights-of-evidence models in landslide susceptibility mapping using GIS. *Geomatics. Natural Hazards and Risk*, 4(2): 93-118. doi:10.1080/19475705.2012.662915
- Pradhan, B., and Lee, S. 2010. "Delineation of landslide hazard areas on Penang Island, Malaysia, by using frequency ratio, logistic regression, and artificial neural network models." *Environmental Earth Sciences* 60(5):1037–1054. Doi:10.1007/s12665-009-0245-8.
- Prokop, A., 2008. Assessing the applicability of terrestrial laser scanning for spatial snow depth measurements. *Cold Regions Science and Technology*, 54(3):155-163. doi: 10.1016/j.coldregions.2008.07.002
- Prokop, A., Schön, P., Singer, F., Gaëtan, P., Naaim, M., Thibert, E., 2013. Determining avalanche modelling input parameters using terrestrial laser scanning technology. *Proceedings of the International Snow Science Workshop, 2013, Chamonix Mont-Blanc, France*, pp. 770–774.
- Rango A. and Itten K.I., 1976. Satellite potentials in snowcover monitoring and runoff prediction. *Nordic Hydrology*, 7: 209-230

- Rao M. et al., 1988. Impact of avalanche problems in some of the hill areas of Himachal Pradesh (1988), National Seminar on Hill Area Development, 27–29 Jun 1988 Shimla (HP).
- Rees, G.W., 2006. Remote sensing of snow and ice. CRC Press, Taylor & Francis Group, 277 pp.
- Regmi A.D., Devkota K.C., Yoshida K., Pradhan B., Pourghasemi H.R., Kumamoto T., Akgun A., 2014. Application of frequency ratio, statistical index, and weights-of-evidence models and their comparison in landslide susceptibility mapping in Central Nepal Himalaya. *Arabian Journal of Geosciences*, 7 (2): 725-742. DOI: 10.1007/s12517-012-0807-z
- Rahmati, O., Ghorbanzadeh, O., Teimurian, T., Mohammadi, F., Tiefenbacher, J.P., Falah, F., Pirasteh, S., Ngo, P.T.T. and Bui, D.T., 2019. Spatial Modeling of Snow Avalanche Using Machine Learning Models and Geo-Environmental Factors: Comparison of Effectiveness in Two Mountain Regions. *Remote Sensing*, 11(24), p.2995.
- Rehman, S., Sahana, M., Dutta, S., Sajjad, H., Song, X., Imdad, K. and Dou, J., 2020. Assessing subsidence susceptibility to coal mining using frequency ratio, statistical index and Mamdani fuzzy models: evidence from Raniganj coalfield, India. *Environmental Earth Sciences*, 79(16), pp.1-18.
- Saaty, T.L., 1980. *The Analytical Hierarchy Process*. McGraw-Hill, New York.
- Saaty TL. 1987. How to handle dependence with the analytic hierarchy process. *Mathematical Modelling*. 9:161–176.
- Saaty TL. 2000. *The Fundamentals of decision making and priority theory with the analytic hierarchy process*, Vol (VI). Pitsburg: RWS publications; 478 pp.
- Saaty TL. 2008. Decision making with the analytic hierarchy process. *Int J Serv Sci*. 1:83–98.
- Sailer R. et al., 2008. Snow avalanche mass-balance calculation and simulation-model verification. *Annals of Glaciology*, 48: 183-192
- Sappington, J. M., K. M. Longshore, and D. B. Thompson. 2007. “Quantifying Landscape Ruggedness for Animal Habitat Analysis: A Case Study using

- Bighorn Sheep in the Mojave Desert.” *The Journal of Wildlife Management* 71 (5): 1419–1426. doi:10.2193/2005-723.
- Scherer, D., Hall, D.K., Hochschild, V., König, M., Winther, J.-G., Duguay, C.R., Pivot, F., Mätzler, C., Rau, F., Seidel, K., Solberg, R. and Walker, A.E., 2013. Remote sensing of snow cover. In: C.R. Duguay and A. Pietroniro (Editors), *Remote Sensing in Northern Hydrology: Measuring Environmental Change*. American Geophysical Union, pp. 7-38.
- Schweizer J., Jamieson J.B., Schneebeli M., 2003. Snow avalanche formation. *Review of Geophysics*, 41: 10-16.
- Schweizer J., Mitterer C., Stoffel L., 2009. On forecasting large and infrequent snow avalanches. *Cold Region Science & Technology*, 59(2–3):234–241
- Schweizer J., Bartelt P., Herwijnen AV., 2015. *Snow avalanches: Snow and Ice-Related Hazards, Risks, and Disasters*
- Selçuk L., 2013. An avalanche hazard model for Bitlis Province, Turkey, using GIS based multicriteria decision analysis, *Turkish Journal of Earth Sciences*, 523-535
- Shahabi H, Khezri S, Ahmad B.B., Hashim M, 2014. Landslide susceptibility mapping at central Zab basin, Iran: A comparison between analytical hierarchy process, frequency ratio and logistic regression models. *Catena*. 115, 55–70.
- Shahabi H., Hashim M., Ahmad B.B., 2015. Remote sensing and GIS-based landslide susceptibility mapping using frequency ratio, logistic regression, and fuzzy logic methods at the central Zab basin, Iran. *Environmental Earth Sciences*. 73, 12:8647-8668
- Sharma S.S., Ganju A. 2000. Complexities of avalanche forecasting in Western Himalaya – an overview; *Cold Regions Science and Technology*, 31: 95 – 102.
- Sharma S.S., Mathur P., Snehmani., 2004. Change detection analysis of avalanche snow in Himalayan region using near infrared and active microwave images. *Adv Space Res* 33:259– 267.

- Singh M.K., Gupta R.D., Snehmani, Bhardwaj A., Ganju A., 2016a. Scenario-Based Validation of Moderate Resolution DEMs Freely Available for Complex Himalayan Terrain. *Pure and Applied Geophysics*, 173, 463–485. DOI: 10.1007/s00024-015-1119-5
- Singh M.K., Gupta R.D., Snehmani, Kumar S., Ganju A., 2016b. Assessment of freely available CartoDEM V1 and V1.1R1 with respect to high resolution aerial photogrammetric DEM in high mountains, 31, 943-955. *Geocarto International*. DOI: 10.1080/10106049.2015.1094524
- Sinickas, A., and Jamieson, B. 2014. “Comparing methods for estimating β points for use in statistical snow avalanche runout models.” *Cold Regions Science and Technology* 104-105: 23-32. doi:10.1016/j.coldregions.2014.04.004.
- Smith, M. J., and D. M. McClung. 1997. “Avalanche Frequency and Terrain Characteristics at Rogers’ Pass, British Columbia, Canada.” *Journal of glaciology* 43: 165–171.
- Snehmani, Singh M.K., Gupta R.D., Ganju A., 2013. DTM Generation and Avalanche Hazard Mapping using Large Format Digital Photogrammetric Data and Geomatics Technique. *Journal of Remote Sensing and GIS*, 4(2): 4-13. ISSN: 2230-7990
- Snehmani, Bhardwaj A., Pandit A., Ganju A., 2014. Demarcation of potential avalanche sites using remote sensing and ground observations: a case study of Gangotri glacier. *Geocarto International*, 29 (5), 520-535. DOI: 10.1080/10106049.2013.807304
- Snow and Avalanche Study Establishment (SASE). 2010. Internal report on avalanche hazard mitigation scheme.
- Snow and Avalanche Study Establishment (SASE). 2014. Internal report on avalanche hazard mitigation scheme.
- Snow and Avalanche Study Establishment (SASE). 2016. Internal report on avalanche hazard mitigation scheme.
- Snow and Avalanche Study Establishment (SASE). 2018. Internal report on avalanche hazard mitigation scheme.

- Sovilla, B., McElwaine, J.N., Schaer, M. and Vallet, J., 2010. Variation of deposition depth with slope angle in snow avalanches: Measurements from Vallée de la Sionne. *Journal of Geophysical Research: Earth Surface*, 115(F2): F02016.10.1029/2009JF001390
- Stoffel A., Meister R., Schweizer J., 1998. Spatial characteristics of avalanche activity in an Alpine valley: A GIS approach. *Annals of Glaciology*, 26:329-336
- Tedesco, M., 2015. Remote sensing of the Cryosphere. The Cryosphere Science Series. Wiley-Blackwell.
- Tracy L., 2001. Using GIS in avalanche hazard management. Proceedings of the 2001 ESRI International User Conference, San Diego.
- Tsai, Y.L.S., Dietz, A., Oppelt, N. and Kuenzer, C., 2019. Remote sensing of snow cover using spaceborne SAR: A review. *Remote Sensing*, 11(12), p.1456.
- Umar Z., Pradhan B., Ahmad A., Jebur M.N., Tehrany M.S., 2014. Earthquake induced landslide susceptibility mapping using an integrated ensemble frequency ratio and logistic regression models in West Sumatera Province, Indonesia. *Catena*, 118: 124–135. DOI:10.1016/j.catena.2014.02.005
- Vallet, J., Skaloud, J. and Koelbl, O., 2000. Development of a Helicopter-Based Integrated System for Avalanche Mapping and Hazard Management. *The International archives of photogrammetry. Remote sensing and spatial information sciences*, 33: 565-572
- Van Den Eeckhaut M, Vanwalleggem T, Poesen J, Govers G, Verstraeten G, Vandekerckhove L. 2006. Prediction of landslide susceptibility using rare events logistic regression: a case-study in the Flemish Ardennes (Belgium). *Geomorphology*. 76:392–410.
- Van Herwijnen, A. and Simenhois, R., 2012. Monitoring glide avalanches using timelapse photography, Proceedings of the International Snow Science Workshop, 2012, Anchorage, Alaska, pp. 899-903.
- Van Herwijnen, A., Berthod, N., Simenhois, R. and Mitterer, C., 2013. Using timelapse photography in avalanche research, Proceedings of the International Snow Science Workshop, 2013, Grenoble, France, pp. 950-954.

- Van Herwijnen, A. and Fierz, C., 2014. Monitoring snow cornice development using time-lapse photography, Proceedings of the International Snow Science Workshop, 2014, Banff, Canada, pp. 865-869.
- Vogel, S., Eckerstorfer, M. and Christiansen, H.H., 2012. Cornice dynamics and meteorological control at Gruvefjellet, Central Svalbard. *The Cryosphere*, 6:157-171.doi:10.5194/tc-6-157-2012
- Westoby, M.J., Brasington, J., Glasser, N.F., Hambrey, M.J. and Reynolds, J.M., 2012. "Structure-from-Motion" photogrammetry: A low-cost, effective tool for geoscience applications. *Geomorphology*, 179: 300-314.doi: 10.1016/j.geomorph.2012.08.021
- Wiesmann, A., Wegmueller, U., Honikel, M., Strozzi, T. and Werner, C.L., 2001. Potential and methodology of satellite based SAR for hazard mapping., IGARSS 2001. IEEE, Sydney, Australia.
- Wiesmann, A., Caduff, R., Strozzi, T., Papke, J. and Mätzler, C., 2014. Monitoring of dynamic changes in alpine snow with terrestrial radar imagery, IGARSS 2014. IEEE, pp. 3662-3665.
- Wirz, V., Schirmer, M., Gruber, S., Lehning, M., 2011. Spatio-temporal measurements and analysis of snow depth in a rock face. *The Cryosphere*, 5:893-905.doi: 10.5194/tc-5-893-2011.
- Xiong, K., Adhikari, B.R., Stamatopoulos, C.A., Zhan, Y., Wu, S., Dong, Z. and Di, B., 2020. Comparison of different machine learning methods for debris flow susceptibility mapping: A case study in the Sichuan Province, China. *Remote Sensing*, 12(2), p.295.
- Xiao, X., Zhang, T., Zhong, X., Shao, W. and Li, X., 2018. Support vector regression snow-depth retrieval algorithm using passive microwave remote sensing data. *Remote sensing of environment*, 210, pp.48-64.
- Yang Q.L., Gao J.R., Wang Y., and Qian B.T. 2011. Debris flows characteristics and risk degree assessment in Changyuan Gully, Huairou District, Beijing; *Procedia Earth and Planetary Science*, 2:262-271.

- Yariyan, P., Avand, M., Abbaspour, R.A., Karami, M. and Tiefenbacher, J.P., 2020. GIS-based spatial modeling of snow avalanches using four novel ensemble models. *Science of the Total Environment*, 745, p.141008.
- Yesilnacar, E., Topal, T., 2005. Landslide susceptibility mapping: a comparison of logistic regression and neural networks methods in a medium scale study, Hendek region (Turkey). *Engineering Geology*, 79 (3-4): 251–266. DOI:10.1016/j.enggeo.2005.02.002
- Yilmaz A. 2007. *Environmental Geology*. Cumhuriyet University, Faculty of Engineering Publications, Sivas, Publication No: 107.
- Zadeh L.A., 1965. Fuzzy sets. *Information and Control*, 8(3): 338-353
- Zhang J, Su Y, Wu J, Liang H. 2015. GIS based land suitability assessment for tobacco production using AHP and fuzzy set in Shandong province of China. *Comput Electron Agricu*. 114:202–211.
- Zischg, A., Fuchs, S., Keiler, M., and Meibl, G., 2005. Modelling the system behaviour of wet snow avalanches using an expert system approach for risk management on high alpine traffic roads, *Natural Hazards and Earth System Science*, 5, 821-832.

APPENDICES

APPENDIX 1: FIRST PAGE OF PLAGIARISM REPORT

<p>Turnitin Originality Report</p> <p>Processed on: 06-Jul-2020 3:32 PM IST ID: 1354070037 Word Count: 31227 Submitted: 1</p> <p>Geospatial Modelling and Mapping of Avalanche Hazard By Satish Kumar</p>		<table border="1"> <tr> <td>Similarity Index</td> <td>6%</td> </tr> </table>	Similarity Index	6%	<table border="1"> <tr> <th colspan="2">Similarity by Source</th> </tr> <tr> <td>Internet Sources:</td> <td>3%</td> </tr> <tr> <td>Publications:</td> <td>3%</td> </tr> <tr> <td>Student Papers:</td> <td>3%</td> </tr> </table>	Similarity by Source		Internet Sources:	3%	Publications:	3%	Student Papers:	3%
Similarity Index	6%												
Similarity by Source													
Internet Sources:	3%												
Publications:	3%												
Student Papers:	3%												

<p>< 1% match (student papers from 19-Jun-2017) Submitted to Indian Institute of Remote Sensing on 2017-06-19</p>
<p>< 1% match (Internet from 20-Jun-2017) http://documents.mx/download/link/science-and-technology-2011</p>
<p>< 1% match (Internet from 12-Oct-2017) http://www.tandfonline.com/doi/full/10.1080/10106049.2016.1206626</p>
<p>< 1% match (publications) Haoyuan Hong, Himan Shahabi, Ataollah Shirzadi, Wei Chen et al. "Landslide susceptibility assessment at the Wuning area, China: a comparison between multi-criteria decision making, bivariate statistical and machine learning methods", Natural Hazards, 2018</p>
<p>< 1% match (publications) Xingzhang Chen, Hui Chen, Yong You, Jinfeng Liu. "Susceptibility assessment of debris flows using the analytic hierarchy process method – A case study in Subao river valley, China", Journal of Rock Mechanics and Geotechnical Engineering, 2015</p>
<p>< 1% match (publications) Eckerstorfer, Markus, Yves Bühler, Regula Frauenfelder, and Eirik Malnes. "Remote sensing of snow avalanches: Recent advances, potential, and limitations", Cold Regions Science and Technology, 2016.</p>
<p>< 1% match (student papers from 09-Oct-2018) Submitted to University of Malaya on 2018-10-09</p>
<p>< 1% match (Internet from 10-Dec-2019) https://www.tandfonline.com/doi/full/10.1080/17499518.2017.1343482</p>
<p>< 1% match (publications) "Laser Scanning Applications in Landslide Assessment", Springer Science and Business Media LLC, 2017</p>
<p>< 1% match (Internet from 27-Apr-2019) https://repository.tudelft.nl/islandora/object/uuid:26845c1a-5248-48fc-9379-7c44d8f85c5b/datastream/OBJ/download</p>
<p>< 1% match (student papers from 23-Jun-2020) Submitted to University of Petroleum and Energy Studies on 2020-06-23</p>
<p>< 1% match (publications) Meimei Zhang, Fang Chen, Bangsen Tian. "Glacial Lake Detection from GaoFen-2 Multispectral Imagery Using an Integrated Nonlocal Active Contour Approach: A Case Study of the Altai Mountains, Northern Xinjiang Province", Water, 2018</p>
<p>< 1% match (Internet from 06-Mar-2020) https://link.springer.com/article/10.1007%2Fs12145-014-0145-7</p>

APPENDIX -2: CURRICULUM VITAE

SATISH KUMAR

Development Manager (GIS System)
Town and Country Planning Department,
Government of Haryana, Sector 18 A,
Chandigarh-160018
Contact No.: +91-7009975441
Email id: satish894@gmail.com



1. EDUCATION:

- Pursuing Ph.D. in Computer Science & Engineering from University of Petroleum and Energy Studies, Dehradun.
- M. Tech. in Computer Science & Engineering from Punjab Technical University Jalandhar with first division.
- B. Tech. in Computer Science & Engineering from Punjab Technical University Jalandhar with first division.
- 12th from Himachal Pradesh Board of School Education Dharamshala with first division.
- 10th from Himachal Pradesh Board of school Education Dharamshala with first division.

2. WORK EXPERIENCE: (11 Years and 07 Months)

Sr. No.	Organization	Period		Months
		From	To	
1	Town and Country Planning Department, Govt. of Haryana, Chandigarh	Mar, 2016	Till date	52 Months
2.	Defence Research & Development Organization (DRDO), Ministry of Defence, SASE-RDC, Chandigarh	Nov, 2012	Feb, 2016	38 Months
3.	Punjab Remote Sensing Centre (A Govt. of Punjab Enterprises), PAU Campus, Ludhiana	Apr, 2012	Nov, 2012	07 Months
4.	Defence Research & Development Organization, Ministry of Defence, SASE-RDC, Chandigarh	Apr, 2009	Mar, 2012	36 Months
5.	Longowal College, Punjab	Oct, 2008	Mar, 2009	06 Months

3. TECHNICAL SKILLS:

- Remote Sensing (Optical and Microwave), Geographical Information System (GIS), Enterprise WebGIS, Photogrammetry, Satellite Image Processing and Analysis and Spatial Databases.
- **Language:** C++, C#, ASP.NET, SQL, JavaScript, HTML and Python
- **Packages, APIs and Libraries:** OpenGeoSuite, Geoserver, OpenLayers, GeoEXT, ArcGIS Server, ArcGIS, LPS, ErdasImagine, ENVI, ArcObjects, ArcGIS APIs, GeoEXT APIs, OpenLayers APIs, Google APIs, and ArcPy
- **Database:** PostgreSQL, SQL Server 2008, ArcSDE, PostGIS and MS Access
- **OGC Standards:** KML, GML, CSW, WMS, WFS, WCS, WPS, TMS, WMS-C, WMTS and REST web services
- **Operating Systems:** Microsoft Windows XP, Windows7, Linux.

4. WORK PROFILE:

- WebGIS development, Management of Spatial Database, Satellite Image Processing and analysis related tasks.
- Manage technical team including allocation of work responsibilities and workflow management
- Development of models/algorithms for snow covers mapping and monitoring of parts of NW Himalayas using multispectral, multi-temporal and multi resolution satellite data.
- Development of an Advanced Algorithm for Fire Detection, Validation, and Characterization using satellite imagery (Under INSAT-3D Utilization Program-ISRO Sponsored Project).
- Extraction of high-resolution Digital Elevation Models (DEMs) from Cartosat-1 Pan Ortho Stereo pair satellite imagery using stereo correlation technique and its accuracy assessment/validation in Manali and nearby region, a part of NW-Himalaya.
- Creation of digital database of rural water supply sources in Sangrur district using Remote Sensing and GIS.
- Creation of digital database of Sikkim using Remote Sensing & GIS.
- **Satellite Data Used:** AWiFS, MODIS, LISS, Cartosat-1, PAN, Landsat7 ETM+, Landsat 8, etc.

5. PROFESSIONAL TRAININGS:

Sr. No.	Organization	Period		Training Detail(s)
		From	To	
1.	Indian Institute of Remote Sensing, Dehradun (ISRO)	Aug 5, 2012	Aug 9, 2012	Open-Source GIS Software Solutions (WebGIS)
2.	Defence Research & Development Organization, Ministry of Defence, SASE RDC Chandigarh	Jul 2014	Jul 2014	Geospatial Technology
3.	Defence Research & Development Organization, Ministry of Defence, SASE RDC Chandigarh	Jul 8, 2013	Jul 12, 2013	Geospatial Technology
4.	Defence Research & Development Organization, Ministry of Defence, SASE RDC Chandigarh	Jul 4, 2011	Jul 8, 2011	Remote Sensing & GIS
5.	Defence Research & Development Organization, Ministry of Defence, SASE RDC Chandigarh	Jul 5, 2010	Jul 9, 2010	Remote Sensing & GIS
6.	Defence Research & Development Organization, Ministry of Defence, SASE-RDC, Chandigarh	Jul 6, 2009	Jul 10, 2009	Remote Sensing & GIS
7.	Punjab Remote Sensing Centre, Ludhiana	Jul, 2007	Jan, 2008	Creation of Digital Database using Remote Sensing & GIS

6. PERSONAL DETAIL:

- Date of Birth: 29-10-1984
- Marital Status: Married
- Sex: Male
- Nationality: Indian
- Permanent Address: S/o Shri Parkash Chand Sapehia, Village Kanol, PO Chanour, Tehsil Dehra, District Kangra, Himachal Pradesh-177113

7. REFERENCES:

- Dr. Snehmani, Scientist 'F', Joint Director, DRDO, SASE, Research & Development Centre (Ministry of Defence), Himparisar, Sector-37A, Chandigarh, Email id: snehmani@sase.drdo.in, snehmani@gmail.com, Contact number: +91-9417839240, 172-2699804-270
- Dr. Pankaj Kumar Srivastava, Professor, Department of Petroleum Engineering and Earth Sciences, University of Petroleum and Energy Studies, Dehradun, India, Email id: pksrivastava@ddn.upes.ac.in, Contact number: +91-9758218896

Date: 14/07/2020

Place: CHANDIGARH

SATISH KUMAR

APPENDIX -3: LIST OF PUBLICATIONS

1. Satish Kumar, Snehmani, Pankaj Kumar Srivastava, Akshay Gore, Mritunjay Kumar Singh, 2016. Fuzzy Frequency Ratio Model for Avalanche Susceptibility Mapping. *International Journal of Digital Earth*, 9 (12): 1168-1184.
DOI:10.1080/17538947.2016.1197328. IF: 3.985
2. Satish Kumar, Pankaj Kumar Srivastava, Snehmani, 2017. GIS Based MCDA-AHP Modelling for Avalanche Susceptibility Mapping of Nubra Valley Region, Indian Himalaya. *Geocarto International*, 32 (11): 1254-1267.
DOI:10.1080/10106049.2016.1206626. IF:2.365
3. Satish Kumar, Pankaj Kumar Srivastava, Snehmani, 2018. Geospatial Modelling and Mapping of Snow Avalanche Susceptibility. *Journal of the Indian Society of Remote Sensing*, 46 (1): 109-119. DOI:10.1007/s12524-017-0672-z. IF: 0.869
4. Satish Kumar, Pankaj Kumar Srivastava, Snehmani, Sanjay Bhatiya, 2019. Geospatial Probabilistic Modelling for Release Area Mapping of Snow Avalanches. *Cold Regions Science and Technology*, 165: 102813. DOI: 10.1016/j.coldregions.2019.102813. IF: 2.767